Noninvasive Glucose Detection Using Infrared Photoacoustic Spectroscopy and Machine Learning

by

Abdulrahman Aloraynan

A thesis
presented to the University of Waterloo
in fulfillment of the
thesis requirement for the degree of
Doctor of Philosophy
in
Electrical and Computer Engineering

Waterloo, Ontario, Canada, 2023

© Abdulrahman Aloraynan 2023

Examining Committee Membership

The following served on the Examining Committee for this thesis. The decision of the Examining Committee is by majority vote.

External Examiner:	Mohamed Bakr Professor, Dept. Electrical & Computer Engineering McMaster University
Supervisor(s):	Dayan Ban Professor, Dept. Electrical & Computer Engineering University of Waterloo
Internal Member:	Bo Cui Professor, Dept. Electrical & Computer Engineering University of Waterloo
	Guo-Xing Miao Associate Professor, Dept. Electrical & Computer Engineering University of Waterloo
Internal-External Member:	Eihab Abdel-Rahman Professor, Dept. System Design Engineering, University of Waterloo

Author's Declaration

I hereby declare that I am the sole author of this thesis. This is a true copy of the thesis, including any required final revisions, as accepted by my examiners.

I understand that my thesis may be made electronically available to the public.

Abstract

The ideal method to monitor diabetes is to obtain the glucose level with a fast, accurate, and pain-free measurement that does not require blood drawing or finger pricking. Although the development of noninvasive devices for blood glucose measurement started three decades ago, no clinically proven devices were commercially released in the market. Among all the noninvasive glucose detection techniques, optical spectroscopy has rapidly advanced, including infrared (IR) and photoacoustic (PA) spectroscopy.

The combination of IR and PA spectroscopy has shown promising developments in recent years as a substitute for invasive glucose monitoring technology. The IR region has a strong relationship with glucose due to the presence of glucose absorption peaks. PA spectroscopy utilizes the vibration modes of the glucose molecules in the IR region and the weak water absorption of acoustic signals as an alternative approach to compensate for the optical losses in the IR transmission and absorbance spectroscopy. The concept of PA spectroscopy relies on generating acoustic waves, by an electromagnetic source, that are distinguishable from one material to another and can be detected by sensitive ultrasonic or piezoelectric sensors.

The first part of the thesis demonstrates the development of the IR and PA system for noninvasive glucose monitoring. The IR and PA system has been developed using a single wavelength quantum cascade laser (QCL), lasing at a glucose fingerprint of 1080 cm^{-1}. In biomedical applications, phantoms are widely used as test models to substitute targeted body objects. Biomedical skin phantoms with similar properties to human skin have been prepared at different glucose concentrations of ±25 mg/dL as test models for the setup. The system shows feasibility in detecting glucose using these skin phantoms, covering the normal and hyperglycemia blood glucose ranges. Machine learning classification models have been employed to enhance the prediction accuracy of glucose levels using unprocessed acoustic signals.

The second part of the thesis extends the development of the IR and PA system. A dual single-wavelength quantum cascade lasers (QCLs) system has been developed using PA spectroscopy for noninvasive glucose monitoring. The glucose detection sensitivity of the IR and PA spectroscopy has improved to ±12.5 mg/dL using dual QCLs lasing at 1080 & 970 cm^{-1}. The artificial skin phantoms have been prepared with other blood components at different glucose concentrations. The dual QCLs system demonstrates sustainability in detecting glucose concentrations in the presence of albumin, sodium lactate, cholesterol, and urea. An ensemble classifier model has been developed to predict the glucose level of skin samples. The model has achieved 96.7% prediction accuracy for samples with and

without blood components, with 100% of the predicted data located in zones A and B of Clarke's error grid analysis (EGA).

After demonstrating the glucose detectability of the IR and PA system for the *in vitro* measurements, the system has progressed to the *in vivo* experiments. The operating power of the QCLs has been lowered to fulfill the safety guidelines of using light sources on human skin. The blood glucose concentration can be potentially measured from the interstitial fluid (ISF) located underneath the skin in the epidermis layer. The glucose diffuses from the blood to the ISF layer, creating a significant opportunity for noninvasive monitoring systems. The *in vivo* measurements of the fiber-coupled dual QCLs and PA system have been assessed by oral glucose tolerance test (OGTT). The preliminary results from the *In vivo* measurements demonstrate that the mid-infrared (MIR) and PA system can detect glucose levels not only in the biological samples but also in real human skin. Finally, a Gaussian Process regression model has been developed to improve the prediction accuracy of the IR and PA system.

Acknowledgements

In the name of Allah, the most merciful and the most compassionate, all praises are due to Allah for his abundant favours abundantly on us. All acknowledgments from the beginning to the end are due to Allah, who eases every difficulty in the way of accomplishing this mission.

I would like to express my sincere gratitude and appreciation to my supervisor, Professor. Dayan Ban, for his precious guidance, encouragement, and continuous support throughout the entire period of my Ph.D. study. Without his knowledge, enthusiasm, availability for discussions at any time, and, most importantly, patience, I could not have made my way through this journey. Their commitment to high-quality research is an inspiration for pursuing excellence and success not only in academic endeavors but in every other aspect of life.

My appreciation and thanks are also extended to Prof. Bo Cui, Prof. Guo-Xing Miao, and Prof. Eihab Abdel-Rahman from the University of Waterloo for serving on my doctoral Advisory Committee and for their insightful comments and feedback. I am also very thankful to Prof. Mohamed Bakr from McMaster University for serving as the external thesis examiner and for his careful reading, wise comments, and insightful observations.

I would like to show my genuine acknowledgment to my entire family, especially my beloved parents, for their continuous devotion, care, generosity, and support. Also, I have countless appreciation for my wife for her infinite patience and love throughout my journey. Wordless thanks to my kids, who are the source of happiness and strength.

With deep appreciation, I would like to thank Umm Al Qura University in the Kingdom of Saudi Arabia, for granting me the scholarship to pursue my graduate studies. I also would like to thank the Ministry of Education, Saudi Arabia, and the Saudi Arabian Cultural Bureau in Canada for their support.

Finally, this thesis would not have been possible without the help, support, and guidance of so many friends who shared happiness and challenging times with me throughout various stages of this study and made my stay memorable. Among them, Dawood Alsaedi, Talal Alharbi, Omar Alrumayh, Yasser Assolami, Abdullah Alshehri, and Hesham Alharbi.

Dedication

To my parents, my grandmother, my wife, my kids, my sisters, and my brothers

Table of Contents

List of Figures xi

List of Tables xiv

List of Abbreviations xv

1 Introduction 1

1.1 Overview . . . 1
1.2 Literature Review of MIR and PA . . . 6
1.3 Motivation . . . 8
1.4 Research Objectives . . . 9
1.5 Dissertation Outline . . . 10

2 Glucose Detection Using IR and PA Spectroscopy 12

2.1 Introduction . . . 12
2.2 IR and PA Spectroscopy . . . 12
2.2.1 The Behaviour of Human Tissue in IR and PA Spectroscopy . . . 14
2.3 PA Spectroscopy Using QCLs . . . 20
2.3.1 Machine Learning Techniques for Glucose Detection . . . 24
2.4 Conclusion . . . 25

3 Glucose Detection Using a Single MIR Wavelength and PA Spectroscopy 26
3.1 Introduction . . . 26
3.2 Methodology . . . 27
3.2.1 Sample Preparation . . . 28
3.2.2 Glucose Detection Measurements . . . 30
3.2.3 Machine Learning for Glucose Detection . . . 31
3.3 Results and Discussion . . . 36
3.3.1 Optical Properties for the Artificial Skin Phantoms . . . 36
3.3.2 System Optimization . . . 36
3.3.3 Glucose Detection . . . 37
3.3.4 Glucose Detection Using Machine Learning . . . 40
3.4 Conclusions . . . 47

4 Dual QCLs for Noninvasive Glucose Detection Using PA Spectroscopy 48
4.1 Introduction . . . 48
4.2 Methodology . . . 49
4.2.1 Sample Preparation . . . 49
4.2.2 Glucose Detection Measurements . . . 52
4.2.3 Machine Learning for Glucose Detection . . . 54
4.3 Results and Discussion . . . 55
4.3.1 Machine Learning Classifier Model . . . 60
4.4 Conclusion . . . 61

5 *In vivo* Blood Glucose Detection Using IR and PA Spectroscopy 63
5.1 Introduction . . . 63
5.2 Methodology . . . 64
5.2.1 *In vivo* Glucose Detection Measurements . . . 66
5.2.2 Machine Learning for *In vivo* Glucose Detection . . . 68

5.3 Results and Discussion 70
5.3.1 Oral Glucose Tolerance Test 72
5.3.2 Machine Learning for *In vivo* Glucose Detection 75
5.4 Conclusion 78

6 Contributions and Future Works **79**
6.1 Summary of Contributions 79
6.2 Accomplished Work 80
6.3 List of Publications 81
6.4 Future Work 82

References **84**

APPENDICES **100**

A Specification Sheets for the QCLs **101**

List of Figures

1.1 Overview of various techniques and active research areas for *in vivo* and *in vitro* glucose monitoring. . . . 3

2.1 A Schematic conduction band diagram of a quantum cascade laser [90]. . . . 13

2.2 A cross-section of human skin [99]. . . . 15

2.3 Glucose solution absorption spectrum obtained by Fourier-transform infrared (FT-IR) [100]. . . . 16

2.4 MIR absorption spectra for glucose, albumin, sodium lactate, cholesterol, and urea [71]. . . . 17

2.5 The PA spectra of a diabetic volunteer with different glucose concentrations at selective wavenumbers using a MIR source [82]. . . . 18

2.6 The absorption spectra of four skin tissue components and the baseline of the scattering equivalent absorption [112]. . . . 19

2.7 The PA spectroscopy for biological samples where $l > \mu_a > \mu_s$. . . . 21

3.1 Schematic of the setup used for glucose detection using MIR and PA spectroscopy. . . . 28

3.2 (**a**) PA cell sketch. (**b**) PA off-resonance. (**c**) PA on-resonance. (**d**) Fabricated copper acoustic cell. (**e**) Simulated resonance frequencies of the PA cell. . . . 29

3.3 **(a)** Gelatin mixture before the heating up process. **(b)** Gelatin mixture after the heating up process. **(c)** Gelatin mixture after adding other ingredients. 30

3.4 Overview of ensemble machine learning technique using random subspace sampling. . . . 33

3.5 Sampling method for the collected acoustic signals for machine learning training purposes. 34
3.6 (**a**) Tissue-mimicking phantoms. (**b**) Absorption spectrum for the phantoms compared to the real human skin spectrum. 37
3.7 (**a**)Acoustic spectrum at different pressure levels. (**b**) Background noise with and without acoustic absorption foam. 38
3.8 Acoustic spectrum for each glucose skin sample from 75 to 300 mg/dL. . . 39
3.9 (**a**) Non-rectified acoustic spectrum of the second peak. (**b**) Rectified acoustic spectrum. (**c**) Normalized acoustic spectrum with carbon. 40
3.10 Relationships between the acoustic signals to the corresponding glucose samples for the three-day measurements. 41
3.11 Confusion matrix of the ensemble model for glucose detection. 42
3.12 (**a**) Clarke's EGA of the prediction model of glucose detection before applying the majority voting algorithm. (**b**) Clarke's EGA of the prediction model after applying the majority voting algorithm. 43
3.13 Confusion matrix of the ensemble model trained with preprocessed data. . . 43
3.14 (**a**) Clarke's EGA of the prediction model with preprocessed data before applying the majority voting algorithm. (**b**) Clarke's EGA of the prediction model with preprocessed data after applying the majority voting algorithm. 44
3.15 Confusion matrices of the support vector machine (SVM), narrow neural networks (NNN), and medium neural networks (MNNs) models for glucose detection. 46
3.16 Clarke's EGA of the SVM, NNN, and MNNs prediction model of glucose detection. 46

4.1 Schematic of the setup used for glucose detection using MIR and PA spectroscopy. 50
4.2 The fiber optic coupling for the QCL light transmitting. 50
4.3 The prepared samples of the main set. 51
4.4 Design of the optical lens. 53
4.5 Background noise in the free space and fiber-coupled light transmission. . . . 56

4.6 Measurements of the first set of glucose phantoms from 100 to 275 mg/dL. . 57
4.7 Acoustic signals to corresponding glucose. 58
4.8 Measurements of the second set of glucose phantoms with blood components from 100 to 275 mg/dL. 59
4.9 Performance of the developed ensemble classification model. 61

5.1 (a) The laser drivers and function generators for the 9.25 & 10.3 μm QCLs (b) The C-Mount for the 9.25 & 10.3 μm QCLs (c) The stage of the photoacoustic system for *in vivo* measurements. 65
5.2 System preparation for the *in vivo* measurement and the targeted fingerspot. 66
5.3 *In vivo* measurements conducted with and without arm support. 70
5.4 Acoustic signals for the carbon, finger, and skin sample. 71
5.5 Acoustic signals for the three-days *in vivo* measurements. 71
5.6 Normalized acoustic signals to corresponding invasive blood glucose levels. 73
5.7 Acoustic signals of the OGTT *in vivo* measurements 75
5.8 Normalized acoustic signals to corresponding invasive blood glucose levels for the OGTT measurements. 76
5.9 Predicted blood glucose levels using Gaussian regression model to the reference levels for the OGTT measurements. 77
5.10 Clarke's EGA of the Gaussian regression model for the OGTT measurements.. 77

List of Tables

1.1 Typical blood glucose levels in adult humans. 2
1.2 Summary of some of the current noninvasive technologies for glucose detection. 5
1.3 Recent progress in PA and MIR combined spectroscopy for glucose detection. 7

2.1 MIR Vibrational absorption frequencies for some blood components [81]. . . 15
2.2 Absorption peaks of glucose in the near-infrared (NIR) regime [18]. 20
2.3 Recent progress in the MIR spectroscopy for Glucose detection 23

3.1 Summary of the measurement procedures for glucose detection for the single wavelength setup. 32
3.2 Dataset arrangement of the glucose acoustic spectrum for machine learning training purposes. 35
3.3 Standard deviation of the three-day measurements using different skin samples. 40

4.1 Summary of the measurement procedures for the dual QCLs system. 53
4.2 Dataset arrangement of the glucose acoustic spectrum for machine learning training purposes. 55
4.3 Summary of the results for the dual QCLs measurements. 60

5.1 Dataset arrangement of the OGTT measurement for ML training purpose. . 69
5.2 Invasive blood glucose levels using the glucometer for the OGTT measurement. 74

List of Abbreviations

R^2 correlation coefficient 7

ANNs artificial neural networks 24

DT decision trees 25, 54

EC external cavity 6, 7, 14

EGA error grid analysis v, xii, xiii, 7–9, 27, 41–49, 60–62, 75–78

FDA Food and Drug Administration 7–10, 24, 31, 38, 41, 42, 45, 47, 51, 56, 60–62, 75, 76, 80, 81

FT-IR Fourier-transform infrared xi, 16, 24, 30

IDF International Diabetes Federation 1, 8

IR infrared iv, v, viii, ix, 4, 6, 9, 10, 12, 25, 28, 29, 36, 52, 63, 64, 79, 80, 82

ISF interstitial fluid v, 1–4, 6, 15, 25, 63

ISO International Organization for Standardization 8, 9, 66

KNN K-nearest neighbor 25

MIR mid-infrared v, viii, ix, xi, xii, xiv, 4–10, 12, 14, 15, 17–19, 21, 22, 24–28, 31, 39, 47, 48, 50, 51, 54, 63, 64, 66–68, 72, 74–76, 78–83

MLR multiple linear regression 24, 25

MNNs medium neural networks xii, 24, 34, 45–47

NIR near-infrared xiv, 4–6, 18–20, 24, 25, 82

NNN narrow neural networks xii, 24, 34, 45–47

NNs neural networks 24

OGTT oral glucose tolerance test v, xiii, 64, 67, 68, 72, 73, 75–78

PA photoacoustic iv, v, viii, ix, xi, xii, xiv, 4–10, 12, 14, 16, 18, 20–22, 24–29, 31, 36, 38, 39, 47–50, 52, 54, 61, 63, 64, 66–68, 72, 74–76, 78–83

PLS partial least square 24

QCL quantum cascade laser iv, xii, 4, 6–10, 13, 14, 17, 26, 27, 37, 39, 47, 49, 50, 52, 53, 55–59, 61, 64, 66, 67, 72, 73, 75, 80

QCLs quantum cascade lasers iv, v, viii–x, xiii, xiv, 6, 7, 10, 12–14, 20, 25, 31, 47–49, 51, 52, 54–61, 64, 65, 79–81, 101

RMSE root-mean-square error 10, 75, 78

SNR signal-to-noise ratio 2, 5, 7, 31, 36, 47, 48, 52, 55

SVM support vector machine xii, 25, 34, 45–47

TEC thermo-electrical cooling 27

Chapter 1

Introduction

1.1 Overview

Diabetes mellitus, commonly known as diabetes, is a metabolic disorder that elevates the glucose percentage in the blood, caused by a dysfunction in the production (type-1) or effectiveness (type-2) of insulin in the body. Worldwide, 530 million people have diabetes, causing more than 6.7 million deaths, according to the International Diabetes Federation (IDF) in 2021 [1]. The number of diagnosed diabetics is rapidly and continuously growing, which draws attention to the demand for developing better functional blood glucose monitors. In addition, hypoglycemia is a condition where the blood glucose concentration is dangerously low. Typical blood glucose levels in adults, under various conditions, are shown in Table 1.1. Both diabetes mellitus and hypoglycemia conditions significantly impact human life and need to be continuously monitored. The current traditional technologies for measuring blood glucose are based on invasive methods. These methods are considered to be painful and inconvenient due to multiple daily blood draws. Also, pricking different body places with needles may lead to infection due to the low immunity of people with diabetes [2–5]. Hence, there is a demand for the development of new noninvasive technologies that will improve the life quality of those living with diabetes.

The blood glucose concentration can be potentially measured directly or indirectly from blood, serum, plasma, urine, saliva, and tear liquid, as per [6–11]. Furthermore, it can be directly determined from the ISF [12], located underneath the skin in the epidermis layer. The ISF is a thin layer of bio-fluid located between the cells, composed of water solvents and blood vessels. It contains sugars, fats, amino acids, hormones, coenzymes, white blood cells, and cell waste products [13]. The glucose diffuses from the blood to the ISF layer

Table 1.1: Typical blood glucose levels in adult humans.

Condition	**Fasting** (mg/dL)	**1 hour after eating** (mg/dL)	**2-3h after Eating** (mg/dL)
Normal	80–110	160-180	<140
Pre-diabetic	80–125	190-220	140-170
Diabetic	80–125	200-250	>180

within a 5 to 10 minutes delay period, creating a significant opportunity for the ISF to be a potential target for noninvasive blood glucose monitoring systems [14].

Researchers have explored various techniques for noninvasive glucose detection, namely, Raman spectroscopy [15–17], electromagnetic sensing [18, 19], optical tomography [20, 21], photothermal radiometry [22, 23], electrochemical sensing [24–26], and impedance spectroscopy [27–30]. Bio-impedance spectroscopy is one of the non-optical techniques used for noninvasive glucose measurement by detecting the change in conductivity of the membranes in red blood cells [31, 32]. Bio-impedance spectroscopy relies on the concept of measuring the difference in resistivity between sodium (Na+) and potassium (K+) ions, which is induced by glucose concentration changes. However, two devices, Pendra and Glucoband, which had been developed based on this method, were withdrawn from the market due to reliability and consistency issues [33]. Metabolic Heat Conformation is another non-optical technology that has been used for glucose monitoring. The glucose concentration is detected by measuring physiological parameters associated with the generation of metabolic heat, and local oxygen [34, 35]. Nevertheless, this method is found to be sensitive to sweat and ambient temperature [36]. Electromagnetic Sensing, which measures the voltage, or current, ratio in the body object to detect glucose molecules, was also found to be temperature sensitive with a low signal-to-noise ratio (SNR) [37–39].

Raman spectroscopy, an optical technique for glucose detection, is based on determining the degree of scattering of monochromatic light based on the Raman effect [40, 41]. The wavelength difference due to the Raman shift represents the difference between the initial and final vibration states of the glucose molecule. Although Raman spectroscopy is less sensitive to temperature changes, the strong interference of other blood components, such as hemoglobin, hinders identifying the glucose signal [15]. Moreover, Raman spectroscopy is susceptible to noise interference and requires a long collection time. Another method to noninvasively measure glucose is optical polarimetry, taking advantage of glucose as chiral molecules [42]. Despite the success of optical polarimetry in detecting other chiral molecules on the aqueous humor in the eye's anterior chamber, it is found unfeasible to

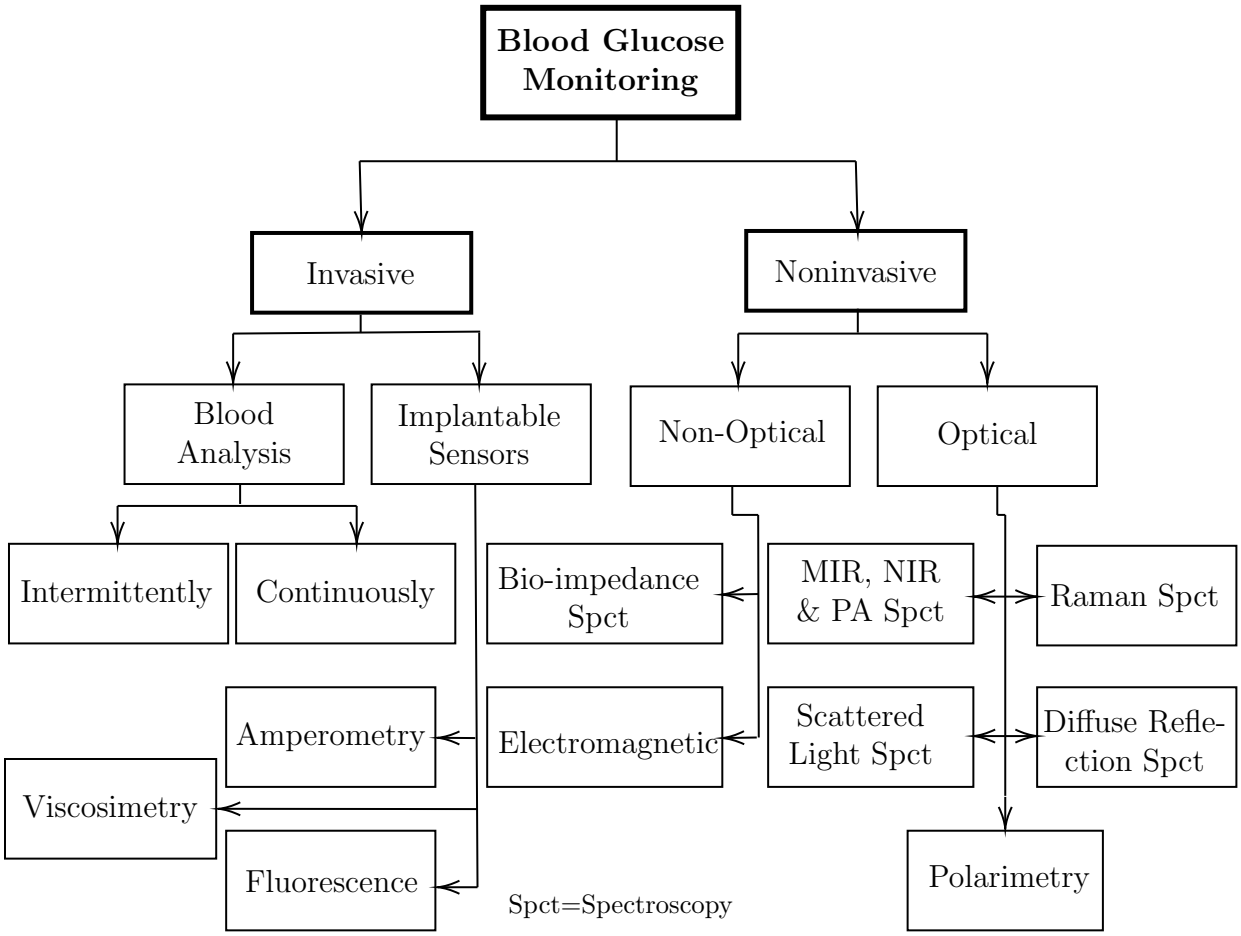


Figure 1.1: Overview of various techniques and active research areas for *in vivo* and *in vitro* glucose monitoring.

detect glucose in the human skin [43]. This is because of other active molecules' presence and the weak correlation to blood glucose.

Nevertheless, none of these approaches have yet met the physiological necessity because of their operational instability and low accuracy [44]. Other minimally invasive techniques have been developed, which require extracting the ISF from the human body without pricking. However, they demand iterative surgical implantation for the sensors and raise a skin irritation dilemma [45]. Figure 1.1 shows some of the current techniques and active research areas for invasive and noninvasive *in vivo* glucose detection.

The ideal method to monitor diabetes is to obtain the glucose concentration with a fast, accurate, and pain-free measurement that does not require blood drawing or surgical operation. Amongst all other noninvasive techniques, optical spectroscopy has advanced rapidly [44, 46, 47]. The IR region, including MIR and NIR, has a strong relationship with glucose due to the presence of glucose overtones. Furthermore, light sources and detectors of both regions are commercially available [48]. The MIR region has strong and distinct glucose fingerprints compared to the NIR [49]. The development of QCL as a MIR regime source in the late 90s has expanded the possibility of implementing this region in glucose detection applications. The QCL demonstrates high efficiency, reliability, compactness, and high power density at the frequency of interest [50].

MIR spectroscopy is a well-established technique in gas-phase detection applications based on absorption mechanisms. MIR spectroscopy can be employed in glucose detection for both *in vivo* and *in vitro* measurements. For *in vivo* measurements, the MIR light is highly scattered by the human skin, making the collection of back-scattered light the most feasible method for blood glucose detection applications compared to transmission and absorption spectroscopy. However, the MIR scattered light might not be directly related to the glucose concentration in the human blood. For *in vitro* measurements, transmission and absorption spectroscopy can be used by placing the solutions or samples inside a transparent MIR micro-cuvette. Nonetheless, MIR transmission and absorption spectroscopy may not be practical for detecting glucose in the blood due to the thickness of the skin [51]. Therefore, there is a demand to integrate IR spectroscopy with other spectroscopy for blood glucose detection.

As one of the most promising imaging and detecting technologies, PA spectroscopy has been well-developed in recent years [52–54]. The PA spectroscopy's extraordinary sensitivity assists the development of the technique in various fields ranging from biomedical, biology, physics, and chemical [55–57]. The concept of PA spectroscopy relies on the effect of generating acoustic waves by an electromagnetic source (modulated light particularly). The radiated electromagnetic waves are absorbed by an object, generating acoustic waves through thermal expansion or pressure. These acoustic waves are distinguishable from one material to another and can be detected by sensitive ultrasonic or piezoelectric sensors.

For glucose detection in human skin, PA spectroscopy utilizes the weak water absorption of acoustic waves compared to MIR waves [58,59]. The generated acoustic signals can travel back with minimum water scattering from the ISF layer in the epidermis. The absorption of the modulated light increases when the glucose level in the blood rises because of the vibration mode of the C —— O —— H bonds of glucose [60,61], generating stronger acoustic signals. The intensity of the light source plays a critical role in generating acoustic waves. Thus, replacing the regular light source with an intensive light source such as a QCL

Table 1.2: Summary of some of the current noninvasive technologies for glucose detection.

Technology	Advantages	Disadvantages
Bio-impedance spectroscopy	- Relatively inexpensive - Simple measurements on human skin	- Long calibration process - Motion and temperature sensitivity - Sensitive to sweat
Metabolic heat conformation	- Physiological parameters are relatively easy to measure	- Sweat and temperature sensitivity - Susceptible to environmental conditions interference
Electromagnetic sensing	- Non-ionized radiation - Cost-effective	- Highly sensitive to temperature
Raman spectroscopy	- Less temperature changes sensitivity - Minimal water sensitivity	- Other blood components interference - Unstable laser intensity - Long collection time and low SNR
Optical polarimetry	- High resolution - Can be miniaturized	- Weak correlation to blood glucose - Motion and temperature sensitivity
NIR spectroscopy	- Strong glucose fingerprints adsorption - Low cost and size-wise - Weak water absorption - Deep penetration to human skin	- Interfering with other blood components - Unstable light intensity at low power - Generate weak acoustic signals
MIR spectroscopy	- Strong glucose fingerprints adsorption - Generating strong acoustic signals - More specific glucose absorption bands - Stable light intensity	- Low penetration depth - Strong water adsorption - Relatively expensive
PA spectroscopy	- Simple method - PAsignals are less scattered by human skin - Can be combined with other spectroscopy	- Susceptible to temperature changes - Relatively low SNR

improves the intensity and quality of acoustic signals. Table 1.2 summarizes the advantages and disadvantages of some of the current noninvasive technologies.

1.2 Literature Review of MIR and PA

IR spectroscopy, including the MIR and NIR regions, is being developed as a promising alternative technique to invasive glucometers [62–70]. Both NIR and MIR regimes demonstrate broad and strong glucose fingerprint absorption. The MIR region has specific glucose fingerprints with a narrower interference with other blood components compared to the NIR region [71–74]. Furthermore, light sources in the MIR region, such as QCLs, have higher power density and more efficient temperature stability [54].

PA spectroscopy utilizes the vibration modes of the glucose molecules in the MIR region as an alternative approach to compensate for the optical losses in the transmission and absorbance spectroscopy. QCLs in the MIR region have the advantage of generating strong, stable, and detectable PA signals. The absorbance of QCLs light in the human skin's ISF layer, where the glucose is diffused, creates acoustic signals that can be used to distinguish the blood glucose level. [75]. These acoustic signals have the capacity to travel back from the ISF layer with minimum water distraction. The generated acoustic signals are eventually collected by a sensitive microphone to show a direct relationship to the blood glucose level.

The combination of MIR and PA spectroscopy has shown promising developments in recent years as a substitute for invasive glucose monitoring technology [75–79]. It was first investigated in 2005 by Lilienfeld-Toal *et al.* [76]. Two separate QCLs were used to generate heat pulses in the forearm of a human body. The first laser was used at a glucose absorption peak at 1080 cm^{-1}, while the second one was used to remove any background noise at 1066 cm^{-1} due to strong water absorption. A sensitive microphone was placed inside an acoustic cell to detect the PA signals from the skin, achieving a correlation factor of 0.61. In 2011, Pleitez *et al.* [78] published a paper to move progress forward with the use of three QCLs in order to detect the glucose level in the palm at two glucose peaks (1084 and 1054 cm^{-1}) and 1100 cm^{-1} for the background. A twin Helmholtz gas-cell was used as an acoustic cell with a resonance frequency of 2 kHz. The linear correlation factor (R) was improved to 0.7 compared to their previous experiment [76].

The development of glucose detection using infrared spectroscopy was accelerated when the external cavity (EC)-QCL became commercially available. The tuning capability and high power density assisted the evolution of the progress. This broadband tunability,

Table 1.3: Recent progress in PA and MIR combined spectroscopy for glucose detection.

Date	Reference	Source	Wavenumber (cm^{-1})	Samples / spot	Glucose (mg/dL)	Correlation / sensitivity	M.L.	Main contributions
2005	Toal *et al.* [76]	QCLs	P: 1080 Bg: 1066	Forearm	0-300	R=0.61	No	The PA & MIR combination
2012	Kottmann *et al.* [77]	QCL	P:1034	Epidermal samples	0-2000	± 100 mg/dL	No	Using tunable QCLs & N2 ventilation
2012	Pleitez *et al.* [78]	EC-QCLs	P: 1054&1084 Bg: 1100	Palm	80-260	R=0.71	R.O.	Selecting three wavelengths
2013	Kottmann *et al.* [81]	EC-QCLs	P:1034	Glucose solution	0-5000	± 57 mg/dL	No	Fiber optics for light delivering
2013	Pleitez *et al.* [82]	EC-QCLs	1000-1220	Hypothenar	40-240	-	R.O.	Removing noise by multivariate models
2016	Kottmann *et al.* [75]	EC-QCLs	P: 1080 Bg: 1180	Fingertip & forearm	90-170	± 30 mg/dL	R.O.	Stability improved by increasing pulse rate
2017	Sim *et al.* [79]	EC-QCLs	950-1245	Fingertip & palm	100-250	70% in zones A	R.O.	Studying skin effect on measurement

M.L.= Machine learning, P= Peak, Bg= Background, & R.O.= Regression only.

which allowed multi-analyte detection, is particularly significant for liquid phase detection of compound chemical compounds [80]. Epidermal skin samples in contact with a glucose solution were studied in vitro with a broadly tunable EC-QCL by Kottmann *et al.* [77]. The tuning range was 1010–1095 cm^{-1} with an 0.90 cm^{-1} tuning step and an open-ended PA cell of 78 mm^3 volume. A glucose detection limit of 100 mg/dL was obtained with a SNR of 1 and correlation coefficient (R^2) = 0.998 at a glucose peak of 1034 cm^{-1} and 1080 cm^{-1}. The cell was ventilated by constant N_2 gas circulation to overcome humidity and water condensation. However, the glucose detection's sensitivity is considered to be inadequate compared to the Food and Drug Administration (FDA) requirement of a ±15 mg/dL accuracy limit for detection. A year later, a flexible, non-toxic silver halide optical fiber was proposed by Kottmann *et al.* [77] for proper light delivery to different spots on the body. A detection limit of 57 mg/dL and SNR = 1 in an aqueous glucose solution was achieved with $R^2 = 0.993$.

In 2016, a dual-wavelength aspect was employed by Kottmann *et al.* [75] at 1080 cm^{-1} for the glucose peak and 1180 cm^{-1} for the background. The acoustic signals were obtained for *in vivo* glucose detection from the forearm and fingertip of a healthy, fasting volunteer. The prediction limit was raised to ±30 mg/dL for a glucose level between 90 and 170 mg/dL at a 90% confidence level. To date, this is the highest glucose detection sensitivity achieved by the MIR and PA spectroscopy in aqueous solutions [16]. In 2018, Sim *et al.* [79] investigated the effect of skin conditions on the PA signals by obtaining the microscopic spatial information of skin during the spectroscopy measurement. An EC-QCL with a tunability range of 900 to 1250 cm^{-1} was employed to detect glucose in the palm and fingertip of five volunteers. The system was evaluated by Clarke's EGA, and 70% of the

measurements fell into Zone A with a mean absolute deviation of 18.5 mg/dL . Table 1.3 summarizes recent progress in PA and MIR combined spectroscopy for glucose detection.

Nevertheless, for clinically approved glucometers, the detection sensitivity has to be within the limit of ±15 mg/dL, according to the FDA) and Health Canada [83, 84]. This requirement has not been fulfilled yet for glucose detection using MIR and PA spectroscopy. The limit of the ±15 mg/dL has to be satisfied by the PA system detection efficiency, not by mathematical algorithms applied to the obtained results. Furthermore, Clarke's EGA is used to assess the clinical accuracy of predicting blood glucose levels compared to the reference values [85]. According to the FDA, 99% of the predicted results must be located within zones A and B in Clarke's EGA [83]. In addition to the aforementioned regulations that have yet to be fulfilled, the MIR and PA system for glucose detection has not been studied using well-controlled objects, such as controlled solid samples.

1.3 Motivation

By 2045, IDF projections show that 1 in 8 adults, approximately 783 million, will be living with diabetes [1]. The number of diagnosed diabetics is rapidly growing, drawing attention to the demand for developing better functional blood glucose monitors. Monitoring blood glucose levels is essential for people with diabetes and needs to be done 3 to 5 times a day to ensure the normal range of glucose levels. The currently available technologies for measuring blood glucose are based on invasive methods. These techniques are considered painful and inconvenient due to multiple daily blood draws. Therefore, there is a necessity for the development of new noninvasive technologies that will improve the life quality of those living with diabetes.

Although the development of noninvasive devices for blood glucose measurement started three decades ago, no clinically proven devices were commercially released in the market [39]. The progress of MIR spectroscopy progress has continued to develop since the first usage of the QCL for glucose detection. However, some challenges remain unsettled and require in-depth investigation, such as the variance of human skin, optimum body spot for employing in measurements, and the interference of other biological fluids on glucose absorption. Each challenge needs to be addressed individually to evolve an understanding of its impact on the glucose spectrum. At the same time, machine learning has not been efficiently utilized to advance glucose detection progress in MIR spectroscopy and overcome the current challenges.

All clinically approved glucose monitors must fulfill the restrictions and guidelines of the FDA and the International Organization for Standardization (ISO) [83, 86]. The first

ISO set of standards for self-monitoring of blood glucose devices was published in 2003 (ISO: 15197:2003), and the second set in 2013 (ISO: 15197:2013). The latter standard stated that 95% of the blood glucose measurement readings should fall within ±15 mg/dL of the laboratory results for concentrations lower than 100 mg/dL, and 20% for higher than 100 mg/dL concentrations. Furthermore, 99% of these results have to be located within zones A and B in the Clarke EGA. In Canada, a precision of 95% is required within ±15 mg/dL for reference glucose concentrations above 100 mg/dL by Health Canada [87]. Despite the extraordinary efforts in developing noninvasive glucose monitors, none have met all of these requirements for *in vivo* measurements.

Another research gap that has yet to be studied is understanding glucose detection using MIR and PA spectroscopy with well-controlled objects. According to the review of MIR and PA, human body objects such as fingertips, forearms, and palms were used for noninvasive glucose detection. Human skin consists of complex components that interfere with each other. The impacts of glucose changes on the collected acoustic signals can not be directly examined for human body objects due to the presence of other blood components. Other parameters, such as skin conditions and blood diseases, may influence the acoustic signals. Glucose solutions with specified glucose concentration were used for *In vitro* measurement to study MIR and PA systems. However, the heat generated by the MIR light sources causes evaporation in the glucose solution, which disturbs the collected acoustic signals. Thus, developing well-controlled objects, such as biological samples, is necessary to study glucose detection using MIR and PA spectroscopy.

1.4 Research Objectives

The main objective of this study is to develop an efficient noninvasive blood glucose monitoring system, utilizing the development of IR and PA spectroscopy. The proposed system is MIR and PA spectroscopy for accurate, convenient, and safe measurements. This blood-free technique avoids finger pricking and provides boundless accessibility for people with diabetes. In order to work toward the development of the MIR and PA system, the main objectives to be achieved are as follows,

- Development of a noninvasive system for blood glucose monitoring using the MIR and PA spectroscopy by a single/dual QCL.
- Improvement in the detection sensitivity limit of glucose to reach ±15 mg/dL by the novel developed system to fulfill FDA and Health Canada requirements.

- Investigation into the glucose detection in the presence of other blood components by the MIR and PA spectroscopy.
- Involvement of machine learning in glucose detection by the MIR and PA system.
- Investigation into the in vivo measurements by the MIR and PA spectroscopy.

1.5 Dissertation Outline

The remaining of this dissertation is organized as follows:

Chapter 2 illustrates the background related to the subject of IR and Photoacoustic Spectroscopy. The mechanism of implementing MIR light sources at the glucose fingerprints to generate acoustic signals in the human skin has been investigated. The behaviour of human tissue in the IR and PA is revisited to determine functional light sources that can generate acoustic signals at the glucose fingerprints. Particularly, the employment of QCLs in PA spectroscopy has been examined, which is the central core of the thesis. Finally, a brief review of the employment of machine learning for glucose detection is introduced.

Chapter 3 introduces the development of MIR and PA spectroscopy using a single wavelength QCL for noninvasive glucose detection. The single wavelength MIR QCL is operated at 1080 cm^{-1} glucose fingerprint. Biomedical skin phantoms with optical properties similar to human skin have been prepared at different glucose concentrations as test models for the developed system. The prepared phantoms are used to determine the feasibility of the developed system in glucose deection. Machine learning classification algorithms are involved in the development of high-accuracy glucose prediction models.

Chapter 4 evolves the single-wavelength MIR system into fiber optics dual QCLs using PA spectroscopy for noninvasive glucose detection. The dual QCLs system assists in the enhancement of the detection sensitivity to fulfill the FDA and Health Canada requirements. Other blood components have been integrated into the biomedical skin phantoms to examine the selectivity of the dual QCLs system. An ensemble classification algorithm is employed to develop high-accuracy glucose prediction models.

Chapter 5 presents the transformation of the MIR and PA system from the in vitro measurements toward the in vivo measurements. Further improvements have been integrated into the setup to accommodate the in vivo measurements. Simultaneous measurements, including invasive and noninvasive systems, are designed to evaluate the MIR and PA spectroscopy for glucose detection. Machine learning regression algorithms are involved in developing low root-mean-square error (RMSE) glucose prediction models.

Chapter 6 summarizes the main contributions, the accomplished works of the thesis, and the future works that will further improve the noninvasive glucose detection system.

Chapter 2

Glucose Detection Using IR and PA Spectroscopy

2.1 Introduction

This chapter illustrates the background review on the subject of IR and Photoacoustic Spectroscopy. A brief introduction to the development of IR light sources is presented. This chapter explains the mechanism of employment of MIR lasers to generate acoustic in the human skin. The behaviour of human tissue in the IR and PA is reviewed to determine functional light sources that can generate acoustic signals at the glucose fingerprints. Specifically, the employment of QCLs in PA spectroscopy has been discussed, which is the central core of the thesis. Finally, a brief review of using machine learning for glucose detection is presented.

2.2 IR and PA Spectroscopy

The obtainable laser sources in the MIR region are QCLs, CO_2, inter-band cascade lasers (ICLs), lead salt lasers, different frequency generation (DFG) lasers, and optical parametric oscillation (OPO) [88]. However, QCLs have the lead because of their merged advantages of high optical power density, stability at room temperature, wide frequency tuneability, and compatibility in continuous- and pulse-wave modes of operation. The modulation capability of QCLs is up to MHz-regime. Furthermore, QCLs provide polarized and coherent light with a 10^4 increase in spectral power density than thermal light sources [89].

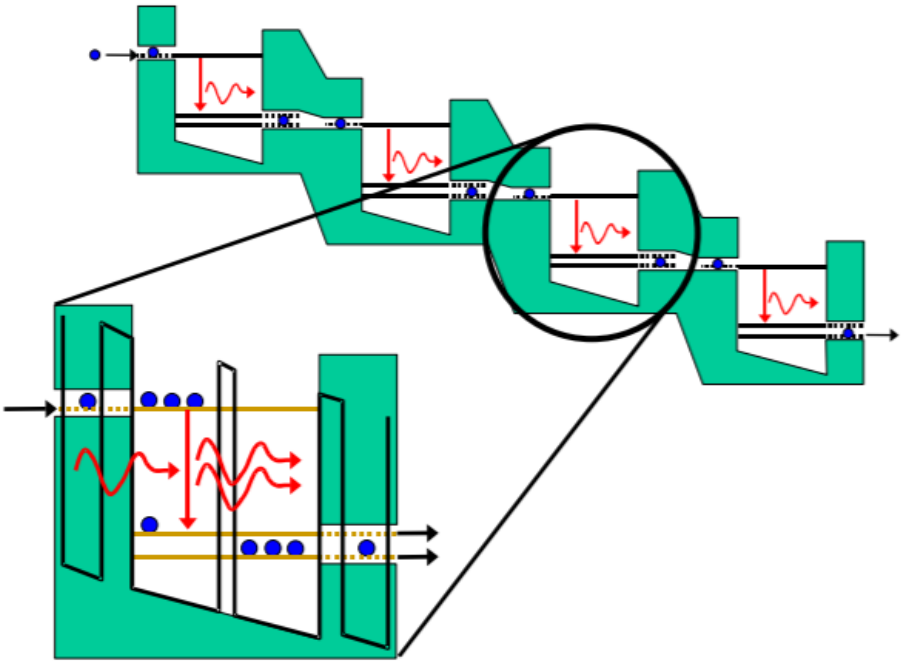


Figure 2.1: A Schematic conduction band diagram of a quantum cascade laser [90].

Fabry-Perot (FP) laser is the simplest form of QCLs where the optical waveguide acts as a gain medium and cleaved face as a parallel mirror. The QCL was first developed by Faist *et al.* in 1994 at Bell Labs [91], which was operated at cryogenic temperature. Later in 2002, a QCL operates at room temperature was realized by Beck *et al.* [92], working in continuous wave (CW) modes. Modern QCLs can now cover the entire infrared regime at operating temperatures higher than 400^{o}K [93].

Quantum cascade lasers are based on designing narrow quantum wells (QWs) where electrons are confined instead of atomic levels. These thin layers of QWs lead to a high electric potential difference across the length of the device. The electric field splits the number of discrete electronic sub-bands where electrons cascade down by emitting a photon at each intersubband transition, as shown in Figure 2.1 [90]. As a result, QCLs outperform typical diode lasers operating by a factor of 10^4 at the same wavelength [94]. The phenomena of a single electron emits multiple photons, raising the quantum efficiency of QCLs greater than one. In principle, the QCL emission's tuneability within the same material depends on the thickness variation of the QW. Also, QCLs can emit multi-wavelengths within the same structure using different materials. Typical QCLs are fabricated either in GaAs/AlGaAs

on a GaAs substrate or by GaInAs/AlInAs on a lattice-matched InP substrate [94].

In order to obtain a single output operation mode in QCLs, a distributed feedback (DFB) system is used. A distributed Bragg reflector (DBR) is integrated on top of the waveguide to force a single-mode operation [95]. The DFB laser can be tuned over a narrow range (1 to 5 cm^{-1}) by tuning the operation temperature and input current. For further tuning range increasing, an EC-QCL is used [96]. EC-QCLs can provide a wide free tuning span of more than 800 cm^{-1}. The QCL is a dynamic candidate for MIR spectroscopy applications because of its long-standing lifetime, small dimension, low energy consumption, and reliable power stability configuration. An extensive review of QCL systems for MIR spectroscopy can be found in [89] and [97], while technical materials for QCLs fabrication are in [90].

2.2.1 The Behaviour of Human Tissue in IR and PA Spectroscopy

MIR Spectroscopy

The human tissues have a simple analytical structure, which mainly consists of three layers. These layers are the epidermis, dermis, and hypodermis, as shown in Figure 2.2. The stratum corneum, the top layer of the epidermis, is about 10-20 μm thick and contains around 20% of water. The next layer is the dermis (1-2 mm), which is filled with approximately 70% of water. This layer is highly permeable for the blood glucose to diffuse [98]. The bottom layer is the hypodermis (1-4 mm), which is filled mostly by fatty tissues.

MIR radiation in the electromagnetic spectrum is from 3 to 12 μm wavelength. This regime is significant for molecules detection due to the presence of strong absorption peaks of some molecular bonds, such as C——C, N——H, N——O, C——H, O——H, C═O, and C≡N. These bonds are referred to as molecular regions for fingerprints [101]. The glucose has a molecular formula of $C_6H_{12}O_6$, which is a kind of monosaccharide in the form of pyranose. The presence of the bending vibrations and stretching of C——H——O bond shows strong absorption peaks for glucose detection using MIR lasers as shown in Figure 2.3 [100]. Blood components, namely albumin, sodium lactate, cholesterol, and urea interfere with the glucose fingerprint in the MIR region as shown in Fig. 2.4 [71].

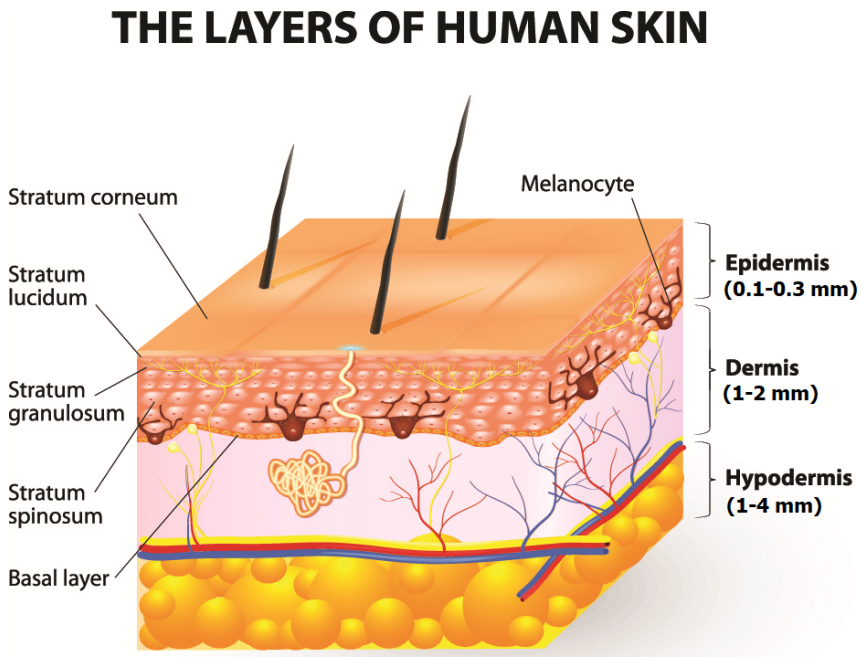


Figure 2.2: A cross-section of human skin [99].

.

Table 2.1: MIR Vibrational absorption frequencies for some blood components [81].

Wavenumber (cm^{-1})	Component	Intensity
1080	β D-glucose absorption	Medium
1080	$v(PO2_2^-)$ symmetric	Medium
1077	v(CC) skeletal trans conformation	Medium
1054	α D-glucose absorption	Very weak
1052	Albumin absorption	Weak
1047	v(C–OP)	Weak
1035	v(CC) skeletal cis conformation	Medium
1034	$\alpha\&\beta$ D-glucose absorption	Medium
1020	Albumin absorption	Very weak

v= stretch

The water absorption is much weaker for the acoustic waves compared to MIR waves. Therefore, acoustic signals can travel deeper with minimum water scattering and easily reach the ISF in the epidermis layer. The absorption of the acoustic waves increases by

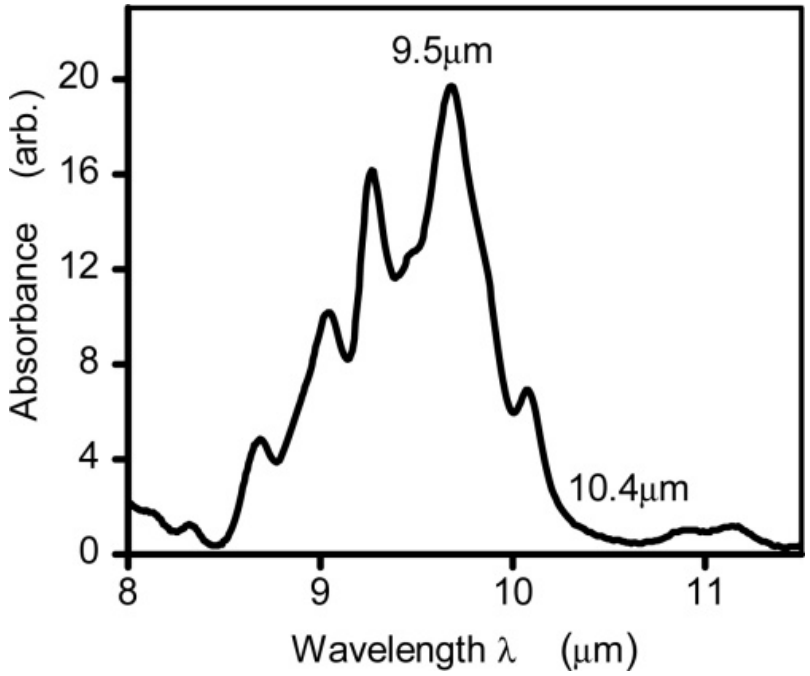


Figure 2.3: Glucose solution absorption spectrum obtained by FT-IR [100].

raising the glucose concentration because of the vibration mode of the C——O——H bonds of sugar [60]. By varying the glucose concentration of a type-1 diabetic volunteer, a gradual increase in the acoustic signal's intensity was obtained from a left hypothenar of the hand as shown in Figure 2.5 [82]. Other blood components were tested by PA spectroscopy to characterize their vibration frequencies to determine the most suitable frequency for glucose detection as listed in table 2.1 [81]. The PA signal intensity varies at different spots of the body object due to the dissimilarities in human skin.

The optical properties of skin for the mid-infrared regime have been investigated on a limited scale [102–104]. The light transmission through the human skin depends on the photon wavelength, skin absorption coefficient, and the tissue's water content. The optical properties of human skin not only significantly fluctuate amongst people but also for the same person at different spots of the skin. The back-scattering light from a porcine skin has been examined *in vitro* by Liakat *et al.* [105] by a mid-infrared light source. The porcine skin's penetration depth was approximately estimated to be around 200 μm to the dermis layer. The back-scattered light intensity was measured and found large and detectable by commercial infrared detectors. The reflected light of human skin was investigated *in vivo* by Pleitez *et al.* [82], and observed that the stratum corneum and living dermis (100 μm

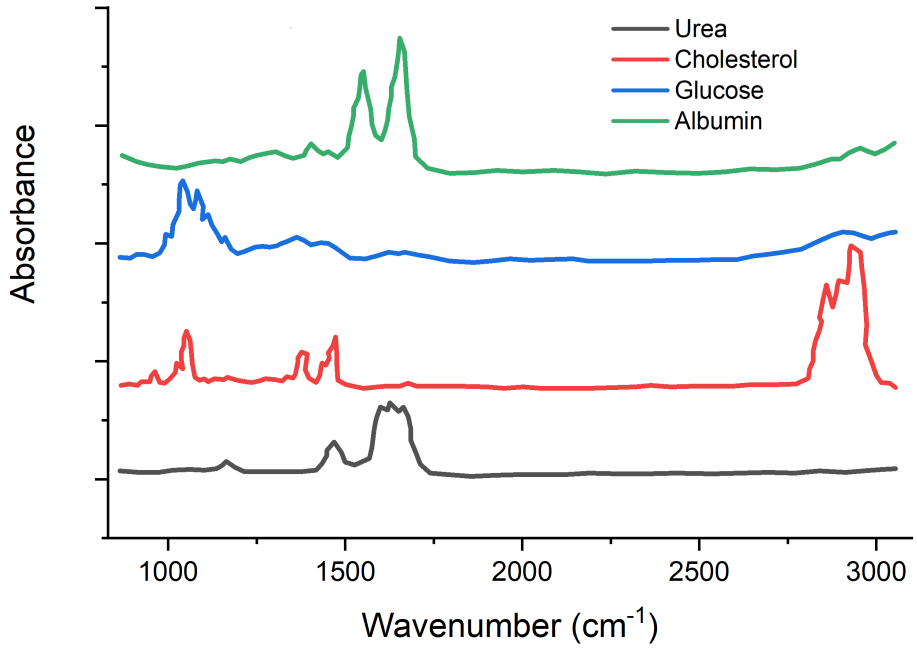


Figure 2.4: MIR absorption spectra for glucose, albumin, sodium lactate, cholesterol, and urea [71].

down of the skin) are the dominant parts of the back-scattered light. However, the diffusely scattered light of the dermis layer (2 mm down of the skin) is weak and hard to detect in normal conditions. The reflected signal collection from the dermis layer can be enhanced by increasing the QCL peak power to 100 mW or an average power of 5 mW [102]. The light absorption in the dermis layer is dominant, compared to scattering, due to collagen fibrils presence, which has strong reflective coefficients [106].

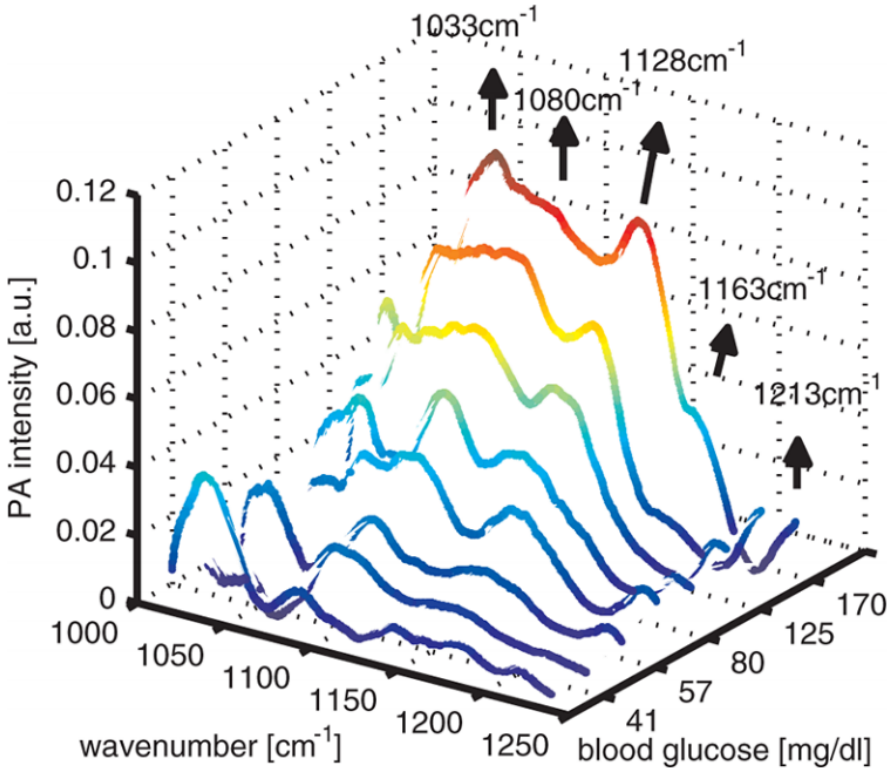


Figure 2.5: The PA spectra of a diabetic volunteer with different glucose concentrations at selective wavenumbers using a MIR source [82].

.

NIR Spectroscopy

The molecules absorption over the NIR region (4000-12800 cm^{-1}) is several orders of magnitude weaker than the MIR region. However, short wavelengths within the NIR spectroscopy (780-2500 nm) can reach deeper into the human skin because of the weak water absorption in this region [107, 108]. Moreover, NIR spectroscopy has the advantage of simpler setups and relatively lower-cost materials [109]. In order to measure the glucose level in the diabetic, transmission spectrum, absorption, and reflection techniques can be used in NIR spectroscopy [47, 110].

The absorption spectrum over the NIR span is broad and overlapped due to the multi-vibrational of fundamental bands of water and other blood components in human tissues. NIR spectroscopy's key challenge is to extract the specific glucose finger-print from the other variable background scattering and overlapping. As a result, some advanced multi-

variant analysis techniques are required to separate the glucose signature in the skin [111].

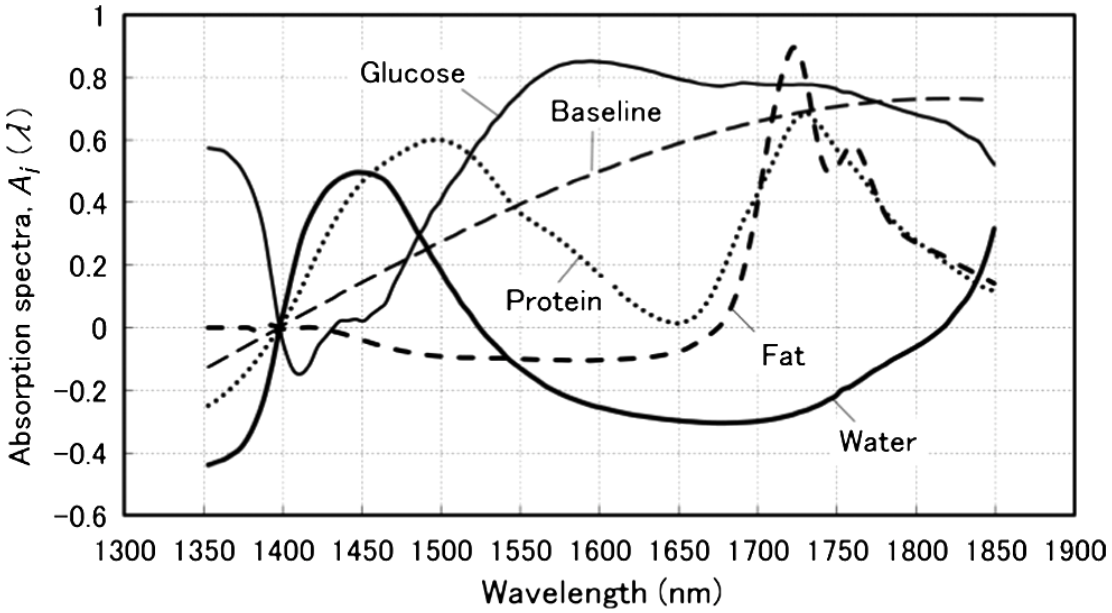


Figure 2.6: The absorption spectra of four skin tissue components and the baseline of the scattering equivalent absorption [112].

The absorption band over the NIR region in the human skin has resulted from overtones combination of O——H, C——H, and N——H vibrations. The absorption spectrum follows the Beer-Lambert law as in the MIR region [113]. The photons in this region have less interaction with some tissue compounds like lipid, water, and hemoglobin. Therefore, the NIR region's penetration length can reach a few millimeters into the skin compared to a few micrometers in the MIR [114]. The radiation of the NIR light can pass through the stratum corneum and epidermis of the skin and reach higher blood concentration regions [115]. However, the NIR region's glucose absorption peaks are weak and overlapped with other complex solutions like protein, albumin, and chromophores within the tissue, as shown in Figure 2.6. Table 2.2 shows the absorption peaks of the glucose functional groups in the NIR region [18]. The NIR spectroscopy has been discussed above in order to examine the opportunity of integrating an NIR source into the system as a future approach.

Table 2.2: Absorption peaks of glucose in the NIR regime [18].

Wavelength (nm)	Stretching Group
910	$4v$CH
930	$3v\mathrm{CH_2}$
939	$3v$OH
1018	vCH combination
1042	vCH combination
1126	$3v$CH
1408	$2v$OH
1536	vOH + vCH
1638	First overtone
1688	$2v$CH
2261	vCH + vCCH
2273	O-H/C-O combination

v= stretch

2.3 PA Spectroscopy Using QCLs

Rosencwaig and Gersho have developed a model [52] to study solid samples by PA spectroscopy. In this model, six special cases of the generated PA signals of the sample can be distinguished based on the ratio of sample length (l), thermal diffusion of the sample (μ_s), and optical absorption depth (μ_a). The PA signal amplitude has an identical dependency on the light intensity and gas coupling properties in all cases. This dependency is defined by a factor (F) as follows [81]:

$$F = \frac{\gamma \cdot P_0 \cdot t(\lambda) \cdot I_0 \cdot \mu_{\mathrm{g}}}{4\sqrt{2} \cdot l_{\mathrm{g}} \cdot T_0} \tag{2.1}$$

where P_0 is the ambient pressure, $t(\lambda)$ is the wavelength-dependent fiber transmission, I_0 is the laser intensity, μ_{g} is the coupling gas thermal diffusion length, l_{g} is the length of the coupling gas, and T_0 is the ambient temperature. The gamma factor (γ) is the specific heat ratio at constant pressure and volume ($\gamma = C_p/C_v$). The thermal diffusing length of the coupling gas, or sample, is defined as follows:

$$\mu_{\mathrm{g},s} = \left(\frac{D_{\mathrm{g},s}}{\pi \cdot f}\right)^{\frac{1}{2}} \tag{2.2}$$

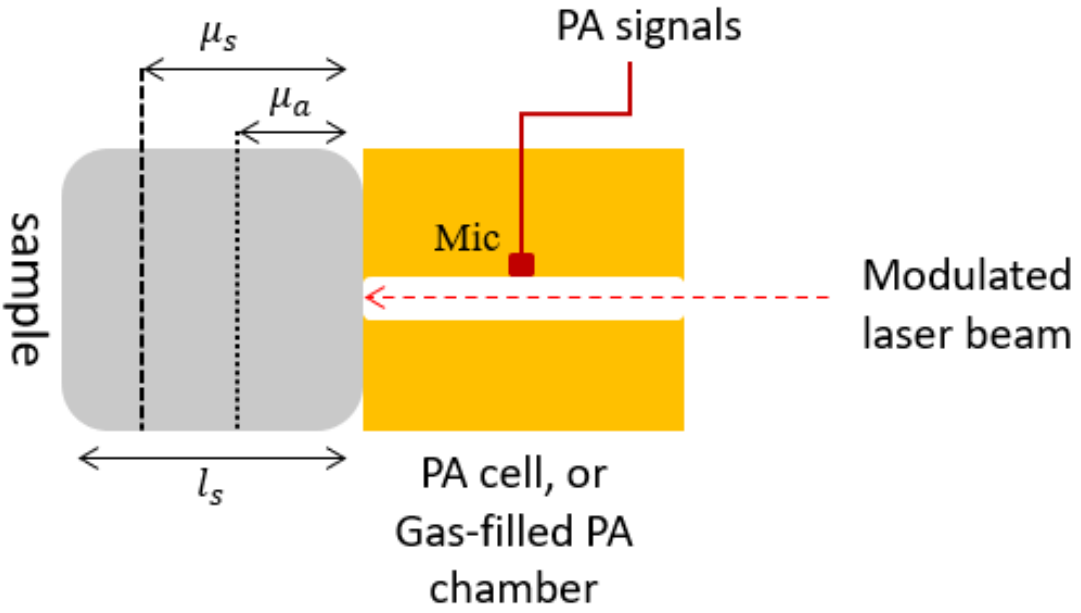


Figure 2.7: The PA spectroscopy for biological samples where $l > \mu_a > \mu_s$.

where D_g, s is the gas, or sample, thermal diffusivity and f is the modulation frequency of the laser. The thermal diffusivity depends on the thermal conductivity (k), density (ρ), and C_p, as follows,

$$D_{\mathrm{g},s} = \frac{k_{\mathrm{g},s}}{\rho_{\mathrm{g},s} \cdot C_{p_{\mathrm{g},s}}}. \tag{2.3}$$

For biological samples, i.e., human skin, which contain high water content, the penetration depth of the NIR, or MIR, light is small compared to the sample's length. In the MIR light, the penetration depth is even smaller due to the stronger water absorption in this region. However, this permeation is adequate for generating informative acoustic signals from the glucose in the human skin, where the glucose molecules are diffused. Therefore, the combination of PA spectroscopy with MIR spectroscopy shows potential for a noninvasive glucose detection system.

The amplitude of the periodical acoustic signal (A_{PA}) is directly proportional to the laser intensity (I_o) and absorption coefficient of the sample (α) as follows:

$$A_{PA} \propto \frac{I_0 \cdot \alpha}{V_0 \cdot f^{\frac{3}{2}}}, \tag{2.4}$$

where V_0 is the volume of the cell, and f is the modulation frequency. Accordingly, by developing an appropriate design of the PA cell and selection of the modulation frequency, the acoustic signals can be improved, leading to enhanced glucose detection sensitivity. Figure 2.7 shows a simple structure of the PA spectroscopy using a modulated laser beam, where the condition of $l > \mu_a > \mu_s$ is fulfilled. A sensitive microphone in a PA cell or in a gas-filled PA chamber of l_g length detects the generated PA signals. The developed system relies on detecting the deviations of the acoustic signals due to the variations of absorption coefficient in the glucose samples. Increasing the glucose concentration in the phantoms strengthens the absorption coefficient, thus stimulating the absorbance in the sample to generate higher acoustic signals. Reference [116] provides intensive background and theoretical details on laser and PA spectroscopy. Other MIR techniques for glucose detection that are not related to PA spectroscopy, such as transmission, absorption, and scattering spectroscopy, have been summarized in Table 2.3 for the benefit of the readers.

Table 2.3: Recent progress in the MIR spectroscopy for Glucose detection

Date	Reference	Source	Wavenumber (cm^{-1})	Samples	G. conc. (mg/dL)	*In vivo*, patients	M.L.	Main contributions [44]
2001	[50]	DFB	P:1067	Aqueous glucose	0	No	R.O.	Separating glucose and fructose
2005	[117]	DFB	P:1036 Bg:1194	Human serum	50-500	No	R.O.	Improving the correlation by two QCLs
2006	[118]	FB-QCL	P:1080&1393	Glucose & sodium acetate solution	1k-5k	No	R.O.	Quasi-simultaneous detection
2006	[119]	QCL	P:1035 Bg:950&1090	Aqueous glucose	40-1000	No	R.O.	Cryogenic free, fiber optics delivering
2010	[120]	EC-QCL	1030-1230	Glucose and sodium acetate solution	0-800	No	R.O.	Multivariant technique
2011	[121]	FB-QCL	1010-1065	Aqueous glucose	4-600	No	R.O.	Fiber based MIR
2012	[122]	EC-QCL	1030-1230	Serum in five analytes	3-400	No	R.O.	Multi-analyte detection & Ni_2 cooling
2013	[123]	EC-QCL	1030-1230	Blood plasma and six analytes	85-264	No	R.O.	Semi-automated multi-analyte detection
2013	[124]	EC-QCL	1000-1200	Serum	5-400	No	R.O.	Isolating the glucose from other fluids in detection
2014	[125]	EC-QCL	1000-1250	Palm	80-160	Yes, 3	R.O.	first *in vivo* human, Hollow core fiber
2014	[126]	QCL	1031	Rat	100-500	Yes	R.O.	First *in vivo* on rats
2016	[127]	QCL	1020-1090	Aqueous glucose	200-1100	No	R.O.	Improving the SNR by laser power &intrgration time
2018	[128]	QCL	980-1200	Oral mucosa (human lips)	60-220	Yes, 6	R.O.	three wavenumbers selected by regression
2018	[129]	EC-QCL	990-1530	Aqueous glucose	35-300	No	R.O.	Relationship between the QCL tuning speed on EC-mirror
2018	[130]	EC-QCL	890-2020	Saliva	-	Yes, 1	R.O.	Introducing ATR with a diamond waveguide
2018	[131]	EC-QCL	1020-1224	Forarm & fingertip	80-150	Yes, 1	R.O.	A Sphere to enhance light collection
2018	[132]	EC-QCL	900-1200& 1500-1750	Aqueous glucose & other saccharides	0-600	No	R.O.	Five selective wavenumbers
2019	[133]	DFB	P:1152 Bg:1186	Oral mucosa (human lips)	100-150	Yes, 1	R.O.	Using ATR & hollow fibers
2019	[134]	QCL	800-1600	Finger	50-160	Yes	R.O.	Introducing pressure sensor
2020	[135]	QCL	900-1250	Fingers, ball of the hand & wrist	50-350	Yes, 100	Yes	*In vivo* Photothermal detection with M.L.

G. conc.=Glucose concentration, P=Peak, Bg= Background, R.O.= Regression only

2.3.1 Machine Learning Techniques for Glucose Detection

Despite the recent outstanding development, machine learning has not been utilized in MIR and PA spectroscopy for noninvasive glucose detection. Machine learning models can assist in improving the detection sensitivity to meet FDA requirements. Furthermore, the employment of machine learning can help to solve the complexity of detecting glucose in the presence of different blood components or in various environmental conditions. In noninvasive optical spectroscopy, machine learning models can be developed to distinguish glucose signals despite the variations in human skin properties for in vivo measurements.

Both classification and regression techniques can be employed for noninvasive glucose detection applications. The classification techniques result in discrete outputs labeled by distinct classes, while the regression models extract quantitative information. In other words, the prediction output of the classification models is a discrete glucose value compared to the regression methods that predict continuous glucose levels. Consequently, the regression methods are constrained to correlate the entire range of interest for glucose measurements. This results in associating the hyperglycemia, normal, and hypoglycemia range of blood glucose levels, which is one of the challenges in regression techniques. In contrast, the classification techniques address each discrete value independently, with no influence on other glucose levels. Therefore, reducing the differences in glucose levels between the discrete classes results in high prediction sensitivity.

Different regression models have been employed for glucose detection, such as partial least square (PLS) [75, 136], principal component (PC) [79], multiple linear regression (MLR) [128], and artificial neural networks (ANNs) [137, 138]. However, these regression models were used only to reduce the correlation coefficient error in associating predicted glucose levels with actual values for the range of interest. In contrast, classification techniques, which have been proposed recently for glucose detection, overcame the challenges in the regression methods [139] based on simulated results. The hidden Markov classification (HMM) model was trained to binary classify the simulated results as normal or abnormal blood glucose levels. A similar approach was followed later, using data obtained from the literature [140], as well as toenail samples [141]. Jernelv *et al.* later employed convolutional neural networks (CNNs) for in vitro glucose detection measurements obtained from online datasets, including NIR and FT-IR measurements [142]. However, no actual experimental measurements were conducted. Liu *et al.* employed four different regression models, namely forward propagation (FP), radial basis function (RBF), recurrent neural networks (RNNs), and backpropagation (BP) to detect glucose in aqueous solutions using PA spectroscopy. Other neural networks (NNs) models were employed for noninvasive glucose detection, such as MNNs and NNN.

In May 2021, Shokrekhodaei *et al.* employed both regression and classification models in Visible-NIR transmission spectroscopy for in vitro glucose detection in aqueous solutions [143]. Five different methods were used, namely MLR and feed-forward neural network (FNN) for regression models, while K-nearest neighbor (KNN), decision trees (DT), and SVM were used as classification models. The study concluded that classification models more efficiently detect broad glucose ranges from hypoglycemia to hyperglycemia. The classification-based models outperform regression methods because of their ability to address each range independently. However, for a narrower blood glucose range, regression models can be more appropriate to detect glucose.

2.4 Conclusion

In this chapter, the concept of IR and PA spectroscopy has been reviewed. The methodology of implementing MIR light sources at the glucose fingerprints to generate acoustic signals in the human skin has been discussed. The glucose molecules diffuse from the human blood to the ISF layer in the human skin. MIR QCLs can reach the ISF layer to generate detectable acoustic signals. When the glucose molecules increase in the blood, stronger acoustic signals are generated, indicating that the blood glucose level has risen. The MIR and PA spectroscopy show promising results for noninvasive glucose detection compared to other explored technologies. Finally, the employment of machine learning in MIR and PA spectroscopy can accelerate the development of noninvasive technology.

Chapter 3

Glucose Detection Using a Single MIR Wavelength and PA Spectroscopy

3.1 Introduction

This chapter investigates the feasibility of the MIR and PA system for noninvasive glucose detection. A single wavelength QCL is employed at a glucose fingerprint to generate acoustic signals that can quantify glucose levels. A PA cell is designed to have resonance frequencies in the range of interest to amplify the acoustic waves. In biomedical applications, phantoms are widely used as test models to substitute targeted body objects. Thus, skin phantoms that have similar properties to human skin have been prepared with different glucose concentrations as test models for the setup. The solid samples are well-controlled and can be used to examine the system's detectability and assist in comprehending the development of the system.

A PA system has been developed using a single wavelength QCL, lasing at a glucose fingerprint of 1080 cm^{-1} for noninvasive glucose monitoring. The system has been examined using artificial skin phantoms, covering the normal and hyperglycemia blood glucose ranges. The detection sensitivity of the system has been improved to ±25 mg/dL using a single wavelength for the entire range of blood glucose. Machine learning has been employed to detect glucose levels using PA spectroscopy in skin samples. Ensemble machine learning models have been developed to measure glucose concentration using classification techniques. The model has achieved a 90.4% prediction accuracy with 100% of the

predicted data located in zones A and B of Clarke's EGA.

3.2 Methodology

The MIR and PA system has been developed using a single wavelength QCL, lasing at a glucose fingerprint of 1080 cm^{-1} (9.25 $m\mu$) for noninvasive glucose monitoring. The MIR and PA experimental setup for the noninvasive glucose detection is shown in Figure 3.1. In this setup, a single wavelength QCL (QD9500CM1, Thorlabs, Newton, NJ, USA) was employed as a light source, lasing at 1080 cm^{-1} where the glucose has a strong fundamental vibration rotation. The maximum laser power in pulse operating mode was about 60 mW with a pulse width of 33 to 100 μs. The laser was operated at 25 °C and had a threshold current of 180 mA. In order to activate the dynamicity of the PA phenomena, the laser current was frequency-modulated from 10 to 30 kHz with square waves of a duty cycle of 40% by a function generator (Agilent 55321A). The datasheet of the 1080 cm^{-1} QCL is attached in Appendix A.

The output light of the laser was collimated using a MID lens and placed close to the lasing facet. The beam diameter of the laser was estimated to be less than 2 mm. This laser beam was then reflected upwards to the incident on the PA cell using a gold-coated parabolic mirror with more than 95% reflectivity. A custom-made thermo-electrical cooling (TEC) system was added to the setup to control the temperature during the measurement to provide a reliable environment. The TEC was controlled by a custom-made proportional-integral-derivative (PID) feedback loop circuit in order to achieve a real-time adjustment [144]. Furthermore, a ventilation system with N_2 flow was added to the setup to control the inside humidity of the chamber, preventing moisture from building up on the biological samples.

The PA cell was designed and simulated using COMSOL [145] to collect and amplify the acoustic signals generated in the skin sample or human skin. The PA cell sketch is shown in Figure 3.2a–c, and the fabricated cell is shown in Figure 3.2d. The PA cell was made from oxygen-free copper, and the surface was electroplated with gold to prevent oxidation, which may cause a degradation in the thermal conductivity. The length of the laser cavity of the PA cell was 5 mm with a diameter of 3 mm, and the length of the microphone channel was 13.5 mm with a 1.5 mm length diameter. The resonance frequencies of the cell were at 16.50 kHz and 21.80 kHz, as shown in Figure 3.2e. A slight shift to the resonance frequency is expected while conducting the *in vivo* and *In vitro* measurements due to the applied pressure on the cavity and other damping effects. A sensitive analog microphone (SPU0410LR5H-QB, Knowles) was attached to the absorption cell for

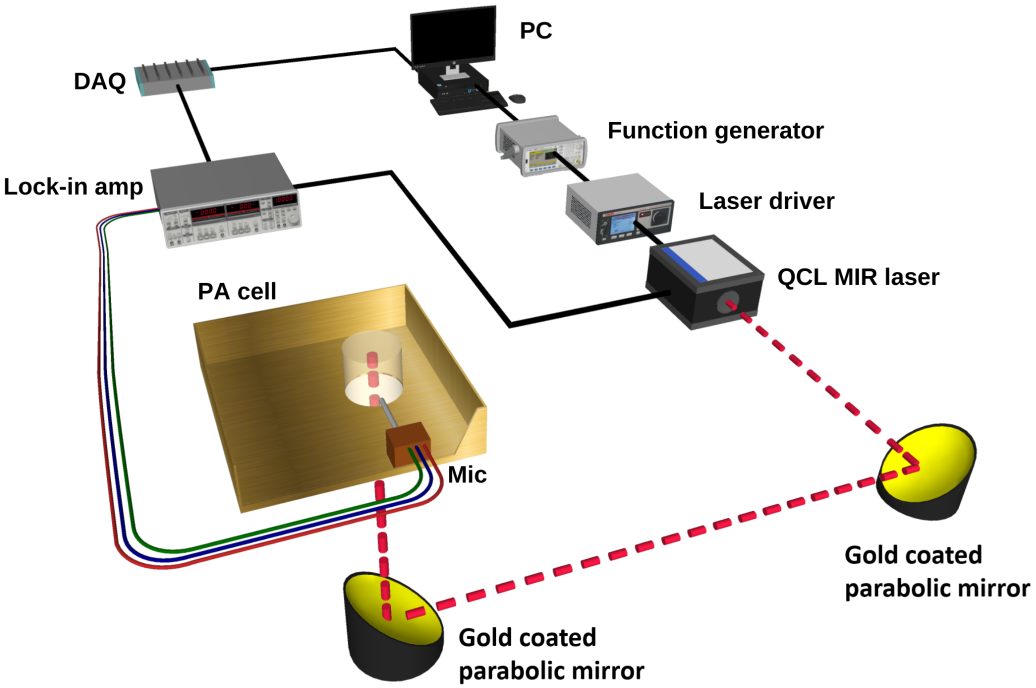


Figure 3.1: Schematic of the setup used for glucose detection using MIR and PA spectroscopy.

collecting the acoustic signal from the PA cell. The microphone has a maximum sensitivity between 15 to 30 kHz in order to synchronize with the PA cell resonance frequencies. The PA cell was designed to accommodate both human fingertips and phantom samples to be perpendicularly irradiated by the MIR laser through the PA cavity. Moreover, the PA cell was surrounded by acoustic absorption panels in order to eliminate any environmental background acoustic noises.

3.2.1 Sample Preparation

Human skin consists of complex components that interfere with each other, influencing the generated PA glucose signals. The IR and PA spectroscopy has yet to be studied using well-controlled samples to develop the detection capacity of the system. Hence, there is a demand to establish well-controlled test models that can assist in understanding the IR and PA spectroscopy. Furthermore, the impact of each blood component on glucose needed to

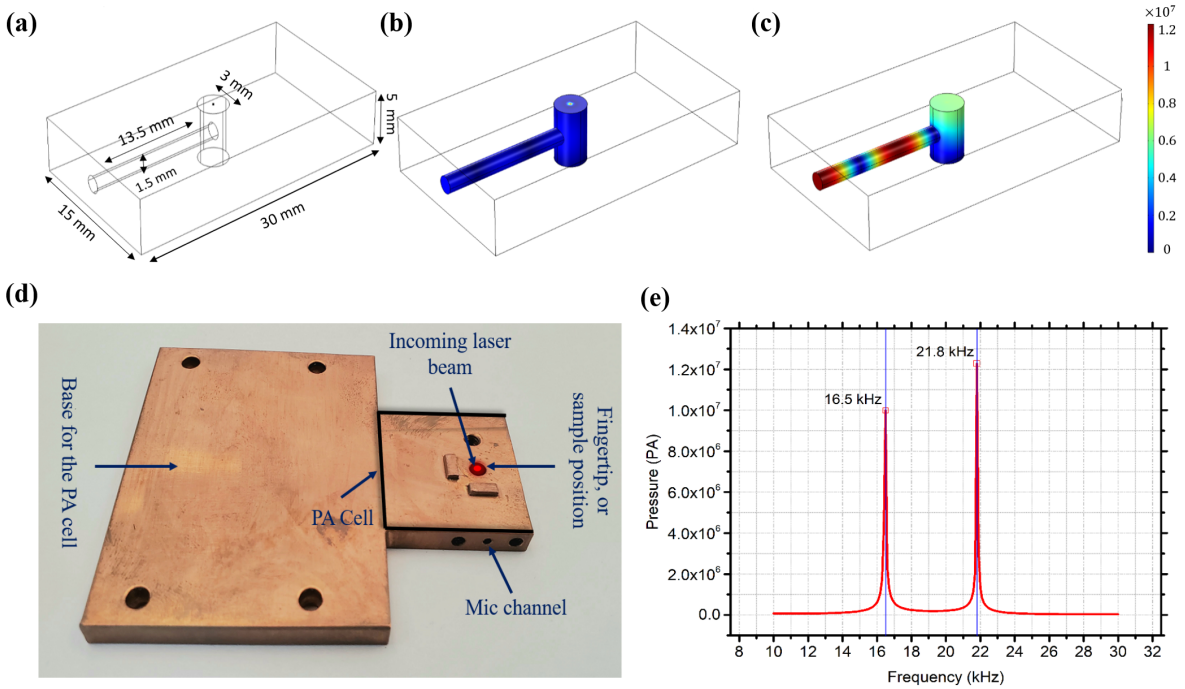


Figure 3.2: (**a**) PA cell sketch. (**b**) PA off-resonance. (**c**) PA on-resonance. (**d**) Fabricated copper acoustic cell. (**e**) Simulated resonance frequencies of the PA cell.

be thoroughly studied in the literature. In biomedical applications, phantoms are widely used as test models to substitute targeted body objects [146–148].

Here, following the work of Lazebnik [149], artificial skin phantoms were prepared at different glucose concentrations to be used as test models for the developed system. These well-controlled test models can be used to determine the detection feasibility of the system and assist in studying the IR and PA spectroscopy. The skin phantoms can also cooperate in investigating the blood components' interference with glucose in a well-controlled environment by studying the effect of each component individually. This advantage assists in studying the impact of human skin variation and blood components on glucose detection.

The oil-in-gelatin phantoms represent the dielectric properties of various human soft tissues over broadband frequency for biomedical studies purposes. A 200-bloom gelatin derived from calfskin (Sigma-Aldrich, Oakville, ON, Canada) was used as the substantial material for the artificial skin samples. A p-toluic acid (powder) and n-propanol were added to deionized (DI) water and mixed with the gelatin before heating the mixture in a double boiler. Figure 3.3 **(a)** shows the gelatine mixture before the heating process.

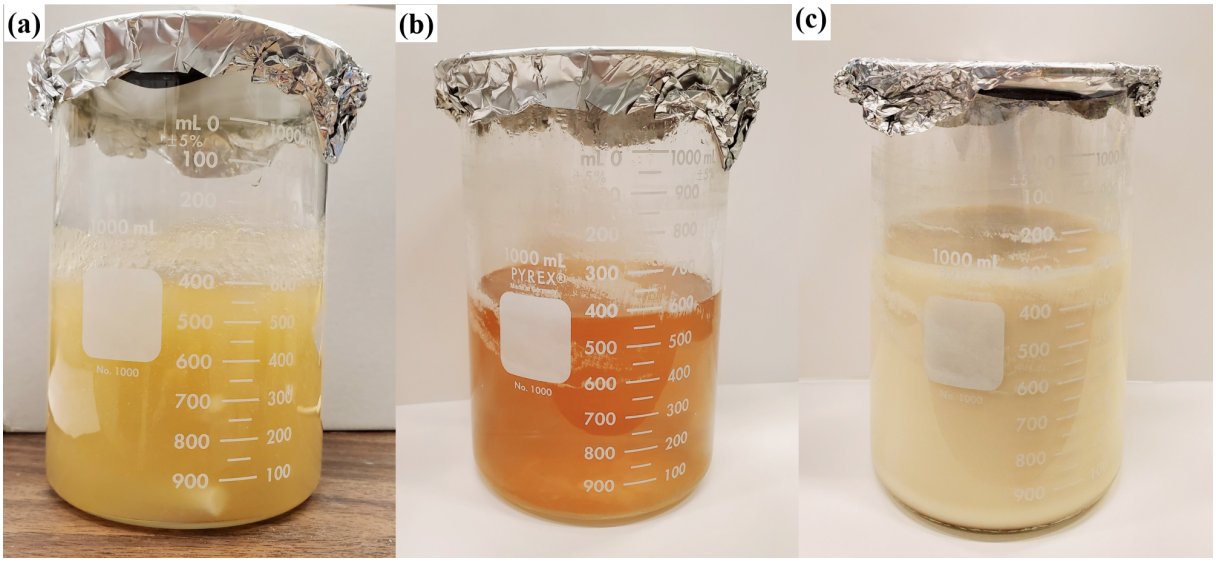


Figure 3.3: **(a)** Gelatin mixture before the heating up process. **(b)** Gelatin mixture after the heating up process. **(c)** Gelatin mixture after adding other ingredients.

After the mixture becomes transparent, as shown in Figure 3.3 **(b)**, the desired oil ratio of 20% is added when the mixture reaches 50 °C. An Ivory-ultra-liquid detergent surfactant was then added with a formaldehyde solution to provide cross-linking with gelatin. Figure 3.3 **(c)** shows the mixture that was finally used to prepare the skin samples. Finally, a D(+)-glucose powder (Sigma-Aldrich) was added to produce glucose concentrations that ranged from 75 to 300 mg/dL with a glucose step of ±25 mg/dL. The mixture was then poured using syringes (to reduce blistering) into specific silicon molds to consolidate for five days. These molds were selected to provide shapes similar to human fingertips (20mm * 20mm * 10mm). Three samples of each glucose concentration were made. Different bakers, syringes, and molds were used for each glucose concentration in the sample preparation procedure. In addition, thinner samples at 0 and 1000 mg/dL were prepared to examine the compatibility of these samples with the optical properties of human skin. The transmission spectra of the thinner samples were measured by an FT-IR (NICOLET iS50R) to obtain the absorbance spectra of the skin samples.

3.2.2 Glucose Detection Measurements

The prepared glucose phantoms, ranging from 75 to 300 mg/dL at ±25 mg/dL glucose differences, were used to investigate the ability of the system for noninvasive glucose de-

tection. The glucose range in the samples covers the scope of interest for blood glucose levels in healthy individuals and those with diabetes. Furthermore, the ±25 mg/dL glucose differences in the phantoms aim to raise the detection sensitivity toward the FDA specifications [83].

The phantom skin samples were individually placed on the PA cell over the resonator cavity at room temperature. A sensitive pressure transducer (400 FSR, Interlink Electronics, Canada) was set beneath the samples to measure the applied pressure and ensure appropriate contact with the cell. Pressure was applied to the samples using a mechanical vice that moves in an XYZ direction. The pressure effect on the acoustic signals was investigated before detecting glucose. The appropriate applied pressure was determined by applying various pressure levels to the sample of the highest glucose concentration, which generates the strongest acoustic signal. The pressure level ranged from 0 to 9 N/cm^2 in order to examine the pressure effect on the acoustic spectrum of the samples. A consistent pressure level of 6 N/cm^2 was eventually applied to all glucose phantoms in the measurements.

The modulated laser beam was focused into the PA cell by a gold-coated parabolic mirror. The 9.25 μm QCLs was operated at 400 mA with an average power of 40 mW. Each sample was scanned from 10 to 30 kHz with a frequency step of 150 Hz. The absorbed laser pulses generate thermal expansions in the skin samples, which are converted to acoustic waves. These waves are amplified inside the PA cavity and detected by a sensitive microphone (SPU0410LR5H-QB) channeled through the PA cell. A lock-in amplifier (SR830) processed the collected PA signals to increase the SNR with a time constant of 300 ms. The measurements were repeated ten times, and the collected acoustic signals were transmitted to the PC through a data acquisition system for further analysis. The experiment was repeated for three days with new samples following similar procedures. Table 3.1 shows the summary of the three-day measurements. The *In vitro* experiment is considered an initial and essential approach in examining the feasibility of the system for noninvasive glucose detection using a single wavelength MIR laser before implementing and developing the setup for *in vivo* measurements.

3.2.3 Machine Learning for Glucose Detection

The architecture of the ensemble classification model, using subspace sampling, is presented in Figure 3.4. Since not all frequencies in the acoustic spectrum provide relevant information for glucose signals, random subspace sampling [150] for the ensemble method was used. The subspace sampling algorithm extracts random features from the spectrum,

Table 3.1: Summary of the measurement procedures for glucose detection for the single wavelength setup.

Index	**Sample no.**	**Glucose level**	**Round 1**	**Round 2**	**...**	**Round 10**	**Class label**
Day 1	1st sample	75 mg/dL	10-30 kHz	10-30 kHz	...	10-30 kHz	75
Day 2	2nd sample	75 mg/dL	10-30 kHz	10-30 kHz	...	10-30 kHz	75
Day 3	3rd sample	75 mg/dL	10-30 kHz	10-30 kHz	...	10-30 kHz	75
Day 1	1st sample	100 mg/dL	10-30 kHz	10-30 kHz	...	10-30 kHz	100
.	.	.	.	.	...	.	.
.	.	.	.	.	...	.	.
.	.	.	.	.	...	.	.
Day 3	3rd sample	275 mg/dL	10-30 kHz	10-30 kHz	...	10-30 kHz	275
Day 1	1st sample	300 mg/dL	10-30 kHz	10-30 kHz	...	10-30 kHz	300
Day 2	2nd sample	300 mg/dL	10-30 kHz	10-30 kHz	...	10-30 kHz	300
Day 3	3rd sample	300 mg/dL	10-30 kHz	10-30 kHz	...	10-30 kHz	300

providing varied outlooks on the data. Thus, individual classifiers are trained using different subspace datasets. The ensemble learning combines several individual models that operate inherently parallel in order to achieve better prediction performance. The ensemble classification learning has shown encouraging results in predictive modeling of type-1 diabetes [151].

In order to generate adequate data for machine learning, each glucose sample was scanned ten times from 10 to 30 kHz, with a frequency step of 150 Hz. Figure 3.5 shows the method of sampling for the acoustic signals collected in the measurement, where each acoustic signal is considered as a single data. The measurement was then repeated for two more days using different samples, creating 4020 datasets for each glucose concentration, which led to 40200 datasets for all glucose samples, ranging from 75 to 300 mg/dL. These datasets represent the acoustic signals collected for the entire measurements. Generating a large number of data points assists the training development of machine learning models, while the arrangement of these data plays a critical role in the efficiency of the models. In machine learning, each column represents a feature, while each row represents an observation or data sampling. Therefore, it is essential to ensure that each value in the column is correlated to create one feature for the algorithm. In this work, the data points at every frequency were assigned to one column to create a unit feature for the model with a given class label. In other words, each round of the measurements was converted into a vector before combining them in one matrix. This data arrangement produced 134 features with 30 datasets for each glucose class, as shown in Table 3.2. The 134 columns represent the

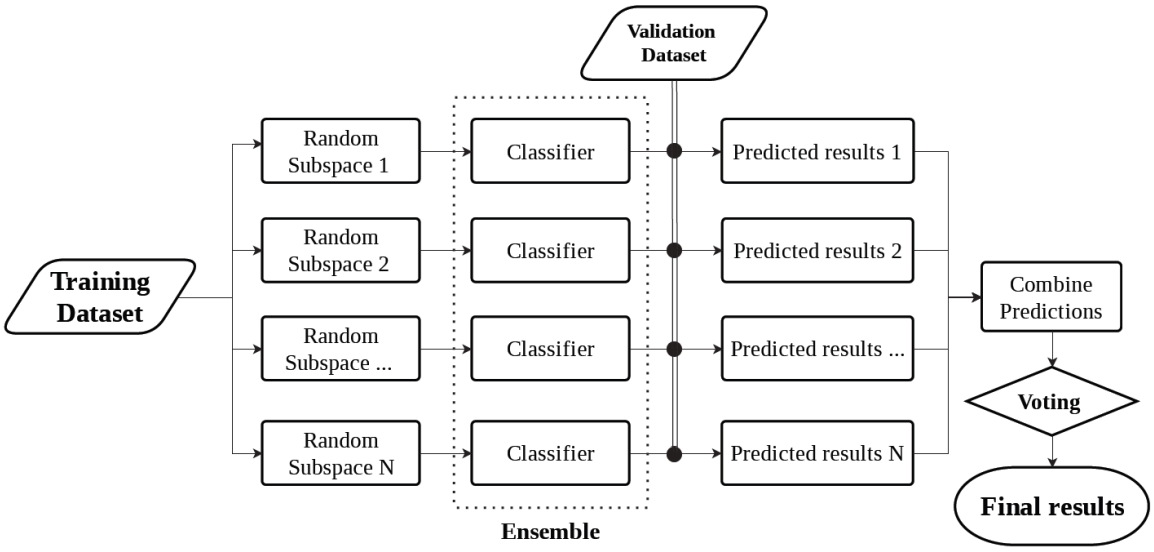


Figure 3.4: Overview of ensemble machine learning technique using random subspace sampling.

frequency range of the measurements from 10 to 30 kHz with a 150 Hz frequency step.

The measured acoustic spectrum for skin phantoms was classified into ten classes based on the glucose concentration of each phantom set. The first six classes cover the glucose level in the normal range (75–200 mg/dL), and the other four classes include the hyperglycemic range (225–300 mg/dL) for fasting and after-eating conditions. The data points of the measurements serve as training data for the machine learning classification algorithm, while the glucose class serves as the training data response.

The classification models are trained to predict the class labels using the unprocessed acoustic spectrum of the skin glucose samples in the presence of water and lipids. The aim was to examine the ability of the machine learning algorithm to classify precisely each glucose concentration without preprocessing to the obtained acoustic signals from the skin samples. The number of learners and the subspace dimension were tuned over the training to maximize the prediction accuracy. The number of learners for the current dataset was tuned between 20 to 50, and 50 to 75 for the subspace dimension. The model was evaluated using the k-fold cross-validation mechanism with 10-fold cross-validation. The dataset is split into ten folds with the same approximate size. One of the nine folds serves as a validation set to evaluate the classifier, while the other nine are used to train the model. This process is repeated until each of the ten folds is employed as a validation set.

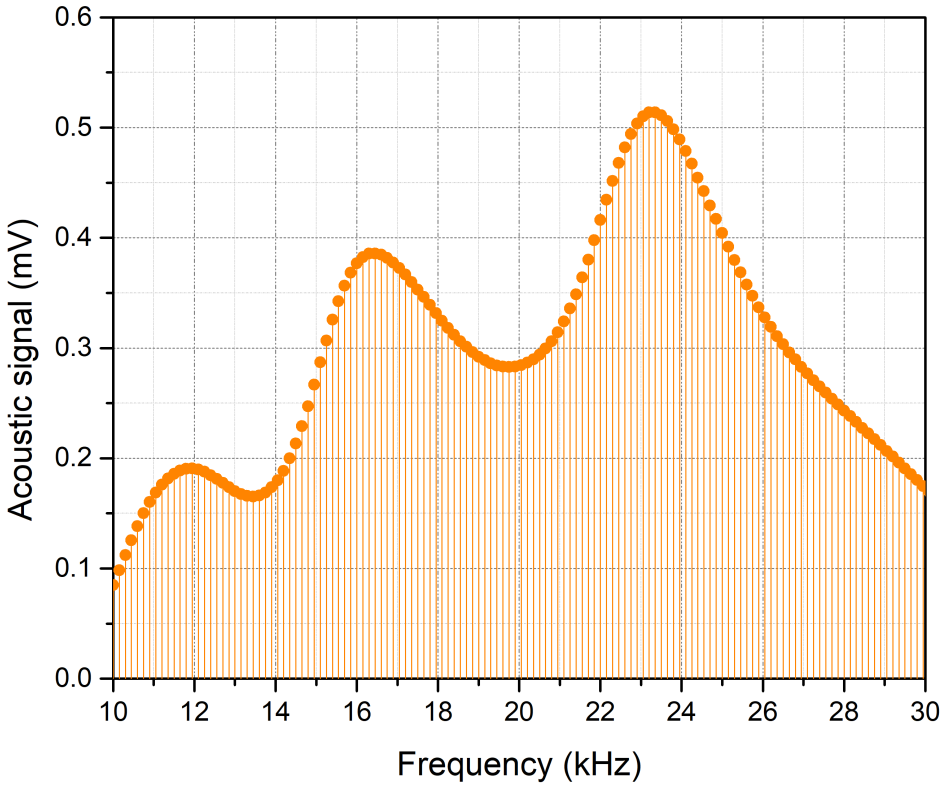


Figure 3.5: Sampling method for the collected acoustic signals for machine learning training purposes.

In the previous step, the ensemble model was trained with the raw acoustic data to investigate the ability of the optimized system to detect glucose without preprocessing the data. A model to remove the outlier using the moving median was then built to preprocess the acoustic spectrums. The moving median detection method was adopted because of the significant variation in the acoustic signal due to the amplification around the resonance frequency. The asymmetric moving window of the model was 10.2 with a threshold factor of 2.3.

SVM, NNN, and MNNs models for Glucose Detection

Three additional classification algorithms, namely SVM, NNN, and MNNs, have been developed and trained using the unprocessed collected acoustic signals only to detect the glucose levels in the skin samples. With 10-fold cross-validation, the model was assessed

Table 3.2: Dataset arrangement of the glucose acoustic spectrum for machine learning training purposes.

Index	**10 kHz**	**10.15 kHz**	**10.30 kHz**	**...**	**20.05 kHz**	**2.20 kHz**	**...**	**30 kHz**	**Class label**
Day 1	round 1	round 1	round 1	...	round 1	round 1	...	round 1	75 mg/dL
	.	.	.	...	.	.	...	.	.
	.	.	.	...	.	.	...	.	.
	round 10	round 10	round 10	...	round 10	round 10	...	round 10	75 mg/dL
Day 1	round 1	round 1	round 1	...	round 1	round 1	...	round 1	100 mg/dL
	.	.	.	...	.	.	...	.	.
	.	.	.	...	.	.	...	.	.
	round 10	round 10	round 10	...	round 10	round 10	...	round 10	100 mg/dL
.	.	.	.	...	.	.	...	.	.
.	.	.	.	...	.	.	...	.	.
.	.	.	.	...	.	.	...	.	.
Day 2	round 1	round 1	round 1	...	round 1	round 1	...	round 1	75 mg/dL
	.	.	.	...	.	.	...	.	.
	.	.	.	...	.	.	...	.	.
	round 10	round 10	round 10	...	round 10	round 10	...	round 10	75 mg/dL
.	.	.	.	...	.	.	...	.	.
.	.	.	.	...	.	.	...	.	.
.	.	.	.	...	.	.	...	.	.
Day 3	round 1	round 1	round 1	...	round 1	round 1	...	round 1	300 mg/dL
	.	.	.	...	.	.	...	.	.
	.	.	.	...	.	.	...	.	.
	round 10	round 10	round 10	...	round 10	round 10	...	round 10	300 mg/dL

using the k-fold cross-validation method. The classification algorithms are trained to predict the glucose class using the unprocessed acoustic spectrum in the presence of water and fat. The goal was to examine the efficiency of the machine learning models to classify each glucose concentration without preprocessing the raw acoustic signals from the skin samples. The dataset is divided into ten folds of approximately equivalent size. The classifier is evaluated using one of the ten folds as a validation set, while the other nine are used to train the model. This procedure is repeated until all ten folds have been used as validation sets.

3.3 Results and Discussion

3.3.1 Optical Properties for the Artificial Skin Phantoms

The prepared tissue-mimicking phantoms, simulating human fingertip size, are shown in Figure 3.6a. The optical properties of phantoms compared to real human skin are shown in Figure 3.6b for 0 and 1000 mg/dL glucose concentrations. The dielectric properties of the phantoms were already tested in the work of Lazebnik [149], where the phantoms were prepared for the first time to confirm the similitude of these phantoms to human skin. Here, the optical properties of the tissue-mimicking phantoms were examined and verified to have properties similar to human skin. Furthermore, the sample with a higher glucose concentration shows higher absorbance due to the glucose molecules. The phantoms that were prepared to examine the optical properties were made thinner to allow the IR lights to be transmitted through the samples using the FT-IR. The C——H absorption peak is clearly shown in the fresh samples due to the presence of oil compared to the dry human skin obtained by Delbeck *et al.* [152]. The oil was added to the sample to examine the glucose detection feasibility in the presence of lipids. This finding enables the employment of these phantoms as test models for biomedical applications that employ optical spectroscopy.

3.3.2 System Optimization

The acoustic absorption panels, which were successfully added to the system, suspend the acoustic background noises with an average of 78% for the entire spectrum, as shown in Figure 3.7a, which increases the SNR of the system. Furthermore, reducing the background noise around the peaks aids in exposing the glucose-buried signals in the acoustic spectrum. The pressure effect is another component that can enhance the SNR of the system. Figure 3.7b shows the collected acoustic signals at different pressure levels for the 300 mg/dL. The acoustic signal was doubled around the second peak when applying 9 N/cm^2 pressure to the sample compared to 0 N/cm^2. Increasing the applied pressure level amplifies the acoustic spectrum, which enhances the SNR and the measurement compatibility of the system. However, at the amplification limit of the PA cell, the acoustic signal reaches saturation point, and increasing the applied pressure will not further amplify the collected signals. These findings lead to a significant consequence: the applied pressure has to be lower than the cell's amplification limit at the highest glucose concentration sample. When the applied pressure exceeds the amplification limit, the acoustic spectrum of the samples will be saturated and will not be further amplified. Thus, the glucose differences among the acoustic spectrum of the samples will be reduced or eliminated. The same concept

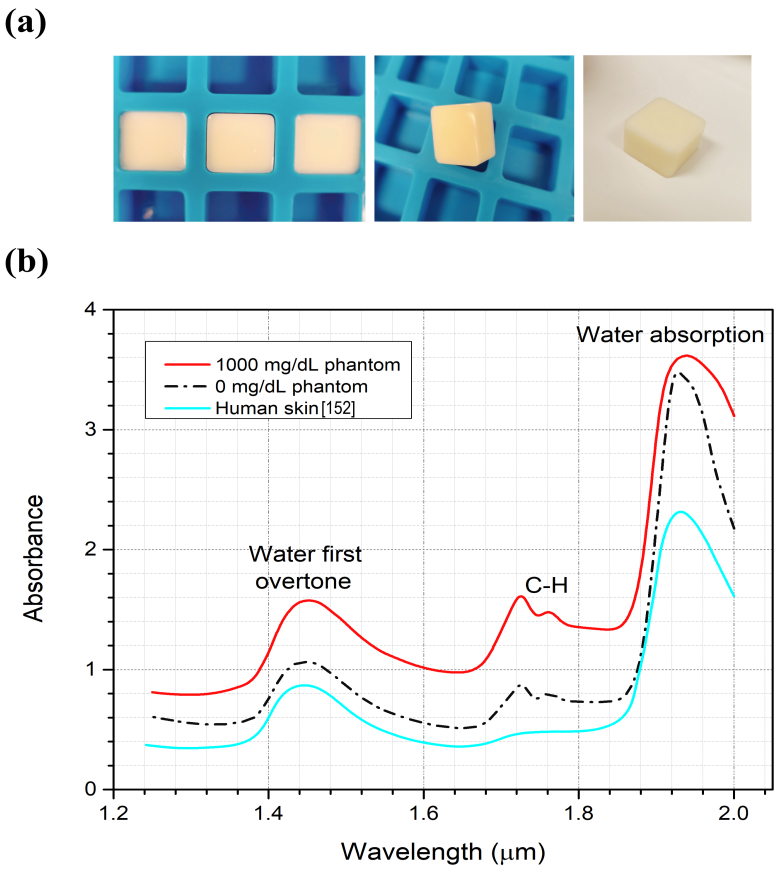


Figure 3.6: (**a**) Tissue-mimicking phantoms. (**b**) Absorption spectrum for the phantoms compared to the real human skin spectrum.

applies to other parameters that may increase the acoustic signal beyond the amplification limit, such as laser intensity, modulation frequency, and ambient temperature.

3.3.3 Glucose Detection

The acoustic spectrum of the glucose phantoms, ranging from 75 to 300 mg/dL, is shown in Figure 3.8, which shows the average of 10 rounds of measurement for each glucose sample using a single QCL, lasing at 9.25 μm. The glucose difference in the samples was set to ±25 mg/dL, aiming to achieve detection sensitivity that leads to fulfilling the

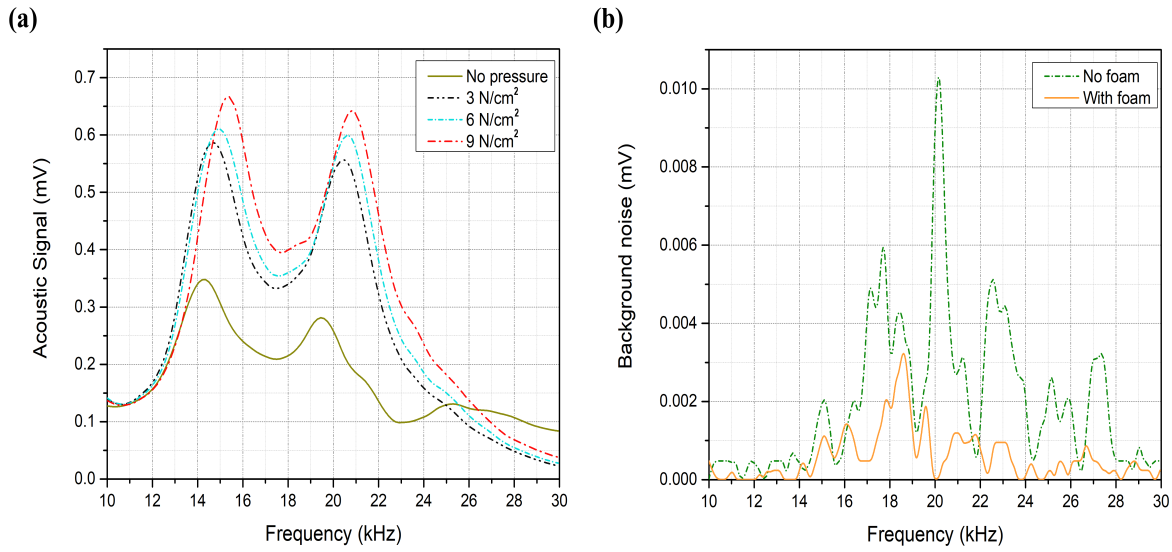


Figure 3.7: (**a**)Acoustic spectrum at different pressure levels. (**b**) Background noise with and without acoustic absorption foam.

FDA requirements. Phantoms with higher glucose concentrations are expected to generate stronger acoustic signals due to the higher absorption of the glucose molecules. The second peak of the collected acoustic spectrum, ranging from 19 to 23 kHz, was found to be sensitive to the glucose levels in the samples. Preliminary results reveal an increment in the acoustic signals along with an increase in the glucose concentrations of the samples. However, frequency shifts were noticed in the spectrum as shown in Figure 3.9a, which induced glucose detection results. These frequency shifts are attributed to the surface contact of the samples with the PA cell. Accordingly, the acoustic signals must be rectified before obtaining the glucose differences from the signals for the selected frequency range. In the rectification process, all acoustic signals were rectified to have their maximum amplitude at the same frequency. From here onwards, the rectification process will be considered a standard procedure in the signal analysis of the acoustic spectrum. The acoustic signals were then normalized with the carbon signal, which was used for the calibration process. The rectification and normalization process is shown in Figure 3.9b,c.

After obtaining the normalized spectrum for the phantoms, the area under the curves of the half-power bandwidth (of the second peak) was integrated to show the relationship between the acoustic signal to the corresponding glucose sample, as shown in Figure 3.10. The results, which were conducted without further processing, show that the system was

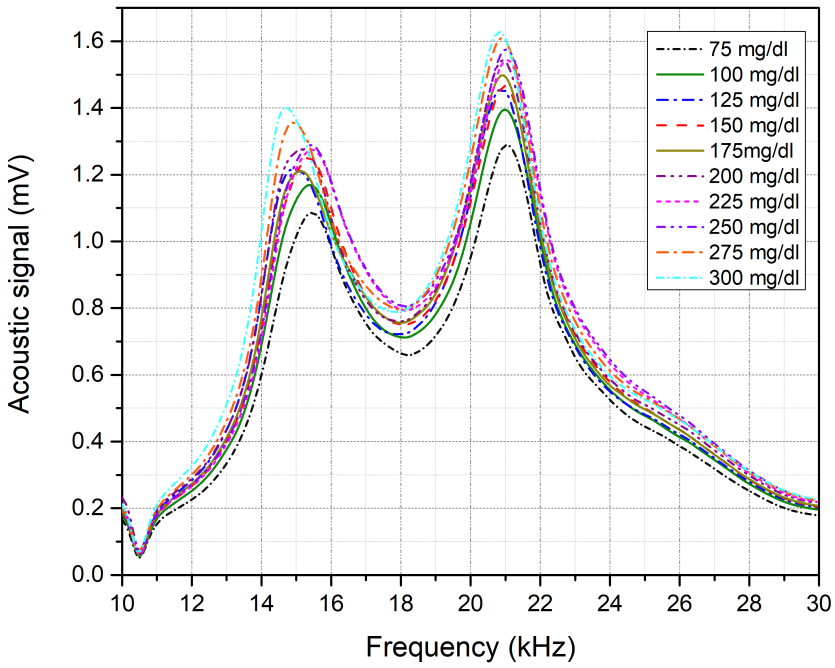


Figure 3.8: Acoustic spectrum for each glucose skin sample from 75 to 300 mg/dL.

able to distinguish the glucose differences in the skin samples in each of the three days. The presence of glucose molecules in the phantoms increases the absorption of the MIR light, which intensifies the PA of the samples that have higher glucose concentrations. The linear correlation factor of the three-day measurement is $R = 0.993$. The average resolution between the acoustic spectrum of two glucose samples with ±25 mg/dL is 2.3%. These findings raise the detection sensitivity to ±25 mg/dL using a single wavelength QCL for the first time. Moreover, it shows that the system is able to detect glucose for the entire range of interest for blood glucose levels in healthy individuals and those with diabetes.

The system shows reliability in detecting glucose in the presence of other blood components, such as water and lipids. Table 3.3 shows the standard deviation for the three-day measurements. The deviation in the measurements is associated with a slight degradation in the glucose phantoms over time for the three-day measurements. Moreover, the PA system is sensitive to environmental conditions, causing a variation in the measurements from one day to another. Nevertheless, introducing the temperature and pressure sensors to

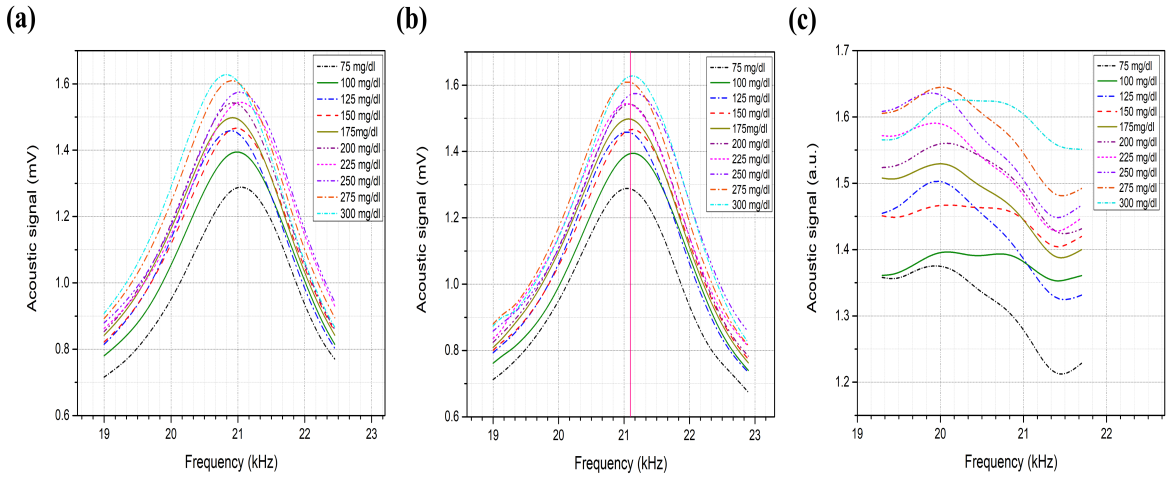


Figure 3.9: (**a**) Non-rectified acoustic spectrum of the second peak. (**b**) Rectified acoustic spectrum. (**c**) Normalized acoustic spectrum with carbon.

Table 3.3: Standard deviation of the three-day measurements using different skin samples.

Glucose level (mg/dL)	75	100	125	150	175	200	225	250	275	300
Standard Deviation $\times 10^{-2}$	2.55	2.71	3.10	2.69	2.76	3.11	2.64	2.54	2.17	1.94

the setup successfully minimized the deviation in the measurements. Further advancement is required for the *in vivo* measurements to affirm the system steadiness in the form of attaching fiber optics and humidity sensors to the setup. Moreover, a comprehensive study is needed to investigate the effect of different skin conditions, such as hydration levels, on the acoustic signals.

3.3.4 Glucose Detection Using Machine Learning

After demonstrating the system's feasibility to detect glucose in the skin phantoms using a single light source, machine learning has been involved in substituting the calibration process for the obtained data. The ensemble classification model was developed using the unprocessed data of the acoustic signals with no rectification or normalization. The ensemble classifier successfully predicted each of the ten classes of glucose concentration from 75 to 300 mg/dL with a prediction accuracy of 86.7%. The optimum number of learners was 30, with a subspace dimension of 67. All features were used to train the ensemble model

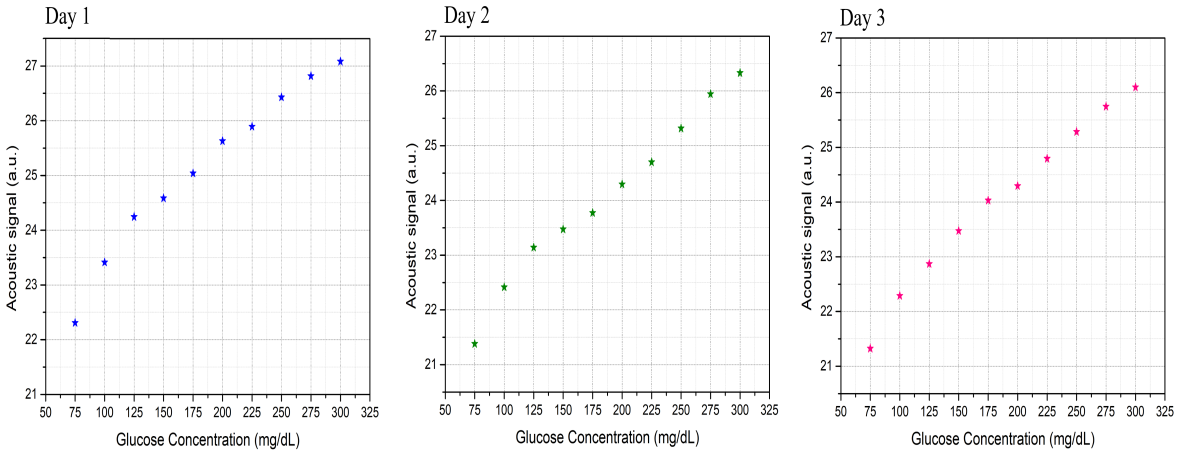


Figure 3.10: Relationships between the acoustic signals to the corresponding glucose samples for the three-day measurements.

to detect glucose in the samples. The produced confusion matrix of the ensemble classifier is shown in Figure 3.11. The confusion matrix visualizes the classifier's performance by representing the true class labels versus the predicted classes. The main diagonal of the confusion matrix demonstrates the number of data samples that are correctly classified. The right-hand side of the confusion matrix shows the percentage of the true-positive rate (TPR) and the false-negative rate (FNR).

According to the FDA, 99% of predicted results have to be located within zones A and B in Clarke's EGA [83], which is used to quantify clinical accuracy for predicted blood glucose measurements to the reference value. In order to evaluate the model's prediction accuracy, the confusion matrix is converted into Clarke's EGA, as shown in Figure 3.12a. The figure shows how many times the classifier predicts the glucose class for each data sample. This results in 93% of the predicted results being located in zone A, while 6.67% and 0.33% are in zones B and D, respectively. A majority voting algorithm was subsequently applied to the prediction data, resulting in reproducing the data in the diagonal line of zone A with 100% accuracy, as shown in Figure 3.12b. The majority voting algorithm nominates the prediction class based on the number of votes of each class in order to determine the final results.

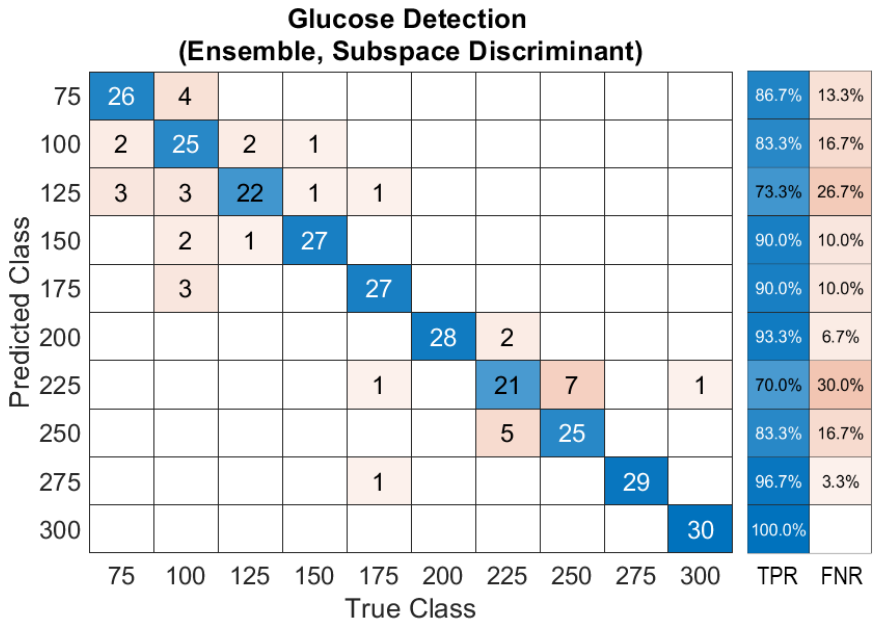


Figure 3.11: Confusion matrix of the ensemble model for glucose detection.

Dataset Preprocessing for Machine Learning

The unprocessed acoustic data has demonstrated sufficient means to train machine learning models in order to achieve conclusive outcomes that fulfill the FDA guidelines. Nevertheless, the acoustic signals are suspected of environmental conditions, which can introduce unrelated inputs to the system. Therefore, building an algorithm that removes outliers from the data is necessary, particularly when merging *in vivo* measurements. Removing outliers reduces the validation dataset of the model yet enhances the prediction accuracy. The median moving algorithm improves the ensemble model's prediction accuracy to 90.4% over the entire glucose range. The confusion matrix of the new ensemble model with the preprocessed data is shown in Figure 3.13. The confusion matrix was converted into Clarke's EGA to quantify clinical accuracy for predicted blood glucose measurements. This results in 96.1% of the predicted results being located in zone A, and with 3.9% in zone B, as shown in Figure 3.14a. Following similar procedures, the majority voting algorithm was applied to the prediction data to obtain 100% accuracy, as presented in Figure 3.14b.

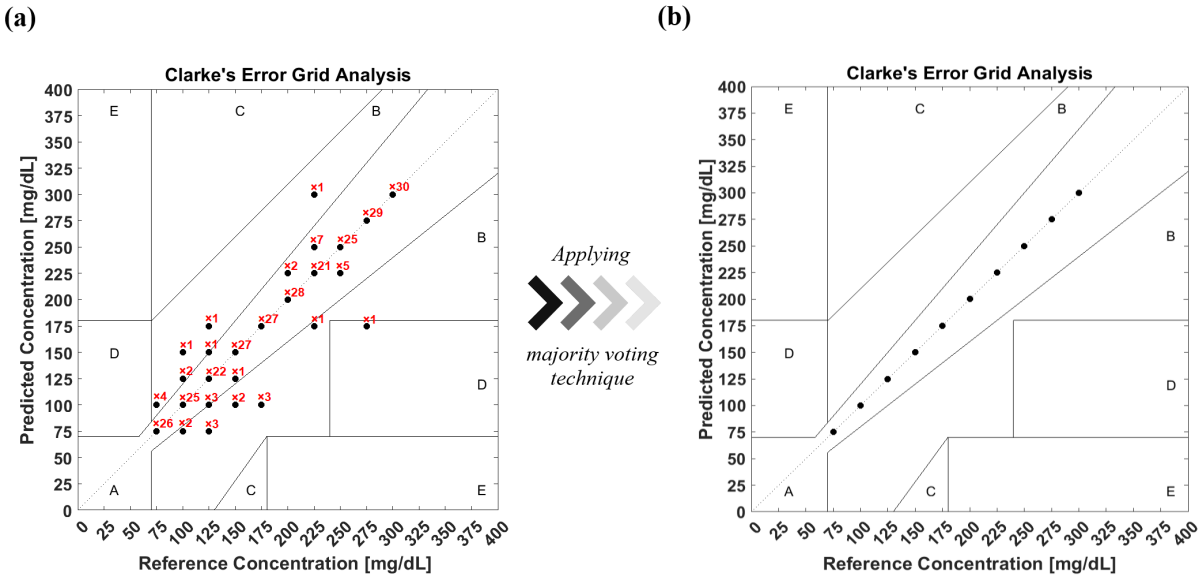


Figure 3.12: (**a**) Clarke's EGA of the prediction model of glucose detection before applying the majority voting algorithm. (**b**) Clarke's EGA of the prediction model after applying the majority voting algorithm.

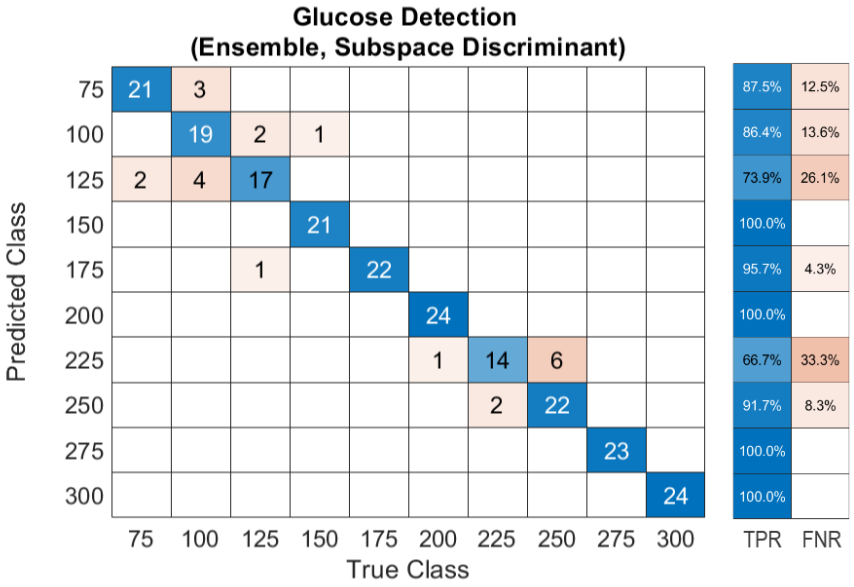


Figure 3.13: Confusion matrix of the ensemble model trained with preprocessed data.

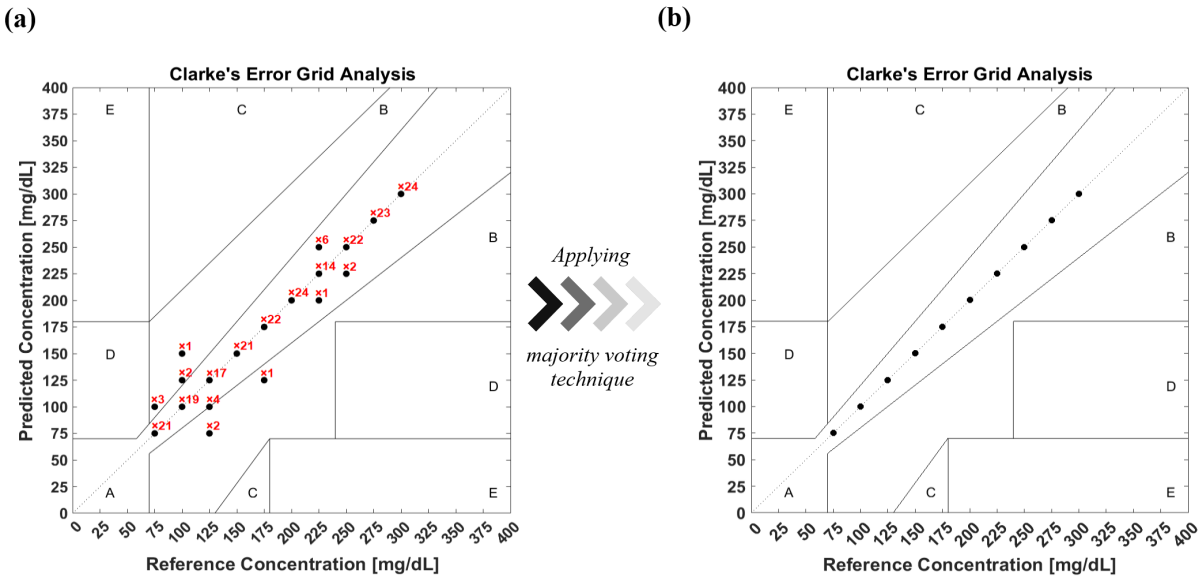


Figure 3.14: (**a**) Clarke's EGA of the prediction model with preprocessed data before applying the majority voting algorithm. (**b**) Clarke's EGA of the prediction model with preprocessed data after applying the majority voting algorithm.

SVM, NNN, and MNNs models Glucose Detection

The unprocessed data of the acoustic signals were used to develop and train additional classification models, namely, SVM, NNN, and MNNs. The SVM algorithm achieved the highest efficiency in predicting glucose concentrations with an accuracy of 83%. The NNN and MNNs classification algorithms obtained prediction precisions of 81.7% and 79.3%, respectively. The produced confusion matrices of the SVM, NNN, and MNNs classifiers are shown in Figure 3.15. The confusion matrix is transformed into Clarke's EGA to evaluate the model's prediction accuracy, as shown in Figure 3.16. The figure illustrates the number of times the classifier predicts the glucose class for each data sample at each glucose concentration. For the SVM, 88.67% of the predicted results are located in zone A, 10% in zone B, 0.67% in zone C, and 0.67% in zone D. This leads to 98.67% of the results being located in zones A and B, which is slightly lower than the FDA requirements. Although the NNN and MNNs prediction models achieved lower prediction accuracy, both techniques successfully fulfilled the FDA requirements by obtaining more than 99% of the predicted results in zones A and B. The NNN model obtained 89% of the results in zone A, 10.33% in zone B, while only 0.67% of the prediction results are located in zone D. For the MNNs algorithm, 89.67% of the predicted results are located in zone A, 10% in zone B, and only 0.33% in zone C. This finding suggests that using machine learning classification techniques such as SVM, NNN, and MNNs can enhance the sensitivity for noninvasive glucose detection to avoid calibration processes for the obtained data and fulfill FDA requirements.

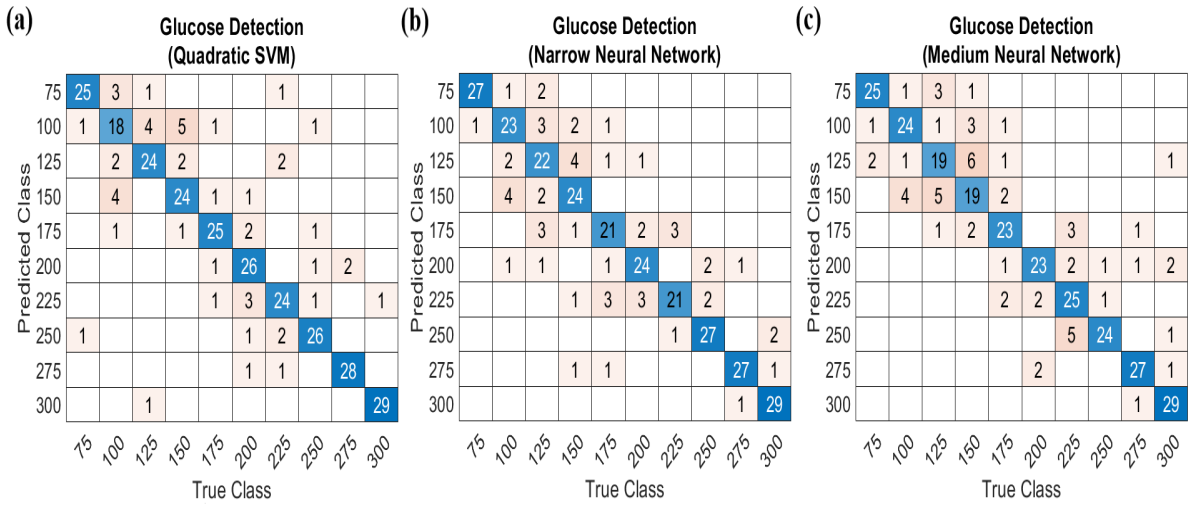


Figure 3.15: Confusion matrices of the SVM, NNN, and MNNs models for glucose detection.

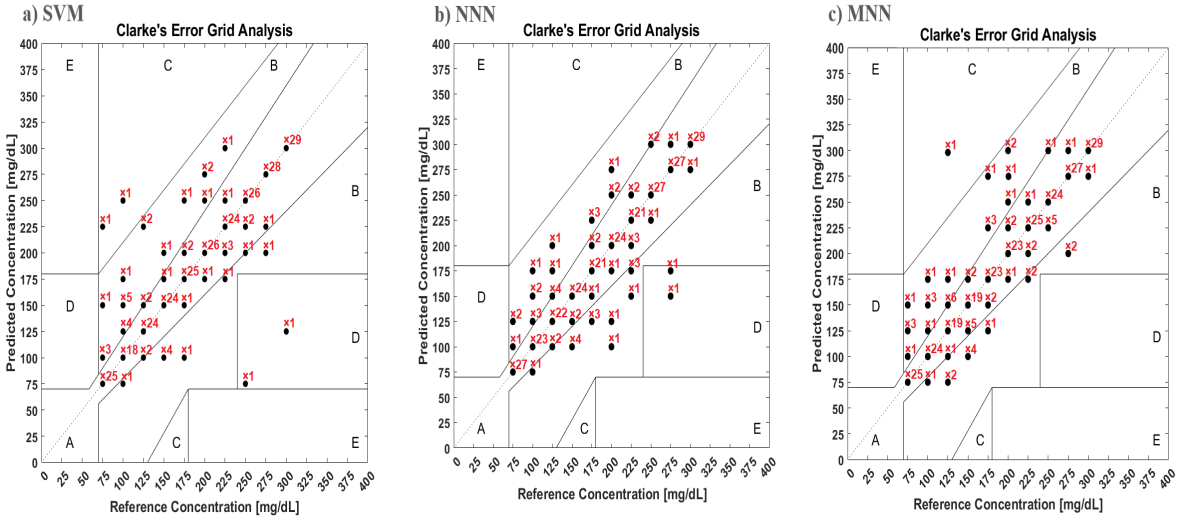


Figure 3.16: Clarke's EGA of the SVM, NNN, and MNNs prediction model of glucose detection.

3.4 Conclusions

A single wavelength QCL has been employed in a PA and MIR spectroscopy on the glucose fingerprint of 1080 cm^{-1} for noninvasive glucose monitoring. Artificial biomedical skin phantoms, having similar properties to real human skin, have been prepared to cover the normal and hyperglycemia blood glucose range. The SNR of the system has been effectively enhanced by introducing acoustic absorption panels and pressure sensors. The pressure level applied to the skin phantoms plays a critical role in detecting glucose differences in the PA signals. The PA signals of the highest glucose concentration sample have to be lower than the amplification limit of the PA cell in order to detect the glucose differences. The signal rectification proposed in this work significantly explicates the glucose signal differences in the PA spectrum. The proposed techniques of MIR and PA spectroscopy enable quantifying the glucose level in the samples with the unprocessed acoustic data. The detection sensitivity has been enhanced to ±25 mg/dL using a single wavelength QCL.

An ensemble machine learning model has been developed to classify the glucose concentration in the samples with a 40200 dataset. The ensemble models trained with an unprocessed and processed dataset achieved 86.7% and 90.4% prediction accuracy, respectively. A majority voting algorithm was applied to both prediction models, resulting in reproducing the data in the diagonal line of zone A of Clarke's EGA with 100% accuracy. These findings satisfy the FDA standards for glucose monitors. Other classification models, namely, SVM, NNN, and MNNs were developed using the unprocessed data to examine the detectability of different machine learning models. Both the NNN and MNNs algorithms, with prediction accuracy of 81.7% and 79.3%, respectively, fulfilled the FDA requirement of 99% of the predicted results in zones A and B.

In vitro measurements conducted in this study are considered to be a significant step in demonstrating the feasibility of the developed PA and MIR system for noninvasive glucose detection. The glucose sensitivity will be further enhanced in the next chapter before merging into *in vivo* experiments. The effect of other blood components, such as protein, urea, and cholesterol, on glucose will be investigated using dual QCLs.

Chapter 4

Dual QCLs for Noninvasive Glucose Detection Using PA Spectroscopy

4.1 Introduction

In this chapter, the MIR and PA system is further developed by integrating a second MIR light source to be employed as a reference for the glucose detection measurements. The reference light source can assist the system's selectivity in detecting glucose in the presence of other blood components. Furthermore, fiber optics have been used for light transmission to enhance the system's SNR and alignment process. The operating power of the MIR sources has been lowered to fulfill the safety requirements in order to qualify the setup for real human skin measurements.

A dual single-wavelength quantum cascade laser system has been developed using PA spectroscopy for noninvasive glucose monitoring. Biomedical skin phantoms with similar properties to human skin have been prepared with blood components at different glucose concentrations as test models for the setup. The detection sensitivity of the system has been improved to ±12.5 mg/dL in the hyperglycemia blood glucose ranges. An ensemble machine learning classifier has been developed to predict the glucose level in the presence of blood components. The model, which was trained with 72360 unprocessed datasets, achieved a 96.7% prediction accuracy with 100% of the predicted data located in zones A and B of Clarke's EGA. These findings fulfill both the US Food and Drug Administration and Health Canada requirements for glucose monitors.

The glucose detection sensitivity of the MIR and PA spectroscopy has improved to ±12.5 mg/dL using dual single-wavelength QCLs (1080 & 970 cm^{-1}) for noninvasive glu-

cose monitoring. The operating power of the QCLs has been lowered to fulfill the safety guidelines of using light sources on human skin. Artificial skin phantoms with similar properties to human skin have been prepared with blood components at different glucose concentrations from 100 to 275 mg/dL as test models for the system. This glucose range covers the scope of interest for blood glucose levels in healthy individuals and those living with diabetes. The dual QCLs system demonstrates sustainability in detecting glucose concentrations in the presence of albumin, sodium lactate, cholesterol, and urea. A machine learning classifier model has been developed to predict the glucose level of skin samples. The model has achieved 96.7% prediction accuracy for samples with and without blood components, with 100% of the predicted data located in zones A and B of Clarke's EGA.

4.2 Methodology

The experimental setup of the dual QCLs and PA spectroscopy for noninvasive glucose detection is shown in Figure 4.1. In the developed setup, two single-wavelength QCLs were employed. The first QCL was lasing at the glucose fingerprint of 9.25 μm (1080 cm^{-1}) (QD9500CM1, Thorlabs, Newton, NJ, USA), and the second was employed as a reference to the measurements lasing at 10.3 μm (970 cm^{-1}) (QD10500CM1, Thorlabs, Newton, NJ, USA). The threshold currents of the 9.25 μm and 10.3 μm QCLs are around 180 mA and 280 mA, respectively. The light beams of the dual QCLs were delivered to the PA cell using fiber optics cables (2FB-HF300LW-SMA-Bk0.5/0.5m, Guiding Photonics, United States), as shown in Figure 4.2. Both lasers were operated in pulsed mode at room temperature with a 40% duty cycle. The laser currents were frequency-modulated from 10 to 40 kHz by a function generator (Agilent 55321A) with a 150 Hz frequency step. The datasheet of the 1080 cm^{-1} and 970 cm^{-1} QCLs are attached in Appendix A.

4.2.1 Sample Preparation

Two main sets of artificial skin phantoms were prepared at different glucose concentrations to be used as the test models for the developed system. Both sets were prepared, ranging from 100 to 275 mg/dL, in order to cover the range of interest for blood glucose levels in healthy individuals and those with diabetes. The glucose skin phantoms were prepared following the work in Chapter 3.2.1. The purpose of the first set was to examine the system's sustainability in detecting glucose at ±25 and ±12.5 mg/dL glucose differences using single and dual QCLs. The first set was split into two categories: the non-diabetic range (100 to 225 mg/dL) and the diabetic range (225 to 275 mg/dL). The glucose difference was set to

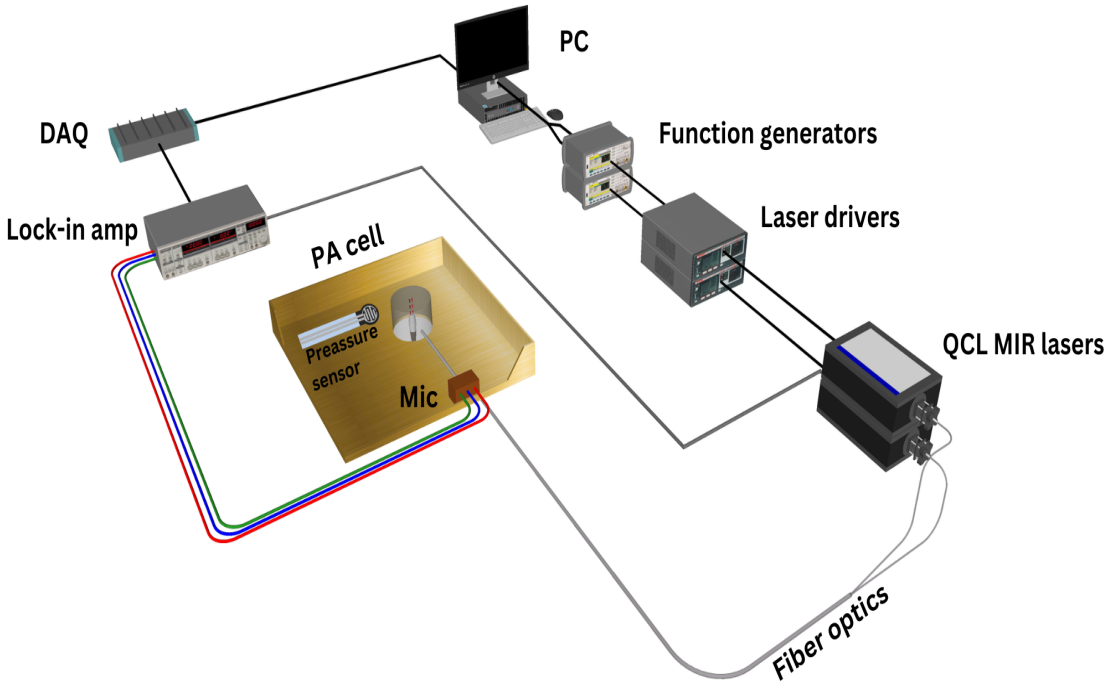


Figure 4.1: Schematic of the setup used for glucose detection using MIR and PA spectroscopy.



Figure 4.2: The fiber optic coupling for the QCL light transmitting.



Figure 4.3: The prepared samples of the main set.

±25 mg/dL in the non-diabetic range, while in the diabetic range, it was reduced to ±12.5 mg/dL. The differences were reduced in the diabetic range, aiming to achieve detection sensitivity within FDA specifications. The prepared samples of the main set are shown in Figure 4.3.

The second set of glucose phantoms was prepared by dissolving the blood components that interfere with the glucose fingerprint in the MIR region [153], namely albumin, sodium lactate, cholesterol, and urea. The MIR spectra of glucose and these blood components are provided in [71]. The components were ground and soaked overnight in deionized water in order to create a uniform solution before adding them to the solution that produced the glucose phantoms. All components were added based on their normal range in human blood in order to examine the detection selectivity and sensitivity of the system using single and dual QCLs. Albumin occupies the largest share of the blood components' weight at 4500 mg/dL, then cholesterol at 160 mg/dL, urea at 15 mg/dL, and sodium lactate at 12 mg/dL. After preparing a homogeneous solution, glucose was added to produce eight different concentrations from 100 to 275 mg/dL with a ±25 mg/dL distinction. All blood components, including glucose, used in the sample preparation were purchased from Sigma-Aldrich, Canada. More information on the preparation of the artificial skin phantoms was provided in Chapter 3.2.1.

4.2.2 Glucose Detection Measurements

The first set of the prepared glucose phantoms, ranging from 100 to 225 mg/dL at ±25 mg/dL and 225 to 275 at ±12.5 mg/dL, were individually placed on the PA cell over the resonator cavity at room temperature. A pressure of 6 N/cm^2 was applied to the samples, measured by a sensitive pressure sensor (400 FSR, Interlink Electronics, Toronto, ON, Canada). Applying constant pressure throughout the measurements is essential to the results' compatibility [154]. The 9.25 μm and 10.3 μm QCLs were operated at 220 mA and 300 mA with an average power of 8 mW and 5 mW, respectively. The fiber-coupled modulated beams of the 10.3 and 9.25 μm QCLs were focused on the PA cell cavity in order to generate the acoustic waves. The 10.3 μm QCL was run first as a reference light source for the measurements. Each sample was scanned from 10 to 40 kHz with a frequency step of 0.15 kHz for both lasers. The frequency sweep extended beyond 30 kHz due to the recognition of a new resonance frequency at 37 kHz. This resonance frequency has been recognized after transforming the light transmitting to the fiber optics, which increases the SNR of the system. The acoustic waves were amplified inside the PA cavity and collected by a sensitive microphone (SPU0410LR5H-QB). A lock-in amplifier (SR830) processed the collected PA signals with a time constant of 300 ms. The measurements were repeated five times per light source, and the collected acoustic signals were transmitted to the PC through a data acquisition system for further analysis. The experiment was repeated for two days with new samples, following similar procedures.

An IR Plano-Convex lens (ZNPX11, NEWPORT, United States) was installed underneath the PA cavity, as shown in Figure 4.4, before conducting the measurements for the second sample set, which contains blood components. The zinc selenide lens is transparent for both lasers and allows them to radiate at the exact spot of the samples, hence generating acoustic waves from an identical source. The last set of measurements was designed to study the effects of the optical lens on the results' precision. In this measurement set, the glucose samples with blood components were subjected to two days of measurements with and without the lens. When the lens was not installed, the two fiber-coupled lasers radiated parallel to the sample with around a 1 mm overlap between their beam spots on the samples. Table 4.1 summarizes the process for the three categories of measurements for both sets of samples.

Table 4.1: Summary of the measurement procedures for the dual QCLs system.

Index	**Sample no.**	**Sample contents**	**Glucose Concentration** (mg/dL)	**9.25** μm **QCL**	**10.3** μm **QCL**
Day 1	1st sample	Glucose only	Non-diabetic range (100:25:225) & diabetic range (225:12.5:275)	5 rounds (10:0.15:40 kHz)	5 rounds (10:0.15:40 kHz)
Day 2	2nd sample				
Day 1	1st sample	Glucose, albumin, urea, sodium lactate, & cholesterol	Diabetic range & non-diabetic range (100:25:275)	5 rounds (10:0.15:40 kHz)	5 rounds (10:0.15:40 kHz)
Day 2	2nd sample				
Day 1	1st sample (with lens)	Glucose, albumin, urea, sodium lactate, & cholesterol	Mid range (150:25:250)	5 rounds (10:0.15:40 kHz)	5 rounds (10:0.15:40 kHz)
Day 2	2nd sample (without lens)				

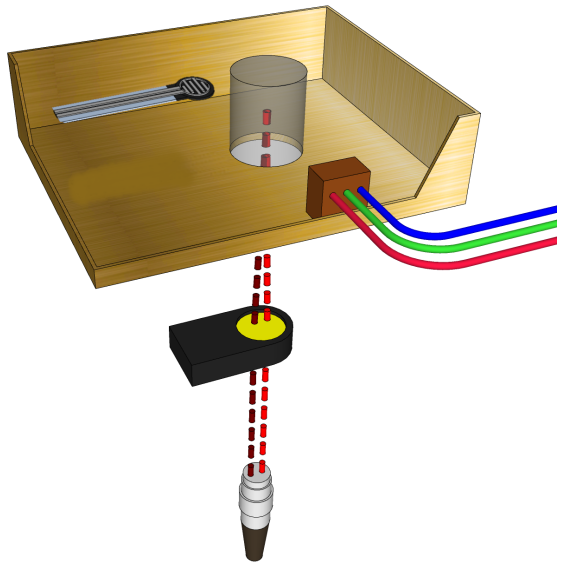


Figure 4.4: Design of the optical lens.

4.2.3 Machine Learning for Glucose Detection

An ensemble of bagged DT classification model was developed using the unprocessed acoustic signals obtained from glucose detection measurements. The bootstrap aggregating models help improve the prediction accuracy and reduce the over-fitting of the algorithms [155]. The model was trained with 72360 datasets of the acoustic signals obtained in the measurements for both sets of phantoms. The development of machine learning models is assisted by producing a large number of datasets for training from both QCLs. In machine learning, each row represents data sampling, while each column represents a feature. In this work, the data from each sampling frequency was assigned to one column to create a coherent feature with a given glucose class label. For example, the data obtained at 20 kHz was designated into one column for all samples versus the class label. The presence of the blood components was assigned into a column in the data arrangement with a binary weight. As a result, the total number of features used in building the model was 403. The data arrangement for the classifier training purposes is shown in table 4.2. The model was trained with all frequency features and without pre-processing the data to investigate the robustness of the acoustic signals obtained in the measurements. The number of learners for the model was tuned over the training to maximize the prediction accuracy. The maximum number of splits for the decision tree technique was optimized during the training. The model was evaluated using the k-fold cross-validation of 10-fold. Implementing machine learning in the MIR and PA spectroscopy may assist the development of *in vivo* measurements, where various stochastic parameters can influence acoustic signals such as human skin differences. Besides, machine learning can effectively substitute the calibration process in order to build a general prediction model for noninvasive glucose detection.

Table 4.2: Dataset arrangement of the glucose acoustic spectrum for machine learning training purposes.

Sample contents	Sample no.	9.25 μm QCL	10.3 μm QCL	Presence of b.c.	Class label
Samples with glucose only	First sample	round 1	round 1	0	100
		.	.	.	.
		.	.	.	.
		round 5	round 5	0	100
	.	.	.	.	.
	.	.	.	.	.
	Last sample	round 1	round 1	0	275
		.	.	.	.
		.	.	.	.
		round 5	round 5	0	275
Samples with other blood components (b.c.)	First sample	round 1	round 1	1	100
		.	.	.	.
		.	.	.	.
		round 5	round 5	1	100
	.	.	.	.	.
	.	.	.	.	.
	Last sample	round 1	round 1	1	275
		.	.	.	.
		.	.	.	.
		round 5	round 5	1	275

4.3 Results and Discussion

The transformation from free space to fiber optics coupling for light transmissions enhanced the SNR of the system with an average of 81% for the entire spectrum, as shown in Figure 4.5. The suspension of the background noises aids in quantifying the glucose signals in the investigated acoustic range. Such an enhancement facilitated achieving the objective of improving the detection sensitivity of the setup to ±12.5 mg/dL. Furthermore, it assisted in refining the correlation factor between the detected glucose signals.

Figures 4.6a and 4.6b show the acoustic signals obtained from the first set of glucose phantoms for the 9.25 μm and 10.3 μm QCLs, respectively. The figures show the average of

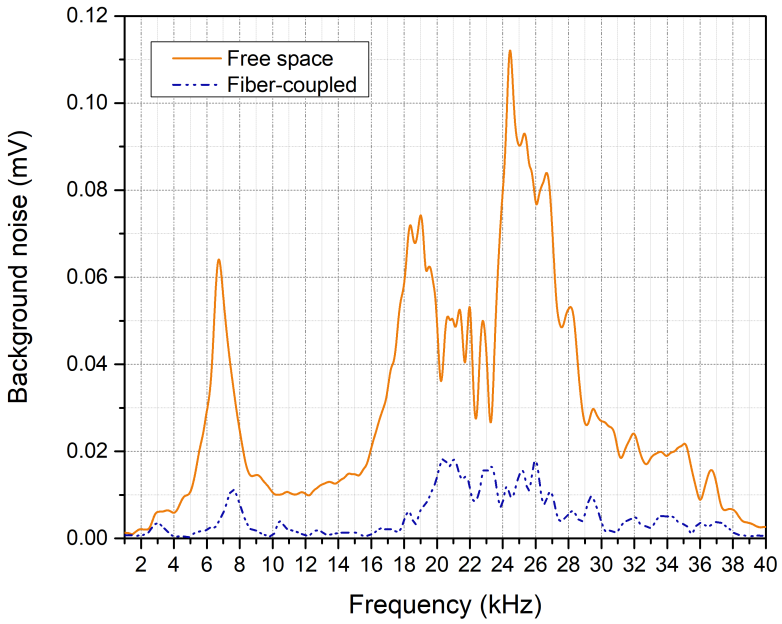
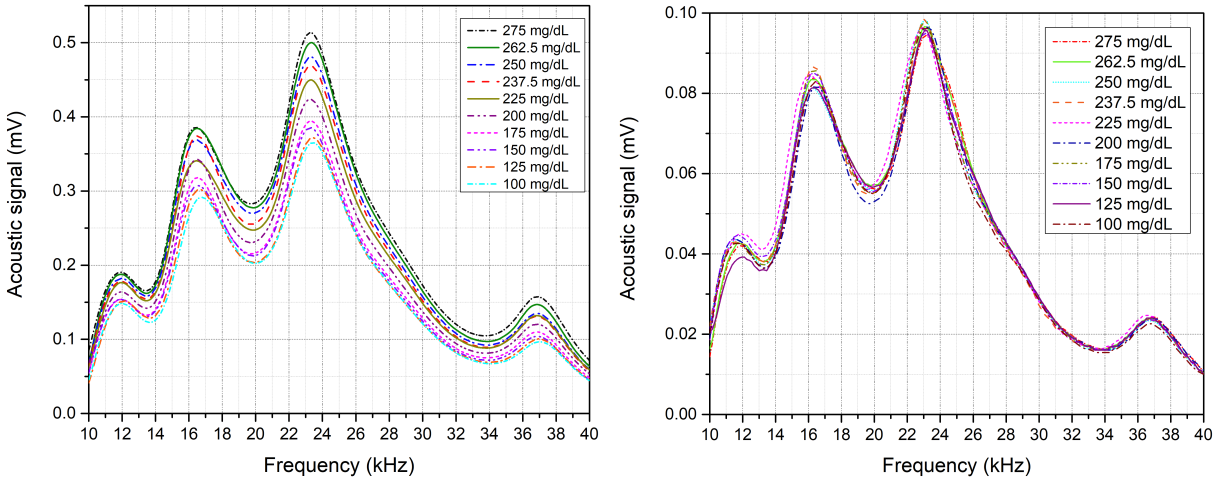


Figure 4.5: Background noise in the free space and fiber-coupled light transmission.

the 10 rounds of the two days' measurement for each light source per glucose concentration. The glucose difference in the samples was set to ±25 mg/dL in the non-diabetic range and ±12.5 mg/dL in the diabetic range, aiming to achieve a detection sensitivity that fulfills the FDA and Health Canada requirements [83, 84]. For the 9.25 μm QCL, lasing at the glucose fingerprint, phantoms with higher glucose concentrations are expected to generate stronger acoustic signals due to the higher absorption of light by the glucose molecules. The third peak of the collected acoustic spectrum, ranging from 21 to 25 kHz, was found to be the most closely correlated to the glucose differences in the samples. In contrast, signals from the 10.3 μm QCL, as intended, have not shown a positive correlation to the glucose differences in the phantoms. This is because the 10.3 μm wavelength does not respond to the glucose molecules. Hence, this wavelength can be used as a reference to subtract the background effects.

After obtaining the acoustic spectrum of the glucose samples for both QCLs, the area under the curves (of the second peak) was integrated to show the relationship between the acoustic signal to the corresponding glucose phantoms. The second peak of the collected acoustic spectrum, ranging from 19 to 23 kHz, was found to be sensitive to the changing of glucose concentrations in the samples. Figure 4.7 shows two cases of the results, one when using only the 9.25 μm QCL and the other when using two QCLs. As for the first



(a) The 9.25 μm QCL measurements.

(b) The 10.3 μm QCL measurements.

Figure 4.6: Measurements of the first set of glucose phantoms from 100 to 275 mg/dL.

case, the integrated signals from the 9.25 μm laser show a positive correlation between the acoustic signals and the glucose concentration with a linear correlation factor of 0.946. The 9.25 μm light source was able to detect the glucose differences in the samples with ±25 and ±12.5 mg/dL glucose differences. The average resolutions between the acoustic signals of two glucose samples with ±25 and ±12.5 mg/dL are 3.8% and 3.5%. These resolutions indicate inconsistency in the differences of the glucose acoustic signals, which shows the importance of adding a reference QCL that does not correspond to glucose molecules to enhance the consistency of the differences. As a result, the 10.3 μm QCL was added to the system as a reference light source. The results of two QCL measurements improved the average resolutions of the glucose samples with ±25 and ±12.5 mg/dL to 4.8% and 2.7%, which enhanced the correlation factor to 0.989, as shown in the second case of Figure 4.7. Moreover, the standard deviation of the results was reduced from 1.51 using a single QCL to 0.79 using two QCLs. The standard deviation was assessed to determine the fluctuation in the differences between the glucose samples for the entire set. In this experiment, the detection sensitivity was improved to ±12.5 mg/dL for the unprocessed data using a single wavelength QCL. The detection sensitivity was further enhanced by adding a reference wavelength to the system to subtract the background effect.

The second set of glucose phantoms was prepared by adding other blood components, namely albumin, sodium lactate, cholesterol, and urea. These blood components were added simultaneously to the glucose samples ranging from 100 to 275 mg/dL. The aim

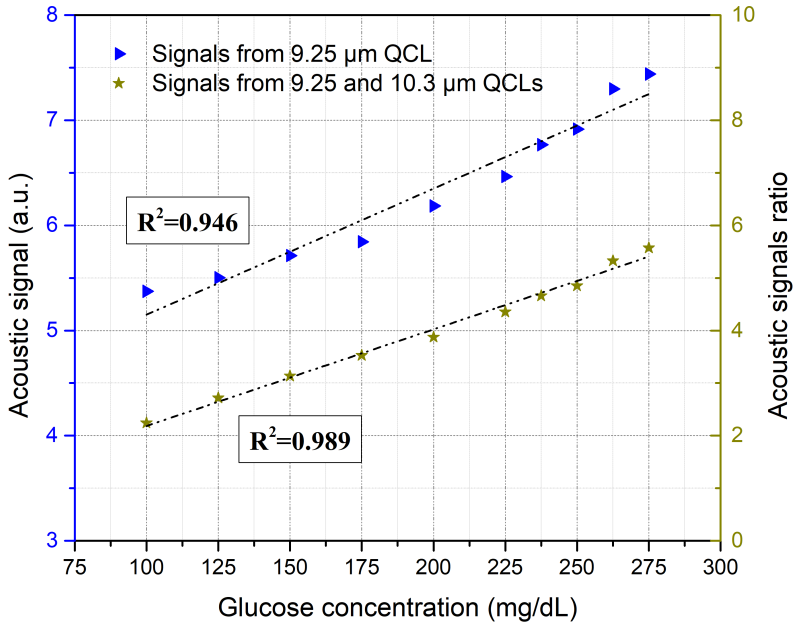
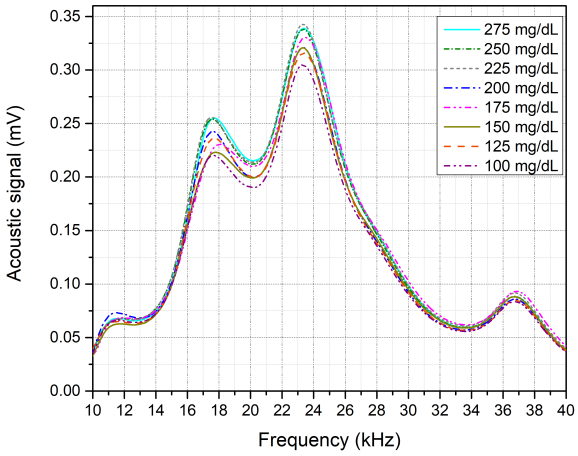
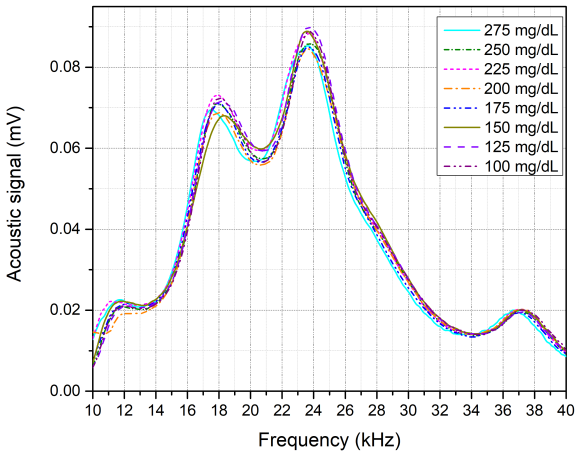


Figure 4.7: Acoustic signals to corresponding glucose.

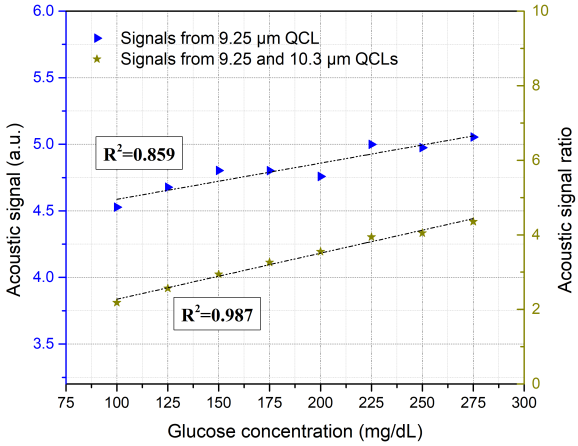
was to examine the detection capacity of the system in the presence of these components that may interfere with the glucose in the in vivo measurements. Figures 4.8a and 4.8b show the average of 10 rounds of acoustic signals per glucose concentration of the two days' measurement using the 9.25 μm and 10.3 μm QCLs. The results show that the blood components that were added to the samples interfered with the glucose signals, which lowered the detection efficiency of the 9.25 μm QCL. The impact of the blood components is distinctly revealed in the linear correlation factor when the area under the curve of the acoustic spectrum is integrated. Figure 4.8c shows the relationship between the acoustic signals to the corresponding glucose phantoms using single and dual QCLs. When only the 9.25 μm QCL was used, the system failed to detect some of the glucose samples correctly. The linear correlation factor of using only the 9.25 μm QCL is 0.859 with 2.01% average resolution between the glucose samples. When the 10.3 μm QCL was used as a reference in the measurements, the correlation factor enhanced to 0.987 with a 2.15% average resolution. The standard deviation of the measurements was reduced from 1.79 using a single QCL to 0.72 using two QCLs. Therefore, in this case, adding a reference light source is essential for eliminating the signals that are received from blood components other than glucose. Moreover, the reference light source assists in subtracting the effects of environmental conditions that vary over the experiment, such as temperature



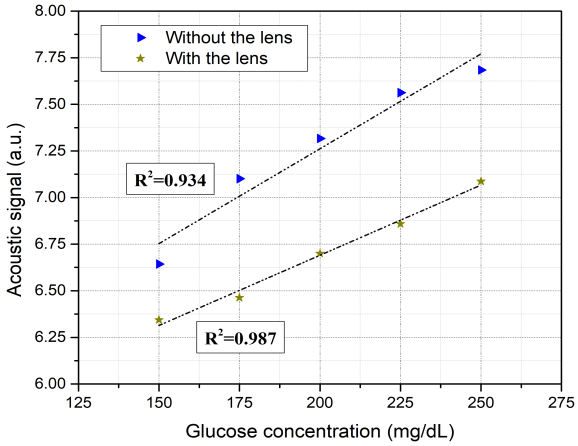
(a) The 9.25 μm QCL measurements.



(b) The 10.3 μm QCL measurements.



(c) Acoustic signals to corresponding glucose in the presence of other blood components.



(d) Acoustic signals to corresponding glucose with and without the lens.

Figure 4.8: Measurements of the second set of glucose phantoms with blood components from 100 to 275 mg/dL.

and humidity, to maintain the results compatible.

The lens effect on the accuracy of the measurements has been studied in order to determine the necessity of installing an optical lens into the system. The primary objective of the lens is to allow both QCLs to radiate at the exact spot of the samples, which assists the detection selectivity in the case of non-uniform distribution of the blood components. Figure 4.8d shows the relationship between the acoustic signals to the corresponding glucose

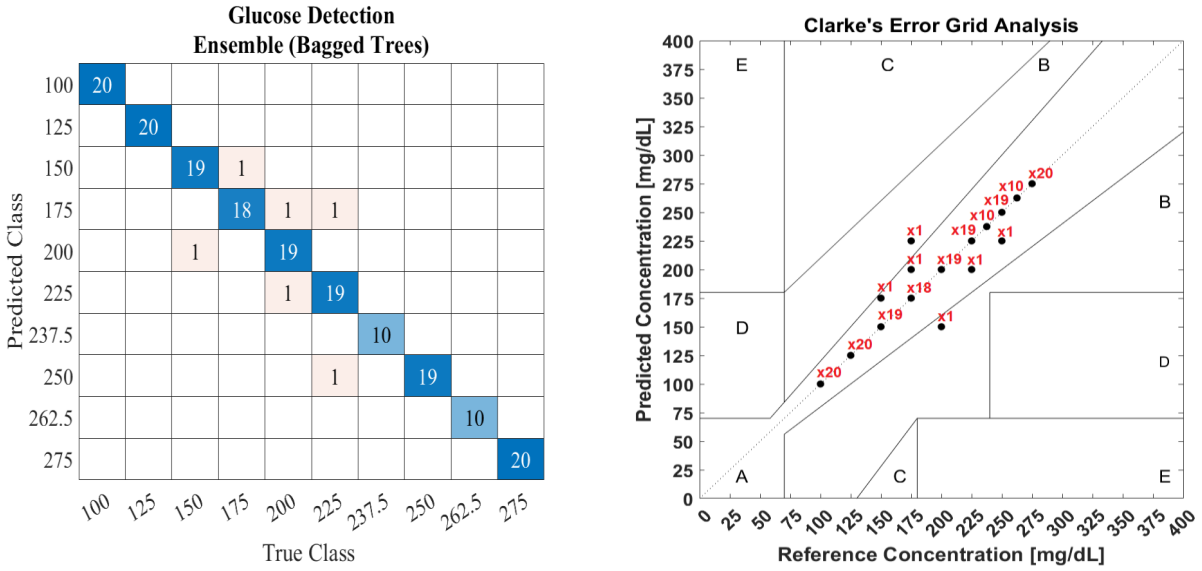
Table 4.3: Summary of the results for the dual QCLs measurements.

Measurements objective	**Glucose level** (mg/dL)	**Sample contents**	**QCL(s)**	(R^2)	Differences standard deviation (σ)
±25 & ±12.5 mg/dL detection sensitivity using a single/dual wavelength	100:25:225 & 225:12.5:275	Glucose only	9.25 μm	0.946	1.51
			9.25 & 10.3 μm	0.989	0.79
Glucose detection in the presence of blood components	100:25:275	Glucose, albumin, urea, cholesterol, & sodium lactate	9.25 μm	0.859	1.79
			9.25 & 10.3 μm	0.987	0.72
Lens effect on the detection selectivity on dual wavelegnths	150:25:250	Glucose, albumin, urea, cholesterol, & sodium lactate	9.25 & 10.3 μm (no lens)	0.934	2.24
			9.25 & 10.3 μm (with lens)	0.987	0.83

samples using dual QCLs with and without an optical lens. The system was able to detect glucose in the presence of the blood components in both cases. Nevertheless, installing an optical lens enhanced the standard deviation in the consistency of the differences by 60%. Furthermore, the correlation factor was improved from 0.934 to 0.987 when the lens was installed into the system. Table 4.3 summarizes the results of the two glucose phantoms and the lens effect.

4.3.1 Machine Learning Classifier Model

After establishing the system's feasibility in detecting glucose in the skin phantoms with and without blood components using dual QCLs, an ensemble classification model was developed using the unprocessed data. The model was trained with the raw acoustic signals of both QCLs with 72360 datasets. The ensemble classifier achieved a prediction accuracy of 96.7% using a decision tree of 30 learners and a maximum split number of 180. The confusion matrix of the ensemble classifier is shown in Figure 4.9a. The confusion matrix visualizes the classifier's performance by representing the predicted classes versus the reference classes. The confusion matrix was then converted into Clarke's EGA, as shown in Figure 4.9b, to evaluate the model according to the FDA requirements. The figure represents the number of times the classifier predicts the glucose class for each data sample. This results in 98.89% of the predicted results being located in zone A, while



(a) Confusion matrix of the ensemble model.

(b) Clarke's EGA of the prediction model.

Figure 4.9: Performance of the developed ensemble classification model.

1.11% is in zone B. Thus, the developed model qualifies for the FDA standards for glucose monitors, which require 99% of the predicted data to be in zones A and B. Further evolution in the machine learning model development is necessary for the *in vivo* measurements to build a robust model. For example, integrating feature selection algorithms can enhance the prediction accuracy of machine learning models and avoid over-fitting issues. Besides, pre-processing the data can assist in removing the noises generated from the background.

4.4 Conclusion

A dual QCL system using PA spectroscopy was developed for noninvasive glucose detection. The developed system shows sustainability in detecting glucose for the skin phantoms using single and dual single-wavelength QCLs. The detection sensitivity of the system was enhanced to ±12.5 mg/dL using a QCL lasing at a glucose fingerprint of 9.25 μm with a correlation factor of 0.946. This correlation factor was improved to 0.989 when a reference QCL, lasing at 10.3 μm, was added to the system. Furthermore, the dual QCL setup demonstrates promising results in detecting glucose in the presence of other blood components that interfere with the glucose fingerprint, namely, albumin, sodium

lactate, cholesterol, and urea. A correlation factor of 0.987 was achieved for the two days' measurements with a standard deviation of 0.72. An optical lens was integrated into the system to allow both lasers to radiate at the exact spot of the samples when the blood components were added to the samples. The correlation factor was enhanced from 0.934 to 0.987 when an optical lens was installed.

The 72360 datasets obtained from the measurements were used to train an ensemble classification model. The acoustic signals from the two sets of phantom skin were used in training. The model successfully predicted the correct classes of phantoms with 96.7% accuracy. All predicted results were located in zones A and B in Clarke's EGA . These findings satisfied both FDA conditions and were considered the final stage before conducting the in vivo measurements.

Chapter 5

In vivo Blood Glucose Detection Using IR and PA Spectroscopy

5.1 Introduction

The ideal procedure to monitor diabetes is to obtain the glucose level with a fast, accurate, and pain-free measurement that does not require blood drawing or finger pricking. For glucose detection in human skin, PA spectroscopy utilizes the weak water absorption of acoustic waves compared to MIR waves. The generated acoustic signals can travel deeper with minimum water scattering and reach the ISF in the epidermis layer. The absorption of the acoustic waves increases by raising the glucose concentration because of the vibration mode of the C —— O —— H bonds of glucose [60].

The blood glucose concentration can be potentially measured directly or indirectly from blood, serum, plasma, urine, saliva, and tear liquid, as per [6–10]. Furthermore, it can be directly determined from the ISF [12], located underneath the skin in the epidermis layer. The ISF is a thin layer of bio-fluid located between the cells, composed of water solvents and blood vessels. It contains sugars, fats, amino acids, hormones, coenzymes, white blood cells, and cell waste products [13]. The glucose diffuses from the blood to the ISF layer within a 5 to 10 minutes delay period, creating a significant opportunity for the ISF to be a potential target for noninvasive blood glucose monitoring systems [14].

The glucose molecules in human skin can absorb the modulated light that lases at the glucose fingerprint. The process of light absorption will eventually generate acoustic signals that can be collected by a sensitive microphone. The laser light absorption by

the human skin increases when the glucose molecules rise, generating stronger acoustic signals. Therefore, these collected acoustic signals can predict the blood glucose level in the human body. Initial *in vivo* measurements have been conducted as a pre-stage before conducting the OGTT. The objective of this experiment is to optimize the parameters of the system in order to detect the blood glucose in the human skin. The OGTT was finally conducted with the employment of a machine learning regression algorithm to determine the feasibility of the developed system.

5.2 Methodology

The fiber-coupled dual QCLs and PA system that has been developed in Chapter 4 was used for the *in vivo* measurements for noninvasive glucose detection. In the developed setup, two single-wavelength QCLs were employed. The first QCL was at a glucose fingerprint of 9.25 μm (1080 cm^{-1}), and the second one was employed as a reference to the measurements lasing at 10.3 μm (970 cm^{-1}). Furthermore, An IR Plano-Convex lens (ZNPX11, NEWPORT, United States) was installed underneath the PA cavity to allow both lasers to radiate at the exact spot of the human skin. Both lasers were operated in pulsed mode with a 40% duty cycle at room temperature. The laser currents were frequency-modulated from 10 to 40 kHz by a function generator with a 0.15 kHz frequency step. Figure 5.1 shows the integrated system for the *in vivo* measurements for noninvasive glucose detection.

The similitude between the previously prepared samples and the human skin was investigated in the PA domain. A skin sample was measured by the MIR and PA system simultaneously with the middle finger of a volunteer. Before the PA measurement, the blood level of the volunteer was measured by an invasive blood glucose monitoring system to select a proper skin sample concentration. The measurement aims to analyze the acoustic spectrum for the skin sample and human skin. For further investigation, the response of a carbon chip was measured by the MIR and PA system.

In order to prepare the system for the *in vivo* measurements, arm support was installed at the same level as the PA cell to provide stability to the arm during the measurements, as shown in Figure 5.2a. Four consecutive scans were conducted on a volunteer finger with and without arm support to examine the impact of the arm support on the consistency of the acoustic signals. Moreover, a pressure sensor with a larger area (402 FSR, Interlink Electronics, Canada) was installed to accommodate various human objects used in the experiments. The consistency and repeatability of the system have been investigated by the 9.25 μm laser using different parts of the hand, namely, the index finger, middle finger, thumb, hypothenar, and wrist. Both index and middle fingers showed consistent

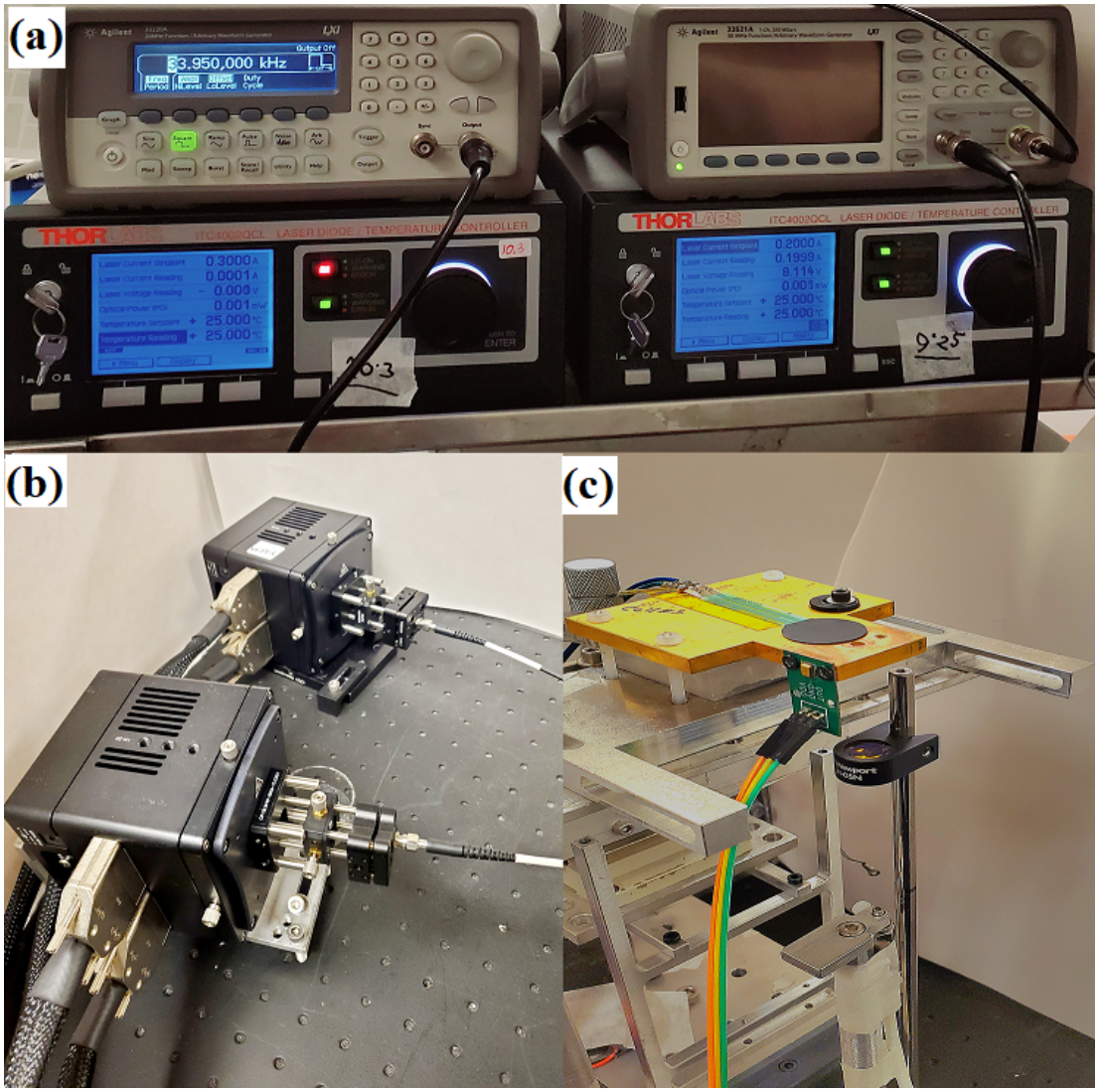
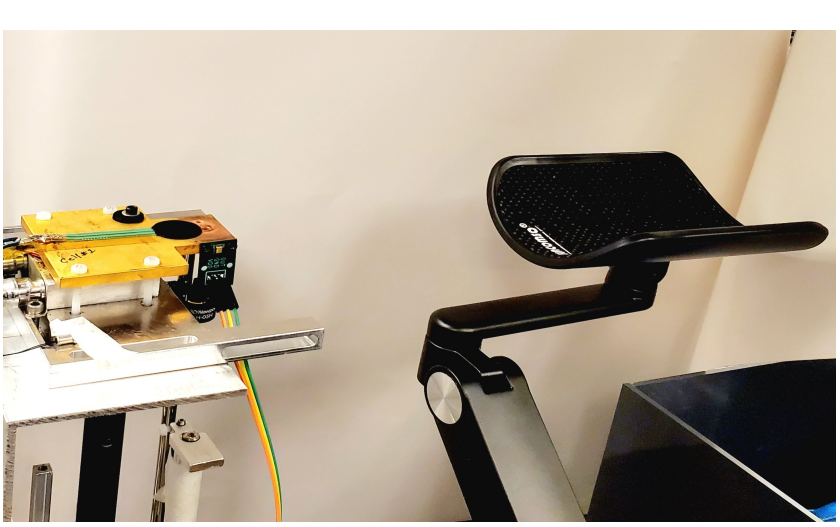


Figure 5.1: (a) The laser drivers and function generators for the 9.25 & 10.3 μm QCLs (b) The C-Mount for the 9.25 & 10.3 μm QCLs (c) The stage of the photoacoustic system for *in vivo* measurements.

and repeatable results. However, the middle finger showed more satisfactory results for the long-run measurements. Thus, the middle finger of the right hand was chosen for conducting the *in vivo* glucose detection measurements. The spot of the middle finger that has been chosen for glucose detection is shown in Figure 5.2b.



(a) The arm support designed for the measurement.



(b) The scanned spot of the middle finger.

Figure 5.2: System preparation for the *in vivo* measurement and the targeted finger-spot.

The pressure effect on the acoustic signals was investigated before detecting glucose in human skin. The applied pressure was determined by applying various pressure levels to the finger. The pressure level ranged from 0 to 9 N/cm^2 in order to examine the pressure effect on the consistency of the acoustic spectrum. A consistent pressure level of 9 N/cm^2, which provided the most consistent results, was eventually applied in all glucose detection measurements for the middle finger.

5.2.1 *In vivo* Glucose Detection Measurements

Random *In vivo* Measurements

The initial *in vivo* measurements have been conducted using the 9.25 μm QCL. The single wavelength QCL was operated at 220 mA with an average power of 8 mW. The *in vivo* measurements were designed by conducting invasive and noninvasive glucose detection simultaneously. The Contour Next One (Ascensia Diabetes Care Canada Inc.) blood glucose monitoring system was used to measure the glucose in the blood by finger pricking. The Contour Next One system exceeded the minimum accuracy requirements of the ISO 15197:2013 standard. As an initial examination of the MIR and PA system, *In vivo*

measurements were designed for three days.

On the first day, the *In vivo* was conducted on a random occasion without observing fasting. For a 40-minute experiment, The middle finger of a healthy volunteer was scanned four times by the 9.25 μm QCL every 10 minutes from 10 to 40 kHz with a frequency step of 0.15 kHz. Laser safety glasses (LG6, Thorlabs, Canada) that are used for MIR laser radiation protection were worn during the measurements. The acoustic waves were amplified in the PA cavity and collected by a sensitive microphone. A lock-in amplifier processed the collected PA signals with a time constant of 300 ms. The collected acoustic signals were transmitted to the PC through a data acquisition system for further analysis. Simultaneously, the blood glucose level was measured every 10 minutes using the CONTOUR NEXT ONE system by pricking the fingertip and extracting a drop of blood onto the test strip.

The experiment was repeated for another day following similar procedures as the first day, but the volunteer was fasting for 4 hours prior to the experiment. Also, after the first measurement round, a light meal of 800 calories was ingested by the healthy volunteer, aiming to increase the glucose in the blood. On the third day, the experiment was extended to 80 minutes with another light meal of 800 calories that was ingested after the first round. The third-day experiment was extended by 40 minutes to observe the decline in blood glucose after ingesting the meal. So, the incline and decline of blood glucose level may be observed on this day.

In these three days measurements, each acoustic signal obtained from the MIR and PA system was labeled by the time and the reading from the invasive glucometer. The middle finger was washed and dried every time before the measurements to avoid the effect of changing skin conditions on the PA signal. Moreover, the scanned area of the middle finger was determined by a marker to ensure the consistency of the scanned area.

Oral Glucose Tolerance Test

The OGTT assesses the human body's response to glucose to diagnose diabetes. Before the test begins, the volunteer has to be fasting for 8 hours before measuring the blood glucose by an invasive glucometer. The OGTT test has been conducted in this section using both invasive and noninvasive methods to evaluate the MIR and PA system.

The OGTT started after the healthy volunteer was fasting for about 6 hours. For a 120-minute experiment, the middle finger of a healthy volunteer was scanned four times by the 9.25 μm QCL every 10 minutes from 10 to 40 kHz with a frequency step of 0.15 kHz. Simultaneously, the blood glucose level was measured using the Contour Next One

system by pricking the fingertip and extracting a drop of blood to the test strip. After three rounds (20 mins), a glucose solution that contains 40 grams was ingested. Usually, the glucose in the blood starts increasing after 20 minutes of drinking the solution. The normal blood glucose results for healthy volunteers have to be less than 200 mg/dL after one hour of ingesting the glucose solution. The blood glucose level starts to decrease after 60-120 minutes for healthy people. Therefore, the 120-minute experiment encounters the rise and decline of blood glucose levels, which will evaluate the detectability of the developed system.

5.2.2 Machine Learning for *In vivo* Glucose Detection

Unlike the measurements on the skin samples, the glucose range in the *In vivo* measurements is narrower. The glucose in skin samples ranged from 75 to 300 mg/dL, while the range was from 93.6 to 117 mg/dL only in the OGTT measurement. Regression models function more appropriately for the narrower and continuous glucose range than the classification models. Therefore, a Gaussian Process regression model was developed using the unprocessed acoustic signals obtained in the OGTT measurement. The Gaussian Process is a nonparametric supervised learning method used to solve regression and probabilistic classification problems. It demonstrates a probabilistic approach to prediction by providing the mean and standard deviation as output when predicting. The Gaussian regression models work well on small datasets and can provide uncertainty measurements on the prediction.

The Gaussian Process regression model was trained with 10,452 datasets obtained in the OGTT measurements. These datasets are represented by the acoustic signals collected during the middle finger scans from 10 to 40 kHz. In machine learning, each row represents data sampling, while each column represents a feature. The data from each sampling frequency was assigned to one column to create a coherent feature with a given glucose label obtained from the Contour Next One glucometer. As a result, the total number of features used in building the model was 201. The model was trained with all frequency features and without pre-processing the data to investigate the robustness of the MIR and PA system. The kernel function and scale of the model have been optimized while building the Gaussian Process model. Implementing machine learning in noninvasive glucose detection can assist the development of *in vivo* measurements, where various stochastic parameters can influence acoustic signals, such as human skin differences or conditions. Moreover, machine learning can effectively substitute the calibration process in order to build a general prediction model for noninvasive glucose detection.

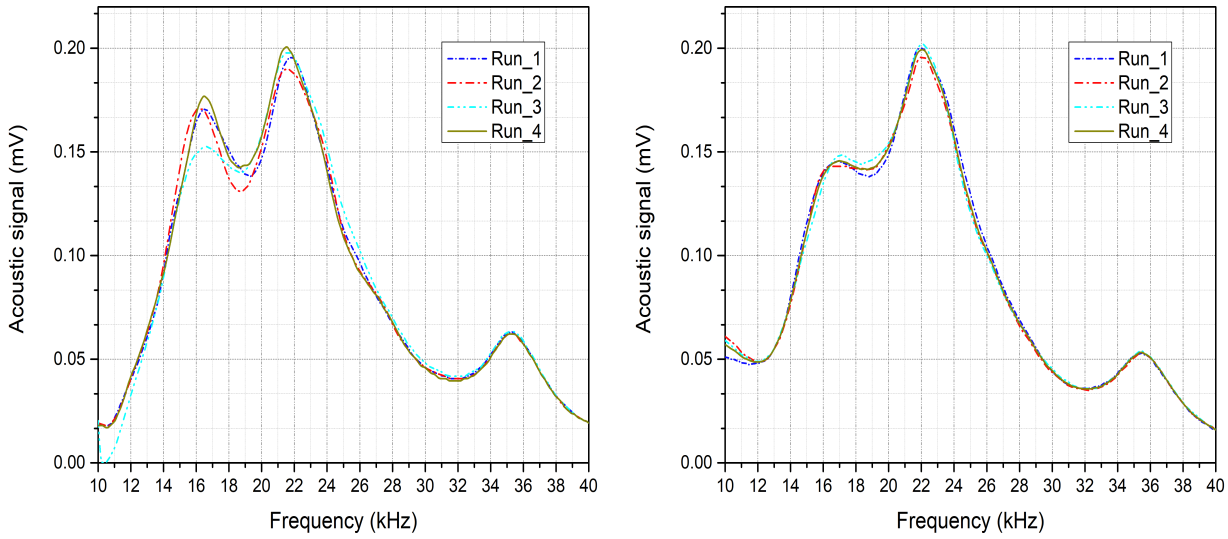
Table 5.1: Dataset arrangement of the OGTT measurement for ML training purpose.

Time (mins)	10 kHz	10.15 kHz	10.30 kHz	...	39.70 kHz	39.85 kHz	40 kHz	Invasive glucose level
00	round 1	round 1	round 1	...	round 1	round 1	round 1	100.8
	.	.	.	...	.	.	.	.
	.	.	.	...	.	.	.	.
	round 4	round 4	round 4	...	round 4	round 4	round 4	100.8
10	round 1	round 1	round 1	...	round 1	round 1	round 1	97.2
	.	.	.	...	.	.	.	.
	.	.	.	...	.	.	.	.
	round 4	round 4	round 4	...	round 4	round 4	round 4	97.2
20	round 1	round 1	round 1	...	round 1	round 1	round 1	93.6
	.	.	.	.	.	.	.	.
	.	.	.	.	.	.	.	.
	round 4	round 4	round 4	...	round 4	round 4	round 4	93.6
.	.	.	.	...	.	.	.	.
.	.	.	.	...	.	.	.	.
.	.	.	.	...	.	.	.	.
110	round 1	round 1	round 1	...	round 1	round 1	round 1	102.6
	.	.	.	.	.	.	.	.
	.	.	.	.	.	.	.	.
	round 4	round 4	round 4	...	round 4	round 4	round 4	102.6
120	round 1	round 1	1	1	round 1	round 1	round 1	97.2
	.	.	.	.	.	.	.	.
	.	.	.	.	.	.	.	.
	round 4	round 4	round 4	...	round 4	round 4	round 4	97.2

The data at each frequency for the multiple scans were assigned to one column to create a unit feature for the model. The invasive glucose reading for each scan was designated as the response column. In other words, each round of the measurements was converted into a vector before being combined into one matrix. This data arrangement produced 201 features of each number of scans for the 120-minute measurement, as shown in Table 5.1. The 201 columns represent the frequency range of the measurements from 10 to 40 kHz with a 150 Hz frequency step.

5.3 Results and Discussion

Figures 5.3a and 5.3b show the acoustic signals for the measurements conducted on the middle finger with and without arm support, respectively. The measurements were consecutively run four times without moving the finger to examine the consistency of the acoustic signals in both cases. The results show that integrating the arm support can potentially reduce the variance in the acoustic signals. This is because the arm support assisted the arm to be stable during the measurement, which provided firmness to the measured finger. The standard deviation of the acoustic signals reduced from 5.49% to 1.85% when the arm support was installed.



(a) No arm support.

(b) With arm support.

Figure 5.3: *In vivo* measurements conducted with and without arm support.

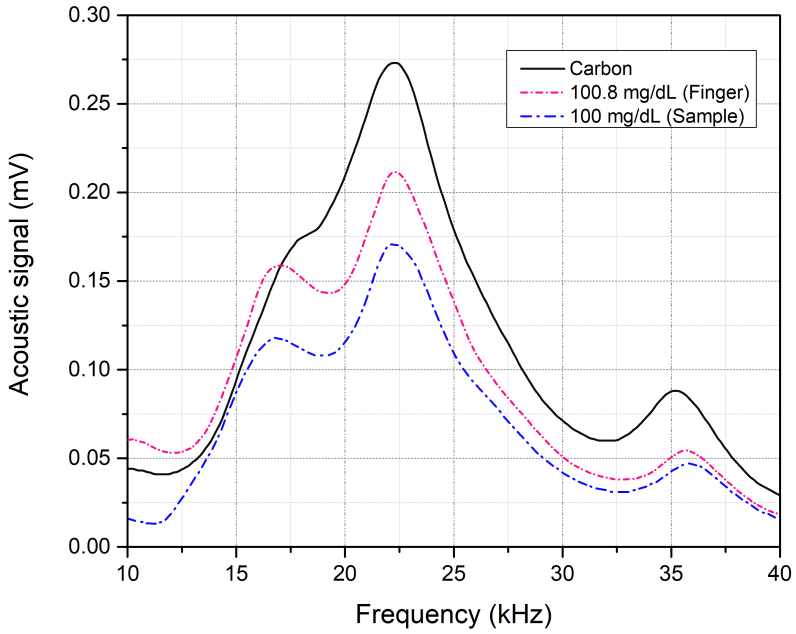
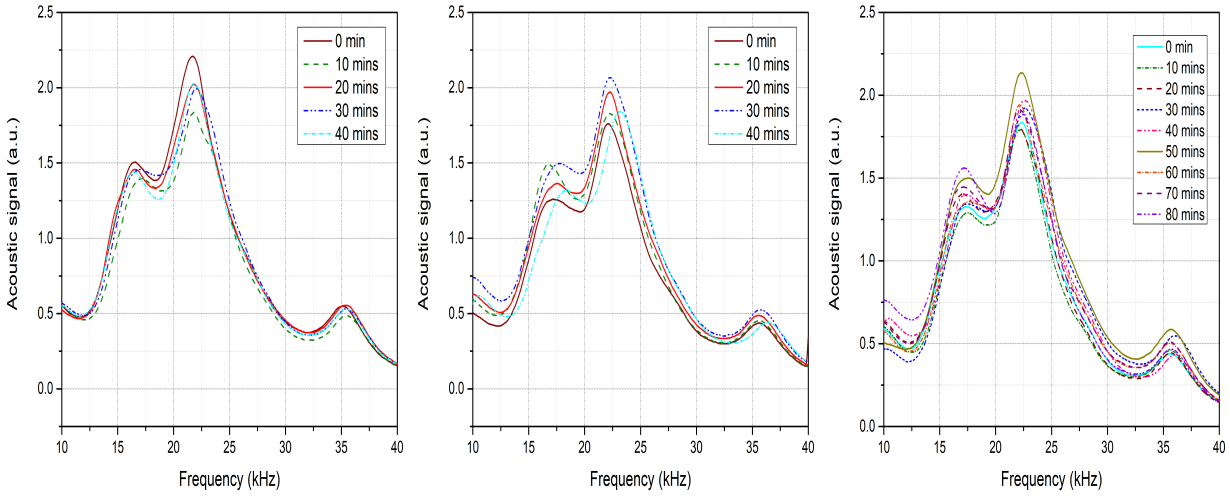


Figure 5.4: Acoustic signals for the carbon, finger, and skin sample.



(a) First-day measurements (40 minutes).

(b) Second-day measurements (40 minutes).

(c) Third-day measurements (80 minutes).

Figure 5.5: Acoustic signals for the three-days *in vivo* measurements.

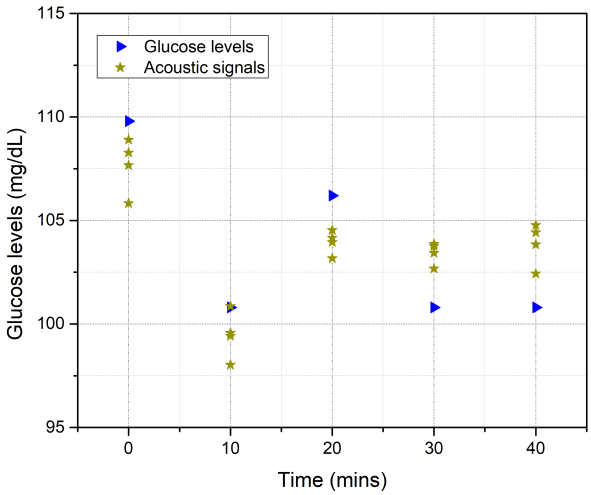
The generated acoustic signals in the real human skin to the skin phantom prepared in previous chapters were tested to examine the compatibility of these phantoms in the PA domain. The carbon signals were used as a reference to visualize the similarities between the real skin and the phantom. Figure 5.4 shows the acoustic spectrum for the carbon, human finger, and skin phantom. The invasive blood glucose monitoring system measured the blood glucose level during the experiment to be 100.8 mg/dL. Therefore, a skin sample with 100 mg/dL glucose concentration was selected for the MIR and PA measurements. The acoustic spectrum of the human finger and skin sample in Figure 5.4 shows compatibility in the spectrum's form compared to the carbon spectrum. This result verifies the employment of the skin samples in the PA spectroscopy.

Figures 5.5a, 5.5b and 5.5c show the acoustic signals obtained from the three days *In vivo* measurements. The figures show the average of the four scans of each measurement round, which was every 10 minutes. The measurements have been conducted using a single wavelength lasing at the glucose fingerprint of 9.25 μm. The spectrum reveals variations in the peak values of the acoustic signals at the resonance frequency of 21.8 kHz, which may indicate varying blood glucose levels. However, slight frequency shifts were noticed in the spectrum, which may have influenced glucose detection results. These frequency shifts are attributed to the bottom surface contact of the finger with the PA cell. The skin curvature or the finger's movement can introduce a slight frequency shift to the acoustic spectrum. Consequently, the acoustic signals must be rectified before investigating the glucose signals. The rectification process has been introduced in detail in Chapter 3.3.3.

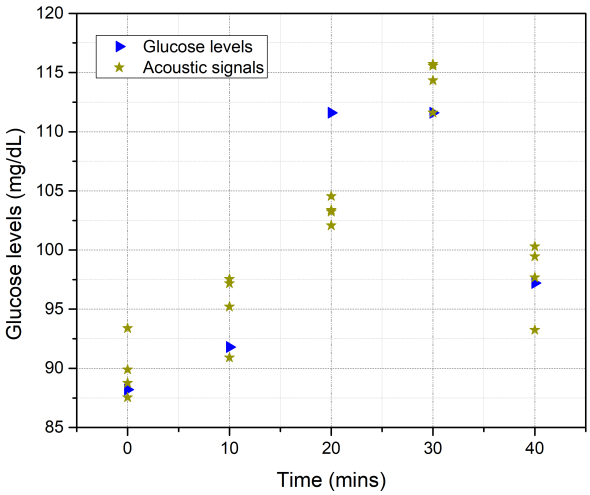
After obtaining the acoustic spectrum of the three days measurements using the 9.25 μm QCL , the area under the curves (of the second peak) was integrated for each round. At each round, the four scans of the middle finger of each round are labeled with the blood glucose readings from the invasive glucometer. In order to show both results, the acoustic signals have been normalized, as seen in Figures 5.6a, 5.6b and 5.6c. The preliminary results reveal that both invasive and noninvasive glucose measurements have similar trends for blood glucose levels. These preliminary outcomes from the initial *In vivo* measurements demonstrate that the MIR and PA system can detect glucose levels not only in the biological samples but also in real human skin.

5.3.1 Oral Glucose Tolerance Test

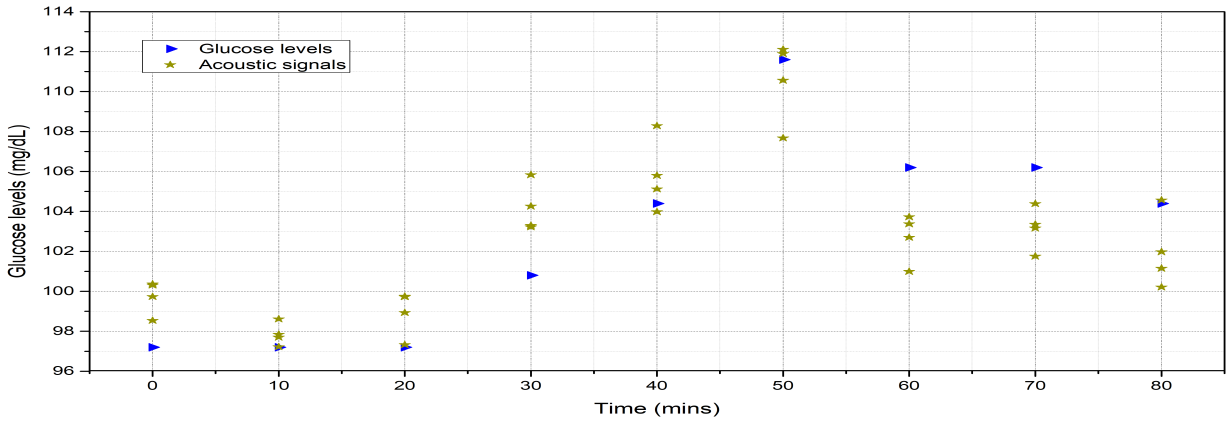
The invasive blood glucose levels using the Contour Next One glucometer for the entire OGTT are shown in Table 5.2. Figure 5.7 shows the average of acoustic signals for each scan obtained from the 120-minute OGTT measurements. The figures show the acoustic



(a) first-day measurements (40 minutes).



(b) Second-day measurements (40 minutes).



(c) Third-day measurements (80 minutes.)

Figure 5.6: Normalized acoustic signals to corresponding invasive blood glucose levels.

spectrum of each measurement round, which was every 10 minutes. The acoustic spectrum has been rectified based on the maxima of the second peak. The OGTT measurements started while the healthy volunteer was fasting, and the glucose solution was ingested after 20 minutes of starting the measurements.

After obtaining the acoustic spectrum of the OGTT measurements using the 9.25 μm QCL, the area under the curves (of the second peak) was integrated for each round. The acoustic signals were then normalized based on the ratio of the first invasive glucose reading to the first acoustic signal, as shown in Figure 5.8. The results demonstrate that invasive

Table 5.2: Invasive blood glucose levels using the glucometer for the OGTT measurement.

Time (minutes)	Invasive glucose levels (mg/dL)
00	100.8
10	95.4
20	95.4
Start drinking glucose solution	
30	93.6
40	109.8
50	113.4
60	117
70	115.2
80	102.6
90	102.6
100	104.4
110	102.6
120	97.2

and noninvasive glucose measurements have similar trends for blood glucose levels. Both measurements show a rise in blood glucose levels after 40 minutes from the start of the test and 20 minutes after ingesting the glucose solution. Furthermore, both measurements show a decline in blood glucose levels after 80 minutes of the test start. The lowest blood glucose level recorded during the measurements by the Contour Next One glucometer was 93.6 mg/dL, while the highest was 117 mg/dL. The difference between the lowest and the highest values was 25%. For the noninvasive blood glucose values, the difference between the lowest and highest acoustic signals was 23.5%. Thus, the MIR and PA system demonstrates promising outcomes compared to the invasive method for detecting blood glucose levels without processing the acoustic signals.

The benefit of representing the raw acoustic signals to the invasive blood glucose levels is to demonstrate the detectability of the noninvasive system itself before employing machine learning algorithms. Here, the noninvasive MIR and PA system established a strong correlation to the reference values that were obtained by the Contour Next One glucometer. Further advancement can be achieved by employing machine learning to develop a prediction model using the dataset obtained in the MIR and PA measurements.

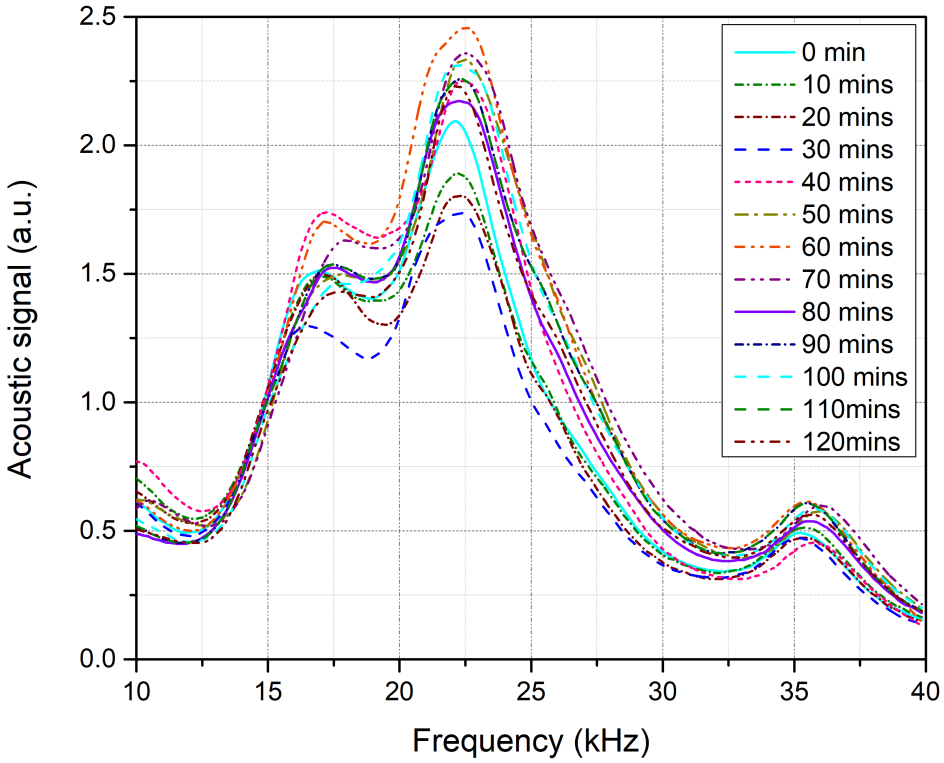


Figure 5.7: Acoustic signals of the OGTT *in vivo* measurements

5.3.2 Machine Learning for *In vivo* Glucose Detection

After establishing the feasibility of the MIR and PA in detecting glucose levels in the human skin, a Gaussian Process regression model was developed with the rational quadratic kernel function using unprocessed acoustic signals. The model was trained with the raw acoustic signals using the 9.25 μm QCL with 10,452 datasets. The Gaussian model was evaluated using the RMSE and the linear correlation factor. The RMSE of the Gaussian regression model for predicting blood glucose level was 1.213 mg/dL with a linear correlation factor of 0.98. In addition to the RMSE value, the mean absolute error (MAE) and Mean squared error (MSE) of the model were 0.622 and 1.47 mg/dL, respectively. The prediction glucose levels versus the reference levels using the developed Gaussian regression model are shown in Figure 5.9.

Clarke's EGA is used to assess the clinical accuracy of the prediction of blood glucose levels compared to the reference values. According to the FDA, 99% of the predicted results have to be located within zones A and B in Clarke's EGA. The Gaussian model

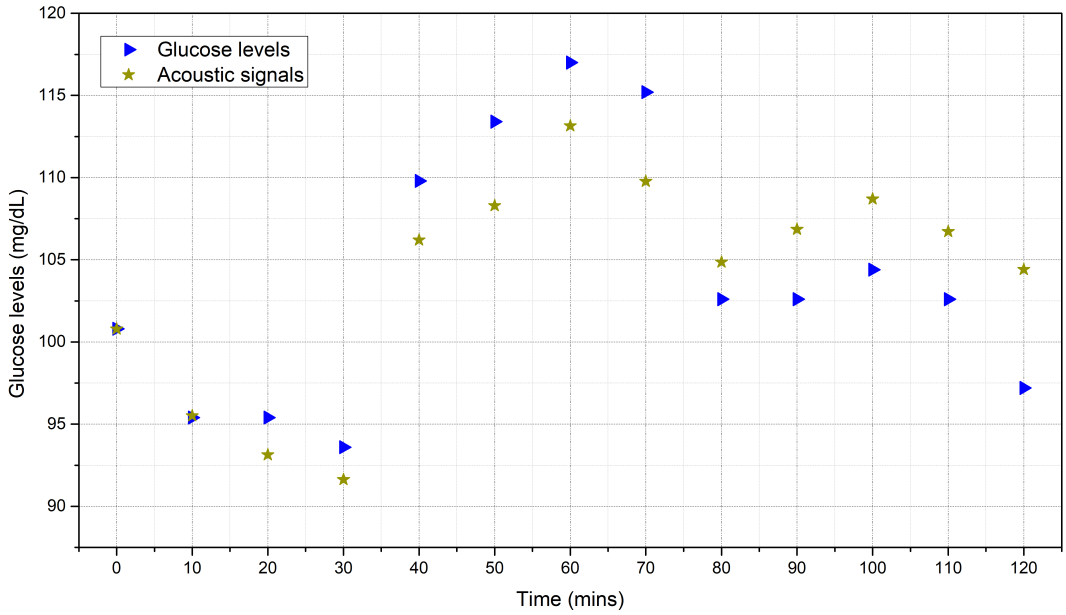


Figure 5.8: Normalized acoustic signals to corresponding invasive blood glucose levels for the OGTT measurements.

was evaluated by Clarke's EGA to assess the prediction model. Figure 5.10 shows Clarke's EGA of the developed regression model, where 100% of the prediction values are located in zone A. This finding reveals that the employment of machine learning with the MIR and PA system leads to fulfilling the FDA requirements.

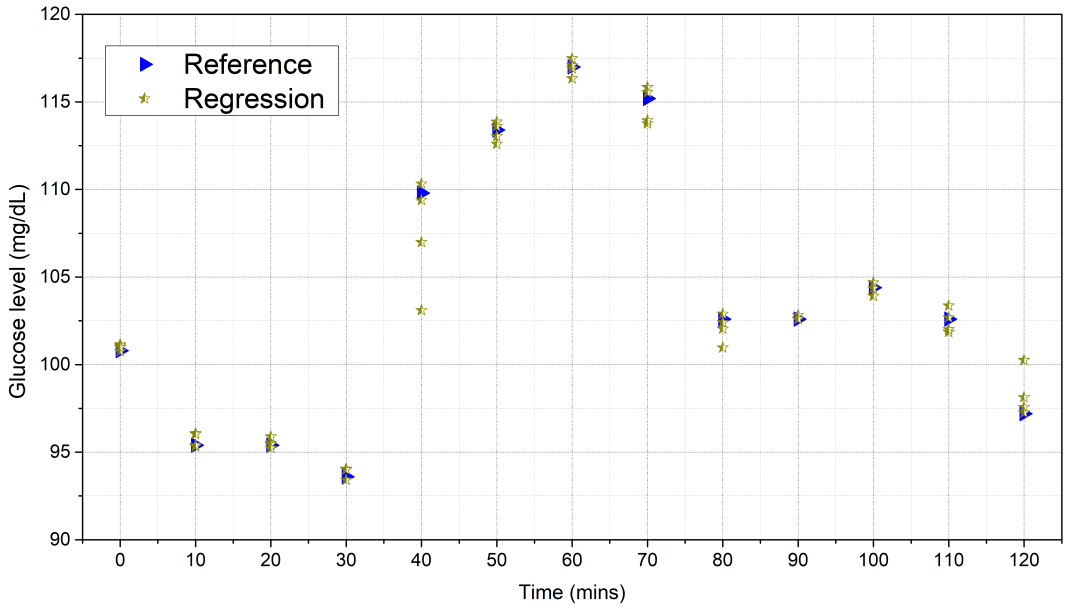


Figure 5.9: Predicted blood glucose levels using Gaussian regression model to the reference levels for the OGTT measurements.

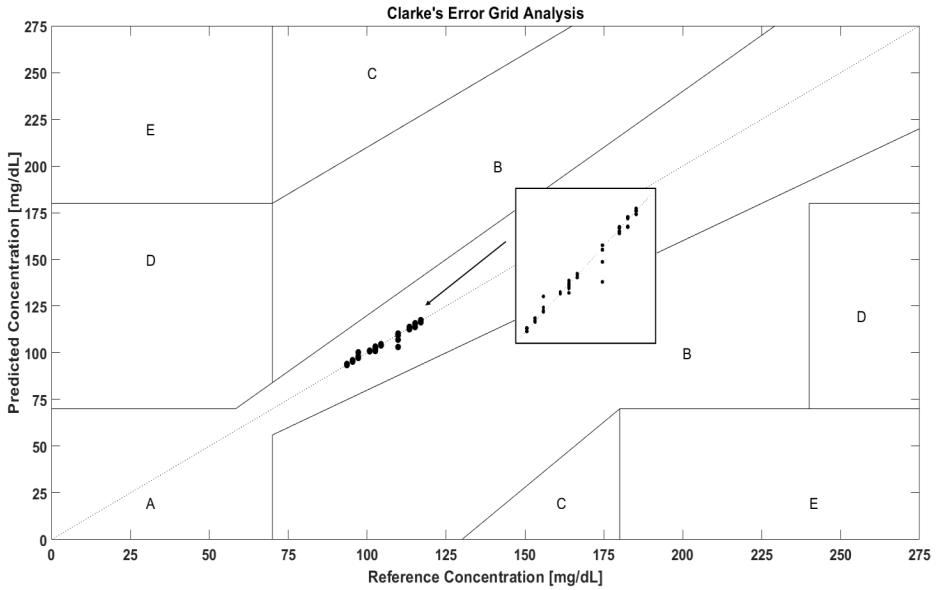


Figure 5.10: Clarke's EGA of the Gaussian regression model for the OGTT measurements..

5.4 Conclusion

In this chapter, the MIR and PA system measurements were moved from the in vitro to the *in vivo* phase. The system was slightly adjusted to accommodate the *in vivo* experiments by installing an arm support and pressure sensor with a larger area. Several initial *in vivo* measurements were conducted to investigate the detectability of the system in the human skin.

A 120-minute OGTT was conducted simultaneously with measuring the blood glucose level by an invasive glucometer. A Gaussian Process regression model was developed using the unprocessed acoustic signals obtained in the OGTT measurement. The RMSE of the Gaussian regression model for predicting blood glucose level was 1.213 mg/dL with a linear correlation factor of 0.98. All blood glucose predicted results were located in zones A and B in Clarke's EGA. These preliminary outputs from the *in vivo* measurements demonstrate that the MIR and PA system can detect glucose levels in biological samples and real human skin. Further investigation is necessary to examine the detectability of the system for a broader range of volunteers, including those who live with diabetes.

Chapter 6

Contributions and Future Works

6.1 Summary of Contributions

This research has conducted a comprehensive study on IR and PA spectroscopy for noninvasive blood glucose detection, focusing on component development, parameter optimization, and system integration. In this section, a qualitative summary of the novelty of this work is provided to highlight the main contributions in the scope of IR and PA spectroscopy for glucose detection.

1. IR and PA system has been developed and studied using well-controlled biomedical skin samples that have similar electrical and optical properties to human skin. These well-controlled samples propose an influential environment to study and enhance each component in order to advance the development of the IR and PA system. The parameters of QCL, photoacoustic cell, function generator, and lock-in amplifier have been investigated, aiming to qualify the IR and PA spectroscopy for noninvasive glucose detection. Consequently, a detection sensitivity of $\pm 12.5\ mg/dL$ has been achieved using a single wavelength MIR source using PA spectroscopy. This detection limit has been reached from the unprocessed data of the developed system for the first time, fulfilling the FDA and Health Canada requirements for noninvasive blood glucose monitors.

2. Further development of IR and PA spectroscopy was demonstrated by employing a single and dual-wavelength QCLs to examine the detectability of the developed system in the presence of other blood components that interfere with glucose in the MIR region. The dual QCLs system establishes sustainability in detecting glucose concentrations in the presence of albumin, sodium lactate, cholesterol, and urea. This sustainability qualifies the

system's advancement from the in vitro to the in vivo phase. The preliminary results of the in vivo measurements reveal the capacity of the system to detect blood glucose levels in individuals.

3. The employment of artificial intelligence has yet to be utilized in IR and PA spectroscopy for glucose detection. In this work, machine learning classification and regression models have been involved in every phase of system development for noninvasive glucose detection. The robustness of artificial intelligence can overcome some of the stochastic parameters, such as the presence of blood diseases, skin conditions, and environmental noises. The machine learning models developed for both single QCL and dual QCLs fulfilled the FDA 's prediction accuracy requirements.

6.2 Accomplished Work

The accomplished contributions of this dissertation can be summarized as follows:

- Development of the research objectives based on the research gaps in the literature review of IR and PA spectroscopy for noninvasive glucose detection. **(Chapter 1)**
- Introduction to IR and PA spectroscopy as one of the advanced techniques for noninvasive glucose detection. **(Chapter 1&2)**
- determination of the capacity of IR and PA spectroscopy for noninvasive glucose detection using QCLs . **(Chapter 1&2)**
- Development of a single wavelength MIR and PA spectroscopy for noninvasive glucose detection. **(Chapter 3)**
- Investigation into the feasibility of a single wavelength MIR and PA system for noninvasive glucose detection with a detection sensitivity of $\pm 25\ mg/dL$. **(Chapter 3)**
- Achievement of a high detection accuracy using a single wavelength MIR and PA system for noninvasive glucose detection. **(Chapter 3)**
- Involvement of machine learning to develop classification models for glucose prediction using a single wavelength MIR and PA system for noninvasive glucose detection. **(Chapter 3)**

- Development of dual QCLs and PA spectroscopy for noninvasive glucose detection. **(Chapter 4)**
- Enhancement of the detection sensitivity to fulfill the FDA and Health Canada requirements for glucose detection using single and dual QCLs and PA spectroscopy for noninvasive glucose detection. **(Chapter 4)**
- Achievement of high detection accuracy in the presence of other blood components using dual QCLs and PA spectroscopy for noninvasive glucose detection. **(Chapter 4)**
- Involvement of machine learning to develop classification models for glucose prediction in the presence of other blood components using dual QCLs and PA system. **(Chapter 4)**
- Investigation into the *in vivo* measurements using a single wavelength MIR and PA spectroscopy for noninvasive glucose detection. **(Chapter 5)**
- Involvement of machine learning to develop regression models for glucose prediction in the *in vivo* measurements using a single wavelength MIR and PA spectroscopy for noninvasive glucose detection. **(Chapter 5)**

6.3 List of Publications

1. A. Aloraynan, S. Rassel, C. Xu, and D. Ban, "A single wavelength mid-infrared photoacoustic spectroscopy for noninvasive glucose detection using machine learning," Biosensors, vol. 12, no. 3, p. 166, 2022. (**Published**) [154]
2. A. Aloraynan, S. Rassel, C. Xu, and D. Ban, "Machine learning classifiers for noninvasive glucose detection using a single wavelength mid-infrared photoacoustic spectroscopy," in Biomedical Spectroscopy, Microscopy, and Imaging II, vol. 12144, pp. 97–102, SPIE, 2022. (**Published**) [156]
3. A. Aloraynan, S. Rassel, M. R. Kaysir, and D. Ban, "Dual quantum cascade lasers for noninvasive glucose detection using photoacoustic spectroscopy," Scientific Reports, vol. 13, no. 1, p. 7927, 2023. (**Published**) [157]
4. S. Rassel, M. R. Kaysir, A. Aloraynan, and D. Ban, "Non-invasive blood sugar detection by cost-effective capacitance spectroscopy," Journal of Sensors and Sensor Systems, vol. 12, no. 1, pp. 21–36, 2023. (**Published**) [158]

5. C. Xu, S. Rassel, S. Zhang, A. Aloraynan, and D. Ban, "Single-wavelength water muted photoacoustic system for detecting physiological concentrations of endogenous molecules," Biomedical optics express, vol. 12, no. 1, pp. 666–675, 2021. (**Published**) [144]

6. M. R. Kaysir, J. Song, S. Rassel, A. Aloraynan, and D. Ban, "Progress and perspectives of mid-infrared photoacoustic spectroscopy for non-invasive glucose detection," Biosensors, vol. 13, no. 7, p. 716, 2023. (**Published**) [54]

7. D. Ban, A. Aloraynan, S. Rassel, and C. Xu, "Mid-infrared Photoacoustic Spectroscopy for Noninvasive Glucose Detection Using Machine Learning," US Provisional Patent, March 2021. (**Patent**)

8. A. Aloraynan, S. Rassel, and D. Ban, "A single wavelength near-infrared photoacoustic spectroscopy for noninvasive glucose detection using machine learning," Sensors. (**Under process**)

6.4 Future Work

The future work plan is designed with the aim of improving the development of the IR and PA system for noninvasive glucose detection by implementing the following aspects:

- **Development** of a prototype for the MIR and PA system. The proposed prototype aims to reduce the cost and size by transforming the analog system into a digital one. Both analog lock-in amplifiers and function generators can be programmed in built-in PIC microcontrollers for the prototype's purpose.

- **Integration** of a NIR source, lasing at the glucose fingerprint of 1.625 μm, into the MIR and PA system as an additional light source. The water absorption in the NIR region has less water absorption than the MIR region; thus, it can penetrate deeper into the skin, reaching the blood vessels.

- **Design** of a chamber with acoustic-absorbing foams to cover the fingertip from the top during the experiments. The chamber will assist in maintaining the finger position while conducting the measurements. The acoustic-absorbing foams will help cancel the environmental acoustic noises.

- **Study** of the impact of each blood component that interferes with glucose absorption in the MIR region individually. The skin samples can simultaneously be prepared with a single blood component with glucose to study the effect of each blood component on the PA signal.

- **Improvement** of the mechanical pressure vice by installing an electric micro-linear actuator (PA-07-1-5, Progressive Automations Inc., Canada) that can apply firm and consistent pressure on the samples while conducting the measurements. Furthermore, the fingertip chamber can be attached to the linear actuator to apply pressure for the *in vivo* experiments.

- **Study** of the effect of human skin/fingertip conditions on the generated acoustic signal by the MIR source. The skin samples can be prepared at different conditions to examine the differences in the PA signal. Moreover, the different fingerprints can be 3D printed on the sample's surface to investigate the effect of the light scattering.

References

[1] "International diabetes federation."

[2] US Centers, *Notes from the Field: Deaths from Acute Hepatitis B Virus Infection Associated with Assisted Blood Glucose Monitoring in an Assisted-Living Facility*, vol. 60. North Carolina: US Centers for Disease Control and Prevention Morbidity and Mortality, Oct 2010.

[3] L. Heinemann, "Finger pricking and pain: a never ending story," *Journal of diabetes science and technology*, vol. 2, no. 5, pp. 919–921, 2008.

[4] E. J. Rayfield, M. J. Ault, G. T. Keusch, M. J. Brothers, C. Nechemias, and H. Smith, "Infection and diabetes: the case for glucose control," *The American journal of medicine*, vol. 72, no. 3, pp. 439–450, 1982.

[5] C. A. Counard, J. F. Perz, P. C. Linchangco, D. Christiansen, L. Ganova-Raeva, G. Xia, S. Jones, and M. O. Vernon, "Acute hepatitis b outbreaks related to fingerstick blood glucose monitoring in two assisted living facilities," *Journal of the American Geriatrics Society*, vol. 58, no. 2, pp. 306–311, 2010.

[6] H. K. Walker, W. D. Hall, and J. W. Hurst, *Peripheral Blood Smear–Clinical Methods: The History, Physical, and Laboratory Examinations*. Butterworths, 1990.

[7] J. Park, J. Kim, S.-Y. Kim, W. H. Cheong, J. Jang, Y.-G. Park, K. Na, Y.-T. Kim, J. H. Heo, C. Y. Lee, *et al.*, "Soft, smart contact lenses with integrations of wireless circuits, glucose sensors, and displays," *Science Advances*, vol. 4, no. 1, p. eaap9841, 2018.

[8] J. T. La Belle, A. Adams, C.-E. Lin, E. Engelschall, B. Pratt, and C. B. Cook, "Self-monitoring of tear glucose: the development of a tear based glucose sensor as an alternative to self-monitoring of blood glucose," *Chemical Communications*, vol. 52, no. 59, pp. 9197–9204, 2016.

[9] V. K. L. Shanbhag and K. Prasad, "Graphene based sensors in the detection of glucose in saliva–a promising emerging modality to diagnose diabetes mellitus," *Analytical Methods*, vol. 8, no. 33, pp. 6255–6259, 2016.

[10] V. Srinivasan, V. K. Pamula, and R. B. Fair, "An integrated digital microfluidic lab-on-a-chip for clinical diagnostics on human physiological fluids," *Lab on a Chip*, vol. 4, no. 4, pp. 310–315, 2004.

[11] A. S. Panchbhai, "Correlation of salivary glucose level with blood glucose level in diabetes mellitus," *Journal of oral & maxillofacial research*, vol. 3, no. 3, 2012.

[12] G. Steil, K. Rebrin, F. Hariri, S. Jinagonda, S. Tadros, C. Darwin, and M. Saad, "Interstitial fluid glucose dynamics during insulin-induced hypoglycaemia," *Diabetologia*, vol. 48, no. 9, pp. 1833–1840, 2005.

[13] G. J. Tortora and B. H. Derrickson, *Principles of anatomy and physiology*. John Wiley & Sons, 2018.

[14] S. N. Thennadil, J. L. Rennert, B. J. Wenzel, K. H. Hazen, T. L. Ruchti, and M. B. Block, "Comparison of glucose concentration in interstitial fluid, and capillary and venous blood during rapid changes in blood glucose levels," *Diabetes Technology & Therapeutics*, vol. 3, no. 3, pp. 357–365, 2001.

[15] R. Pandey, S. K. Paidi, T. A. Valdez, C. Zhang, N. Spegazzini, R. R. Dasari, and I. Barman, "Noninvasive monitoring of blood glucose with raman spectroscopy," *Accounts of chemical research*, vol. 50, no. 2, pp. 264–272, 2017.

[16] V. P. Rachim and W.-Y. Chung, "Wearable-band type visible-near infrared optical biosensor for non-invasive blood glucose monitoring," *Sensors and Actuators B: Chemical*, vol. 286, pp. 173–180, 2019.

[17] K. Maruo, M. Tsurugi, J. Chin, T. Ota, H. Arimoto, Y. Yamada, M. Tamura, M. Ishii, and Y. Ozaki, "Noninvasive blood glucose assay using a newly developed near-infrared system," *IEEE Journal of selected topics in quantum electronics*, vol. 9, no. 2, pp. 322–330, 2003.

[18] R. Zhang, S. Liu, H. Jin, Y. Luo, Z. Zheng, F. Gao, and Y. Zheng, "Noninvasive electromagnetic wave sensing of glucose," *Sensors*, vol. 19, no. 5, p. 1151, 2019.

[19] J. Hanna, M. Bteich, Y. Tawk, A. H. Ramadan, B. Dia, F. A. Asadallah, A. Eid, R. Kanj, J. Costantine, and A. A. Eid, "Noninvasive, wearable, and tunable electromagnetic multisensing system for continuous glucose monitoring, mimicking vasculature anatomy," *Science Advances*, vol. 6, no. 24, p. eaba5320, 2020.

[20] R. O. Esenaliev, K. V. Larin, I. V. Larina, and M. Motamedi, "Noninvasive monitoring of glucose concentration with optical coherence tomography," *Optics letters*, vol. 26, no. 13, pp. 992–994, 2001.

[21] R. V. Kuranov, V. V. Sapozhnikova, D. S. Prough, I. Cicenaite, and R. O. Esenaliev, "Prediction capability of optical coherence tomography for blood glucose concentration monitoring," 2007.

[22] X. Guo, A. Mandelis, A. Matvienko, K. Sivagurunathan, and B. Zinman, "Wavelength-modulated differential laser photothermal radiometry for blood glucose measurements," in *Journal of Physics: Conference Series*, vol. 214, p. 012025, IOP Publishing, 2010.

[23] X. Guo, A. Mandelis, and B. Zinman, "Applications of ultrasensitive wavelength-modulated differential photothermal radiometry to noninvasive glucose detection in blood serum," *Journal of biophotonics*, vol. 6, no. 11-12, pp. 911–919, 2013.

[24] Y. Chen, S. Lu, S. Zhang, Y. Li, Z. Qu, Y. Chen, B. Lu, X. Wang, and X. Feng, "Skin-like biosensor system via electrochemical channels for noninvasive blood glucose monitoring," *Science advances*, vol. 3, no. 12, p. e1701629, 2017.

[25] T. Chang, H. Li, N. Zhang, X. Jiang, X. Yu, Q. Yang, Z. Jin, H. Meng, and L. Chang, "Highly integrated watch for noninvasive continual glucose monitoring," *Microsystems & nanoengineering*, vol. 8, no. 1, pp. 1–9, 2022.

[26] C. Hsueh, M. Janyasupab, Y. Lee, and C. Liu, "Electrochemical glucose sensors," *Encyclopedia of Applied Electrochemistry, eds Kreysa G, Ota Ki, Savinell RF (Springer, New York)*, pp. 479–485, 2014.

[27] C. Amaral and B. Wolf, "Effects of glucose in blood and skin impedance spectroscopy," in *AFRICON 2007*, pp. 1–7, IEEE, 2007.

[28] S. Ollmar, I. Nicander, P. Åberg, and J. Bolinder, "Facts and artefacts regarding correlation between skin electrical impedance spectroscopy (eis) and blood glucose," in *Journal of Physics: Conference Series*, vol. 434, p. 012071, IOP Publishing, 2013.

[29] A. Caduff, F. Dewarrat, M. Talary, G. Stalder, L. Heinemann, and Y. Feldman, "Non-invasive glucose monitoring in patients with diabetes: A novel system based on impedance spectroscopy," *Biosensors and Bioelectronics*, vol. 22, no. 5, pp. 598–604, 2006.

[30] J. Huang, Y. Zhang, and J. Wu, "Review of non-invasive continuous glucose monitoring based on impedance spectroscopy," *Sensors and Actuators A: Physical*, vol. 311, p. 112103, 2020.

[31] S. A. Weinzimer, "Analysis: Pendra: the once and future noninvasive continuous glucose monitoring device?," *Diabetes technology & therapeutics*, vol. 6, no. 4, pp. 442–444, 2004.

[32] A. Nawaz, P. Øhlckers, S. Sælid, M. Jacobsen, and M. N. Akram, "Non-invasive continuous blood glucose measurement techniques," *Journal of Bioinformatics and Diabetes*, vol. 1, no. 3, p. 01, 2016.

[33] I. Wentholt, J. Hoekstra, A. Zwart, and J. DeVries, "Pendra goes dutch: lessons for the ce mark in europe," *Diabetologia*, vol. 48, no. 6, pp. 1055–1058, 2005.

[34] O. K. Cho, Y. O. Kim, H. Mitsumaki, and K. Kuwa, "Noninvasive measurement of glucose by metabolic heat conformation method," *Clinical chemistry*, vol. 50, no. 10, pp. 1894–1898, 2004.

[35] F. Tang, X. Wang, D. Wang, and J. Li, "Non-invasive glucose measurement by use of metabolic heat conformation method," *Sensors*, vol. 8, no. 5, pp. 3335–3344, 2008.

[36] S. K. Vashist and J. H. Luong, *Point-of-care glucose detection for diabetic monitoring and management*. CRC Press, 2017.

[37] A. Tura, S. Sbrignadello, D. Cianciavicchia, G. Pacini, and P. Ravazzani, "A low frequency electromagnetic sensor for indirect measurement of glucose concentration: in vitro experiments in different conductive solutions," *Sensors*, vol. 10, no. 6, pp. 5346–5358, 2010.

[38] M. Gourzi, A. Rouane, R. Guelaz, M. Alavi, M. McHugh, M. Nadi, and P. Roth, "Non-invasive glycaemia blood measurements by electromagnetic sensor: study in static and dynamic blood circulation," *Journal of medical engineering & technology*, vol. 29, no. 1, pp. 22–26, 2005.

[39] W. Villena Gonzales, A. T. Mobashsher, and A. Abbosh, "The progress of glucose monitoring—a review of invasive to minimally and non-invasive techniques, devices and sensors," *Sensors*, vol. 19, no. 4, p. 800, 2019.

[40] G. S. Bumbrah and R. M. Sharma, "Raman spectroscopy–basic principle, instrumentation and selected applications for the characterization of drugs of abuse," *Egyptian Journal of Forensic Sciences*, vol. 6, no. 3, pp. 209–215, 2016.

[41] A. M. Enejder, T. G. Scecina, J. Oh, M. Hunter, W. Shih, S. Sasic, G. L. Horowitz, and M. S. Feld, "Raman spectroscopy for noninvasive glucose measurements," *Journal of biomedical optics*, vol. 10, no. 3, p. 031114, 2005.

[42] B. H. Malik and G. L. Coté, "Real-time, closed-loop dual-wavelength optical polarimetry for glucose monitoring," *Journal of biomedical optics*, vol. 15, no. 1, p. 017002, 2010.

[43] R. Rawer, W. Stork, and C. F. Kreiner, "Non-invasive polarimetric measurement of glucose concentration in the anterior chamber of the eye," *Graefe's Archive for Clinical and Experimental Ophthalmology*, vol. 242, no. 12, pp. 1017–1023, 2004.

[44] S. Rassel, C. Xu, S. Zhang, and D. Ban, "Noninvasive blood glucose detection using a quantum cascade laser," *Analyst*, vol. 145, no. 7, pp. 2441–2456, 2020.

[45] P. Sanchez, S. Ghosh-Dastidar, K. S. Tweden, and F. R. Kaufman, "Real-world data from the first us commercial users of an implantable continuous glucose sensor," *Diabetes Technology & Therapeutics*, vol. 21, no. 12, pp. 677–681, 2019.

[46] H. W. Siesler, Y. Ozaki, S. Kawata, and H. M. Heise, *Near-infrared spectroscopy: principles, instruments, applications*. John Wiley & Sons, 2008.

[47] M. R. Robinson, R. P. Eaton, D. M. Haaland, G. W. Koepp, E. V. Thomas, B. R. Stallard, and P. L. Robinson, "Noninvasive glucose monitoring in diabetic patients: a preliminary evaluation," *Clinical chemistry*, vol. 38, no. 9, pp. 1618–1622, 1992.

[48] M. Steiner, A. Duerkop, and O. S. Wolfbeis, "Optical methods for sensing glucose," *Chemical Society Reviews*, vol. 40, no. 9, pp. 4805–4839, 2011.

[49] M. A. Franceschini, S. Fantini, A. Cerussi, B. Barbieri, B. Chance, and E. Gratton, "The effect of water in the quantitation of hemoglobin concentration in a tissue-like phantom by near-infrared spectroscopy," in *Biomedical Optical Spectroscopy and Diagnostics*, p. AP16, Optical Society of America, 1996.

[50] A. Edelmann, C. Ruzicka, J. Frank, B. Lendl, W. Schrenk, E. Gornik, and G. Strasser, "Towards functional group-specific detection in high-performance liquid chromatography using mid-infrared quantum cascade lasers," *Journal of Chromatography A*, vol. 934, no. 1-2, pp. 123–128, 2001.

[51] K. J. Jeon, I. D. Hwang, S. J. Hahn, and G. Yoon, "Comparison between transmittance and reflectance measurements in glucose determination using near infrared spectroscopy," *Journal of Biomedical Optics*, vol. 11, no. 1, p. 014022, 2006.

[52] A. Rosencwaig and A. Gersho, "Theory of the photoacoustic effect with solids," *Journal of Applied Physics*, vol. 47, no. 1, pp. 64–69, 1976.

[53] H. A. MacKenzie, H. S. Ashton, S. Spiers, Y. Shen, S. S. Freeborn, J. Hannigan, J. Lindberg, and P. Rae, "Advances in photoacoustic noninvasive glucose testing," *Clinical chemistry*, vol. 45, no. 9, pp. 1587–1595, 1999.

[54] M. R. Kaysir, J. Song, S. Rassel, A. Aloraynan, and D. Ban, "Progress and perspectives of mid-infrared photoacoustic spectroscopy for non-invasive glucose detection," *Biosensors*, vol. 13, no. 7, p. 716, 2023.

[55] E. L. Holthoff, D. A. Heaps, and P. M. Pellegrino, "Development of a mems-scale photoacoustic chemical sensor using a quantum cascade laser," *IEEE Sensors Journal*, vol. 10, no. 3, pp. 572–577, 2010.

[56] P. Beard, "Biomedical photoacoustic imaging," *Interface focus*, vol. 1, no. 4, pp. 602–631, 2011.

[57] T. Repenko, S. Fokong, L. De Laporte, D. Go, F. Kiessling, T. Lammers, and A. J. Kuehne, "Water-soluble dopamine-based polymers for photoacoustic imaging," *Chemical communications*, vol. 51, no. 28, pp. 6084–6087, 2015.

[58] R. Zhang, Y. Luo, H. Jin, F. Gao, and Y. Zheng, "Time-domain photoacoustic waveform analysis for glucose measurement," *Analyst*, 2020.

[59] J. Y. Sim, C.-G. Ahn, E. Jeong, and B. K. Kim, "Photoacoustic spectroscopy that uses a resonant characteristic of a microphone for in vitro measurements of glucose concentration," in *2016 38th Annual International Conference of the IEEE Engineering in Medicine and Biology Society (EMBC)*, pp. 4861–4864, IEEE, 2016.

[60] C. Pratywi, S. Marantika, P. Dwijananti, *et al.*, "Characterization of starch degradation during simple heating for bioethanol production from the avocado seed," in *Materials Science and Engineering Conference Series*, vol. 432, p. 012042, 2018.

[61] W. B. Martin, S. B. Mirov, and R. Venugopalan, "Using two discrete frequencies within the middle infrared to quantitatively determine glucose in serum," *Journal of Biomedical Optics*, vol. 7, no. 4, pp. 613–618, 2002.

[62] S. K. Vashist, "Non-invasive glucose monitoring technology in diabetes management: A review," *Analytica chimica acta*, vol. 750, pp. 16–27, 2012.

[63] C.-F. So, K.-S. Choi, T. K. Wong, and J. W. Chung, "Recent advances in noninvasive glucose monitoring," *Medical Devices (Auckland, NZ)*, vol. 5, p. 45, 2012.

[64] M. Brandstetter, L. Volgger, A. Genner, C. Jungbauer, and B. Lendl, "Direct determination of glucose, lactate and triglycerides in blood serum by a tunable quantum cascade laser-based mid-ir sensor," *Applied Physics B*, vol. 110, no. 2, pp. 233–239, 2013.

[65] K. Yoshioka, S. Kino, and Y. Matsuura, "Blood glucose measurement with multiple quantum cascade lasers using hollow-optical fiber-based atr spectroscopy," in *Optical Fibers and Sensors for Medical Diagnostics and Treatment Applications XVIII*, vol. 10488, p. 104880D, International Society for Optics and Photonics, 2018.

[66] J. Tenhunen, H. Kopola, and R. Myllylä, "Non-invasive glucose measurement based on selective near infrared absorption; requirements on instrumentation and spectral range," *Measurement*, vol. 24, no. 3, pp. 173–177, 1998.

[67] J. J. Burmeister, M. A. Arnold, and G. W. Small, "Infrared spectroscopy spectroscopic considerations for noninvasive blood glucose measurements with near infrared spectroscopy," *LEOS LEOS®*, vol. 61, p. 6, 1998.

[68] K. H. Hazen, M. A. Arnold, and G. W. Small, "Measurement of glucose and other analytes in undiluted human serum with near-infrared transmission spectroscopy," *Analytica Chimica Acta*, vol. 371, no. 2-3, pp. 255–267, 1998.

[69] A. A. Al-Mbaideen, T. Rahman, and M. Benaissa, "Determination of glucose concentration from near-infrared spectra using principle component regression coupled with digital bandpass filter," in *2010 IEEE Workshop On Signal Processing Systems*, pp. 243–248, IEEE, 2010.

[70] E.-Y. Park, J. Baik, H. Kim, S.-M. Park, and C. Kim, "Ultrasound-modulated optical glucose sensing using a 1645 nm laser," *Scientific Reports*, vol. 10, no. 1, pp. 1–9, 2020.

[71] R. A. Shaw and H. H. Mantsch, "Infrared spectroscopy of biological fluids in clinical and diagnostic analysis," *Encyclopedia of Analytical Chemistry: Applications, Theory and Instrumentation*, 2006.

[72] L. Tang, S. J. Chang, C.-J. Chen, and J.-T. Liu, "Non-invasive blood glucose monitoring technology: a review," *Sensors*, vol. 20, no. 23, p. 6925, 2020.

[73] J. Yadav, A. Rani, V. Singh, and B. M. Murari, "Prospects and limitations of non-invasive blood glucose monitoring using near-infrared spectroscopy," *Biomedical signal processing and control*, vol. 18, pp. 214–227, 2015.

[74] M. R. Riley and H. M. Crider, "The effect of analyte concentration range on measurement errors obtained by nir spectroscopy," *Talanta*, vol. 52, no. 3, pp. 473–484, 2000.

[75] J. Kottmann, J. M. Rey, and M. W. Sigrist, "Mid-infrared photoacoustic detection of glucose in human skin: towards non-invasive diagnostics," *Sensors*, vol. 16, no. 10, p. 1663, 2016.

[76] H. Von Lilienfeld-Toal, M. Weidenmüller, A. Xhelaj, and W. Mäntele, "A novel approach to non-invasive glucose measurement by mid-infrared spectroscopy: The combination of quantum cascade lasers (qcl) and photoacoustic detection," *Vibrational spectroscopy*, vol. 38, no. 1-2, pp. 209–215, 2005.

[77] J. Kottmann, J. M. Rey, J. Luginbühl, E. Reichmann, and M. W. Sigrist, "Glucose sensing in human epidermis using mid-infrared photoacoustic detection," *Biomedical optics express*, vol. 3, no. 4, pp. 667–680, 2012.

[78] M. Pleitez, H. Von Lilienfeld-Toal, and W. Mäntele, "Infrared spectroscopic analysis of human interstitial fluid in vitro and in vivo using ft-ir spectroscopy and pulsed quantum cascade lasers (qcl): Establishing a new approach to non invasive glucose measurement," *Spectrochimica Acta Part A: Molecular and Biomolecular Spectroscopy*, vol. 85, no. 1, pp. 61–65, 2012.

[79] J. Y. Sim, C.-G. Ahn, E.-J. Jeong, and B. K. Kim, "In vivo microscopic photoacoustic spectroscopy for non-invasive glucose monitoring invulnerable to skin secretion products," *Scientific reports*, vol. 8, no. 1, pp. 1–11, 2018.

[80] R. Maulini, *Broadly tunable mid-infrared quantum cascade lasers for spectroscopic applications*. PhD thesis, Université de Neuchâtel, 2006.

[81] J. Kottmann, U. Grob, J. M. Rey, and M. W. Sigrist, "Mid-infrared fiber-coupled photoacoustic sensor for biomedical applications," *Sensors*, vol. 13, no. 1, pp. 535–549, 2013.

[82] M. A. Pleitez, T. Lieblein, A. Bauer, O. Hertzberg, H. Von Lilienfeld-Toal, and W. Mantele, "In vivo noninvasive monitoring of glucose concentration in human epidermis by mid-infrared pulsed photoacoustic spectroscopy," *Analytical chemistry*, vol. 85, no. 2, pp. 1013–1020, 2013.

[83] U.S. Food & Drug Administration (FDA)., "Blood glucose monitoring devices," May 2019.

[84] Health Canada, "New requirements for medical device licence applications for lancing devices and blood glucose monitoring systems," Sept 2014.

[85] W. L. Clarke, D. Cox, L. A. Gonder-Frederick, W. Carter, and S. L. Pohl, "Evaluating clinical accuracy of systems for self-monitoring of blood glucose," *Diabetes care*, vol. 10, no. 5, pp. 622–628, 1987.

[86] ISO, "15197:2013."

[87] Health Canada, "Notice: New requirements for medical device licence applications for lancing devices and blood glucose monitoring systems," Sep 2014.

[88] A. Krier, *Mid-infrared semiconductor optoelectronics*, vol. 118. Springer, 2007.

[89] A. Schwaighofer, M. Brandstetter, and B. Lendl, "Quantum cascade lasers (qcls) in biomedical spectroscopy," *Chemical Society Reviews*, vol. 46, no. 19, pp. 5903–5924, 2017.

[90] M. Razeghi, *Quantum Cascade Lasers*, pp. 271–319. Boston, MA: Springer US, 2010.

[91] J. Faist, F. Capasso, D. L. Sivco, C. Sirtori, A. L. Hutchinson, and A. Y. Cho, "Quantum cascade laser," *Science*, vol. 264, no. 5158, pp. 553–556, 1994.

[92] M. Beck, D. Hofstetter, T. Aellen, J. Faist, U. Oesterle, M. Ilegems, E. Gini, and H. Melchior, "Continuous wave operation of a mid-infrared semiconductor laser at room temperature," *Science*, vol. 295, no. 5553, pp. 301–305, 2002.

[93] M. S. Vitiello, G. Scalari, B. Williams, and P. De Natale, "Quantum cascade lasers: 20 years of challenges," *Optics express*, vol. 23, no. 4, pp. 5167–5182, 2015.

[94] R. Pecharromán-Gallego, "An overview on quantum cascade lasers: origins and development," in *Quantum Cascade Lasers*, IntechOpen, 2017.

[95] K. Namjou, S. Cai, E. A. Whittaker, J. Faist, C. Gmachl, F. Capasso, D. L. Sivco, and A. Y. Cho, "Sensitive absorption spectroscopy with a room-temperature distributed-feedback quantum-cascade laser," *Optics letters*, vol. 23, no. 3, pp. 219–221, 1998.

[96] G. Luo, C. Peng, H. Le, S. Pei, W.-Y. Hwang, B. Ishaug, J. Um, J. N. Baillargeon, and C.-H. Lin, "Grating-tuned external-cavity quantum-cascade semiconductor lasers," *Applied Physics Letters*, vol. 78, no. 19, pp. 2834–2836, 2001.

[97] L. Hvozdara, N. Pennington, M. Kraft, M. Karlowatz, and B. Mizaikoff, "Quantum cascade lasers for mid-infrared spectroscopy," *Vibrational Spectroscopy*, vol. 30, no. 1, pp. 53–58, 2002.

[98] Y.-H. Kim, A. Ghanem, and W. Higuchi, "Model studies of epidermal permeability.," in *Seminars in Dermatology*, vol. 11, pp. 145–156, 1992.

[99] J. M. Abdo, N. A. Sopko, and S. M. Milner, "The applied anatomy of human skin: a model for regeneration," *Wound Medicine*, vol. 28, p. 100179, 2020.

[100] X. Guo, A. Mandelis, and B. Zinman, "Noninvasive glucose detection in human skin using wavelength modulated differential laser photothermal radiometry," *Biomedical optics express*, vol. 3, no. 11, pp. 3012–3021, 2012.

[101] C. P. Lawrence, A. Rodger, and R. G. Compton, *Foundations of physical chemistry*. No. 40, Oxford University Press, USA, 1996.

[102] A. P. Michel, S. Liakat, K. Bors, and C. F. Gmachl, "In vivo measurement of mid-infrared light scattering from human skin," *Biomedical optics express*, vol. 4, no. 4, pp. 520–530, 2013.

[103] M. A. Pleitez, T. Lieblein, A. Bauer, O. Hertzberg, H. Von Lilienfeld-Toal, and W. Mäntele, "Windowless ultrasound photoacoustic cell for in vivo mid-ir spectroscopy of human epidermis: Low interference by changes of air pressure, temperature, and humidity caused by skin contact opens the possibility for a non-invasive monitoring of glucose in the interstitial fluid," *Review of Scientific Instruments*, vol. 84, no. 8, p. 084901, 2013.

[104] A. Schönhals, H. Tholl, M. Glasmacher, N. Kröger-Lui, A. Pucci, and W. Petrich, "Optical properties of porcine dermis in the mid-infrared absorption band of glucose," *Analyst*, vol. 142, no. 8, pp. 1235–1243, 2017.

[105] S. Liakat, A. P. Michel, K. A. Bors, and C. F. Gmachl, "Mid-infrared (λ= 8.4–9.9 μ m) light scattering from porcine tissue," *Applied Physics Letters*, vol. 101, no. 9, p. 093705, 2012.

[106] R. R. Anderson, J. A. Parrish, *et al.*, "The optics of human skin.," *Journal of investigative dermatology*, vol. 77, no. 1, pp. 13–19, 1981.

[107] K. Xu, Q. Qiu, J. Jiang, and X. Yang, "Non-invasive glucose sensing with near-infrared spectroscopy enhanced by optical measurement conditions reproduction technique," *Optics and lasers in engineering*, vol. 43, no. 10, pp. 1096–1106, 2005.

[108] Y. Uwadaira, N. Adachi, A. Ikehata, and S. Kawano, "Factors affecting the accuracy of non-invasive blood glucose measurement by short-wavelength near infrared spectroscopy in the determination of the glycaemic index of foods," *Journal of Near Infrared Spectroscopy*, vol. 18, no. 5, pp. 291–300, 2010.

[109] R. Liu, B. Deng, W. Chen, and K. Xu, "Next step of non-invasive glucose monitor by nir technique from the well controlled measuring condition and results," *optical and quantum electronics*, vol. 37, no. 13-15, pp. 1305–1317, 2005.

[110] R. Liu, W. Chen, Y. Chen, and K. Xu, "Influence of temperature on the precision of noninvasive glucose sensing by near-infrared spectroscopy," in *Optical Diagnostics and Sensing VIII*, vol. 6863, p. 68630Q, International Society for Optics and Photonics, 2008.

[111] N. Oliver, C. Toumazou, A. Cass, and D. Johnston, "Glucose sensors: a review of current and emerging technology," *Diabetic Medicine*, vol. 26, no. 3, pp. 197–210, 2009.

[112] K. Maruo and Y. Yamada, "Near-infrared noninvasive blood glucose prediction without using multivariate analyses: introduction of imaginary spectra due to scattering change in the skin," *Journal of biomedical optics*, vol. 20, no. 4, p. 047003, 2015.

[113] D. F. Swinehart, "The beer-lambert law," *Journal of chemical education*, vol. 39, no. 7, p. 333, 1962.

[114] U. Müller, B. Mertes, C. Fischbacher, K. Jageman, and K. Danzer, "Non-invasive blood glucose monitoring by means of near infrared spectroscopy: methods for improving the reliability of the calibration models," *The International journal of artificial organs*, vol. 20, no. 5, pp. 285–290, 1997.

[115] L. A. Nelson, J. C. McCann, A. W. Loepke, J. Wu, B. Ben-Dor, and D. C. Kurth, "Development and validation of a multiwavelength spatial domain near-infrared oximeter to detect cerebral hypoxia-ischemia," *Journal of biomedical optics*, vol. 11, no. 6, p. 064022, 2006.

[116] D. Kliger, *Ultrasensitive laser spectroscopy*. Elsevier, 2012.

[117] W. B. Martin, S. Mirov, and R. Venugopalan, "Middle infrared, quantum cascade laser optoelectronic absorption system for monitoring glucose in serum," *Applied spectroscopy*, vol. 59, no. 7, pp. 881–884, 2005.

[118] S. Schaden, A. Domínguez-Vidal, and B. Lendl, "Simultaneous measurement of two compounds in aqueous solution with dual quantum cascade laser absorption spectroscopy," *Applied Physics B*, vol. 83, no. 1, pp. 135–139, 2006.

[119] A. Lambrecht, T. Beyer, K. Hebestreit, R. Mischler, and W. Petrich, "Continuous glucose monitoring by means of fiber-based, mid-infrared laser spectroscopy," *Applied spectroscopy*, vol. 60, no. 7, pp. 729–736, 2006.

[120] M. Brandstetter, A. Genner, K. Anic, and B. Lendl, "Tunable external cavity quantum cascade laser for the simultaneous determination of glucose and lactate in aqueous phase," *Analyst*, vol. 135, no. 12, pp. 3260–3265, 2010.

[121] C. Vrančić, A. Fomichova, N. Gretz, C. Herrmann, S. Neudecker, A. Pucci, and W. Petrich, "Continuous glucose monitoring by means of mid-infrared transmission laser spectroscopy in vitro," *Analyst*, vol. 136, no. 6, pp. 1192–1198, 2011.

[122] M. Brandstetter and B. Lendl, "Tunable mid-infrared lasers in physical chemosensors towards the detection of physiologically relevant parameters in biofluids," *Sensors and Actuators B: Chemical*, vol. 170, pp. 189–195, 2012.

[123] M. Brandstetter, T. Sumalowitsch, A. Genner, A. E. Posch, C. Herwig, A. Drolz, V. Fuhrmann, T. Perkmann, and B. Lendl, "Reagent-free monitoring of multiple clinically relevant parameters in human blood plasma using a mid-infrared quantum cascade laser based sensor system," *Analyst*, vol. 138, no. 14, pp. 4022–4028, 2013.

[124] S. Liakat, K. A. Bors, T.-Y. Huang, A. P. Michel, E. Zanghi, and C. F. Gmachl, "In vitro measurements of physiological glucose concentrations in biological fluids using mid-infrared light," *Biomedical optics express*, vol. 4, no. 7, pp. 1083–1090, 2013.

[125] S. Liakat, K. A. Bors, L. Xu, C. M. Woods, J. Doyle, and C. F. Gmachl, "Noninvasive in vivo glucose sensing on human subjects using mid-infrared light," *Biomedical optics express*, vol. 5, no. 7, pp. 2397–2404, 2014.

[126] C. Vrancic, N. Kroger, N. Gretz, S. Neudecker, A. Pucci, and W. Petrich, "A quantitative look inside the body: minimally invasive infrared analysis in vivo," *Analytical chemistry*, vol. 86, no. 21, pp. 10511–10514, 2014.

[127] K. Haase, N. Kröger-Lui, A. Pucci, A. Schönhals, and W. Petrich, "Advancements in quantum cascade laser-based infrared microscopy of aqueous media," *Faraday discussions*, vol. 187, pp. 119–134, 2016.

[128] R. Kasahara, S. Kino, S. Soyama, and Y. Matsuura, "Noninvasive glucose monitoring using mid-infrared absorption spectroscopy based on a few wavenumbers," *Biomedical optics express*, vol. 9, no. 1, pp. 289–302, 2018.

[129] M. Grafen, S. Delbeck, H. Busch, H. Heise, and A. Ostendorf, "Evaluation and benchmarking of an ec-qcl-based mid-infrared spectrometer for monitoring metabolic blood parameters in critical care units," in *Optical Diagnostics and Sensing XVIII: Toward Point-of-Care Diagnostics*, vol. 10501, p. 105010A, International Society for Optics and Photonics, 2018.

[130] J. Haas, E. V. Catalán, P. Piron, M. Karlsson, and B. Mizaikoff, "Infrared spectroscopy based on broadly tunable quantum cascade lasers and polycrystalline diamond waveguides," *Analyst*, vol. 143, no. 21, pp. 5112–5119, 2018.

[131] A. Werth, S. Liakat, A. Dong, C. M. Woods, and C. F. Gmachl, "Implementation of an integrating sphere for the enhancement of noninvasive glucose detection using quantum cascade laser spectroscopy," *Applied Physics B*, vol. 124, no. 5, p. 75, 2018.

[132] K. Isensee, N. Müller, A. Pucci, and W. Petrich, "Towards a quantum cascade laser-based implant for the continuous monitoring of glucose," *Analyst*, vol. 143, no. 24, pp. 6025–6036, 2018.

[133] Y. Matsuura and T. Koyama, "Non-invasive blood glucose measurement using quantum cascade lasers," in *Quantum Sensing and Nano Electronics and Photonics XVI*, vol. 10926, p. 1092606, International Society for Optics and Photonics, 2019.

[134] J. Y. Chen, Q. Zhou, G. Xu, R. T. Wang, E. G. Tai, L. Xie, Q. Zhang, Y. Guan, and X. Huang, "Non-invasive blood glucose measurement of 95% certainty by pressure regulated mid-ir," *Talanta*, vol. 197, pp. 211–217, 2019.

[135] T. Lubinski, B. Plotka, S. Janik, L. Canini, and W. Mäntele, "Evaluation of a novel noninvasive blood glucose monitor based on mid-infrared quantum cascade laser technology and photothermal detection," *Journal of Diabetes Science and Technology*, vol. 15, no. 1, pp. 6–10, 2021.

[136] A. Bauer, O. Hertzberg, A. Küderle, D. Strobel, M. A. Pleitez, and W. Mäntele, "Ir-spectroscopy of skin in vivo: Optimal skin sites and properties for non-invasive glucose measurement by photoacoustic and photothermal spectroscopy," *Journal of biophotonics*, vol. 11, no. 1, p. e201600261, 2018.

[137] J. Yadav, A. Rani, V. Singh, and B. Mohan Murari, "Investigations on multisensor-based noninvasive blood glucose measurement system," *Journal of Medical Devices*, vol. 11, no. 3, 2017.

[138] T. Liu, Z. Ren, C. Zhang, and G. Liu, "Combined effect of multiple factors on the photoacoustic detection of glucose solution based on neural networks," in *AOPC 2020: Optical Spectroscopy and Imaging; and Biomedical Optics*, vol. 11566, p. 115660W, International Society for Optics and Photonics, 2020.

[139] Y. Zhu, "Automatic detection of anomalies in blood glucose using a machine learning approach," *Journal of Communications and Networks*, vol. 13, no. 2, pp. 125–131, 2011.

[140] A. Z. Woldaregay, E. Årsand, T. Botsis, D. Albers, L. Mamykina, and G. Hartvigsen, "Data-driven blood glucose pattern classification and anomalies detection: machine-learning applications in type 1 diabetes," *Journal of medical Internet research*, vol. 21, no. 5, p. e11030, 2019.

[141] J. A. Carter, C. S. Long, B. P. Smith, T. L. Smith, and G. L. Donati, "Combining elemental analysis of toenails and machine learning techniques as a non-invasive diagnostic tool for the robust classification of type-2 diabetes," *Expert Systems with Applications*, vol. 115, pp. 245–255, 2019.

[142] I. L. Jernelv, D. R. Hjelme, Y. Matsuura, and A. Aksnes, "Convolutional neural networks for classification and regression analysis of one-dimensional spectral data," *arXiv preprint arXiv:2005.07530*, 2020.

[143] M. Shokrekhodaei, D. P. Cistola, R. C. Roberts, and S. Quinones, "Non-invasive glucose monitoring using optical sensor and machine learning techniques for diabetes applications," *IEEE Access*, vol. 9, pp. 73029–73045, 2021.

[144] C. Xu, S. Rassel, S. Zhang, A. Aloraynan, and D. Ban, "Single-wavelength water muted photoacoustic system for detecting physiological concentrations of endogenous molecules," *Biomedical optics express*, vol. 12, no. 1, pp. 666–675, 2021.

[145] COMSOL Multiphysics®, "COMSOL AB," *v5.3a*, Stockholm, Sweden.

[146] J. J. Burmeister, H. Chung, and M. A. Arnold, "Phantoms for noninvasive blood glucose sensing with near infrared transmission spectroscopy," *Photochemistry and photobiology*, vol. 67, no. 1, pp. 50–55, 1998.

[147] V. V. Tuchin, A. Bashkatov, E. Genina, V. Kochubey, V. Lychagov, S. Portnov, N. Trunina, D. Miller, S. Cho, H. Oh, *et al.*, "Finger tissue model and blood perfused skin tissue phantom," in *Dynamics and Fluctuations in Biomedical Photonics VIII*, vol. 7898, p. 78980Z, International Society for Optics and Photonics, 2011.

[148] M. A. Arnold, J. J. Burmeister, and G. W. Small, "Phantom glucose calibration models from simulated noninvasive human near-infrared spectra," *Analytical chemistry*, vol. 70, no. 9, pp. 1773–1781, 1998.

[149] M. Lazebnik, E. L. Madsen, G. R. Frank, and S. C. Hagness, "Tissue-mimicking phantom materials for narrowband and ultrawideband microwave applications," *Physics in Medicine & Biology*, vol. 50, no. 18, p. 4245, 2005.

[150] T. K. Ho, "The random subspace method for constructing decision forests," *IEEE transactions on pattern analysis and machine intelligence*, vol. 20, no. 8, pp. 832–844, 1998.

[151] E. I. Georga, D. I. Fotiadis, and S. K. Tigas, *Personalized Predictive Modeling in Type 1 Diabetes*. Academic Press, 2017.

[152] S. Delbeck, T. Vahlsing, S. Leonhardt, G. Steiner, and H. M. Heise, "Non-invasive monitoring of blood glucose using optical methods for skin spectroscopy—opportunities and recent advances," *Analytical and bioanalytical chemistry*, vol. 411, no. 1, pp. 63–77, 2019.

[153] I. L. Jernelv, K. Strøm, D. R. Hjelme, and A. Aksnes, "Infrared spectroscopy with a fiber-coupled quantum cascade laser for attenuated total reflection measurements towards biomedical applications," *Sensors*, vol. 19, no. 23, p. 5130, 2019.

[154] A. Aloraynan, S. Rassel, C. Xu, and D. Ban, "A single wavelength mid-infrared photoacoustic spectroscopy for noninvasive glucose detection using machine learning," *Biosensors*, vol. 12, no. 3, p. 166, 2022.

[155] L. Breiman, "Bagging predictors," *Machine learning*, vol. 24, pp. 123–140, 1996.

[156] A. Aloraynan, S. Rassel, C. Xu, and D. Ban, "Machine learning classifiers for noninvasive glucose detection using a single wavelength mid-infrared photoacoustic spectroscopy," in *Biomedical Spectroscopy, Microscopy, and Imaging II*, vol. 12144, pp. 97–102, SPIE, 2022.

[157] A. Aloraynan, S. Rassel, M. R. Kaysir, and D. Ban, "Dual quantum cascade lasers for noninvasive glucose detection using photoacoustic spectroscopy," *Scientific Reports*, vol. 13, no. 1, p. 7927, 2023.

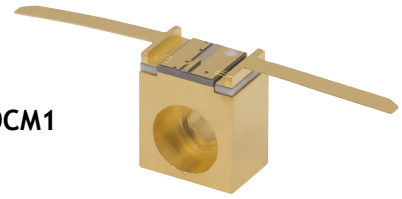
[158] S. Rassel, M. R. Kaysir, A. Aloraynan, and D. Ban, "Non-invasive blood sugar detection by cost-effective capacitance spectroscopy," *Journal of Sensors and Sensor Systems*, vol. 12, no. 1, pp. 21–36, 2023.

APPENDICES

Appendix A

Specification Sheets for the QCLs

Quantum Cascade Laser, 60 mW, CWL Between 9 and 10 µm



QD9500CM1

Description

The QD9500CM1 is a single spatial mode, single longitudinal mode, Distributed Feedback Quantum Cascade Laser designed and manufactured by Thorlabs. This laser operates in Continuous Wave (CW) mode at room temperature. The QD9500CM1 is mounted on an open heatsink C-mount package with both the cathode and the anode isolated from the heatsink base. This discrete semiconductor laser is a compact light source suited to many applications. There is no monitor photodiode.

Specifications

QD9500CM1	
LD Reverse Voltage (Max)	1 V
PD Reverse Voltage (Max)	N/A
Absolute Max Current	Varies Between Devices[a]
Absolute Max Output Power	300 mW
Operating Temperature[b]	15 to 50 °C
Storage Temperature[b]	-40 to 85 °C

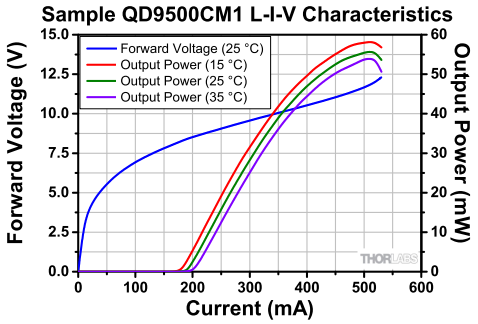
[a]The absolute maximum current is determined on a device-by-device basis and is listed on the device's data sheet.

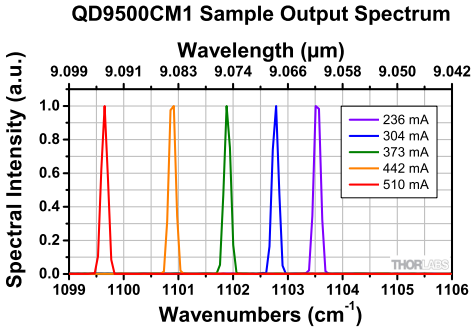
[b]Non-condensing environment. Single mode performance is tested and guaranteed at 25 °C.

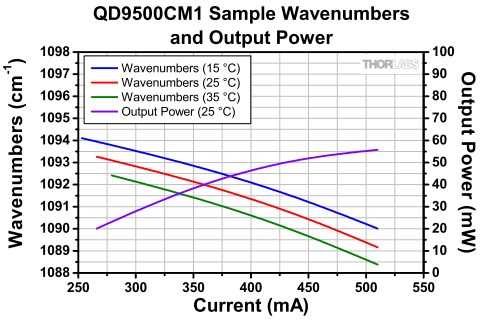
T_{Case} = 25 °C, CW Operation

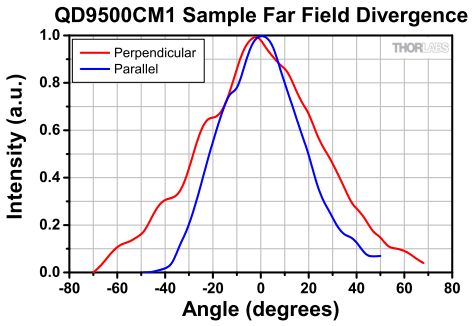
QD9500CM1				
	Symbol	**Min**	**Typical**	**Max**
Wavelength at Minimum Operating Current	λ_c	9.00 µm	-	10.00 µm
Tuning Range	TR	1.5 cm^{-1}	2.5 cm^{-1}	-
Temperature Tuning	$\Delta\bar{\nu}/\Delta T$	-	-0.08 cm^{-1}/ °C	-
Side Mode Suppression	SMSR	20 dB	-	-
Optical Output Power	P_{out}	10 mW	60 mW	-
Operating Current	I_{pp}	-	-	800 mA
Threshold Current	I_{TH}	-	300 mA	-
Forward Voltage	V_F	-	9.5 V	14.0 V
Perpendicular Beam Divergence Angle (FWHM)	$\theta_\perp$	-	55°	-
Parallel Beam Divergence Angle (FWHM)	$\theta_\parallel$	-	40°	-
Slope Efficiency, Front Facet	$\Delta P/\Delta I$	-	0.3 W/A	-

Sample Performance Plots



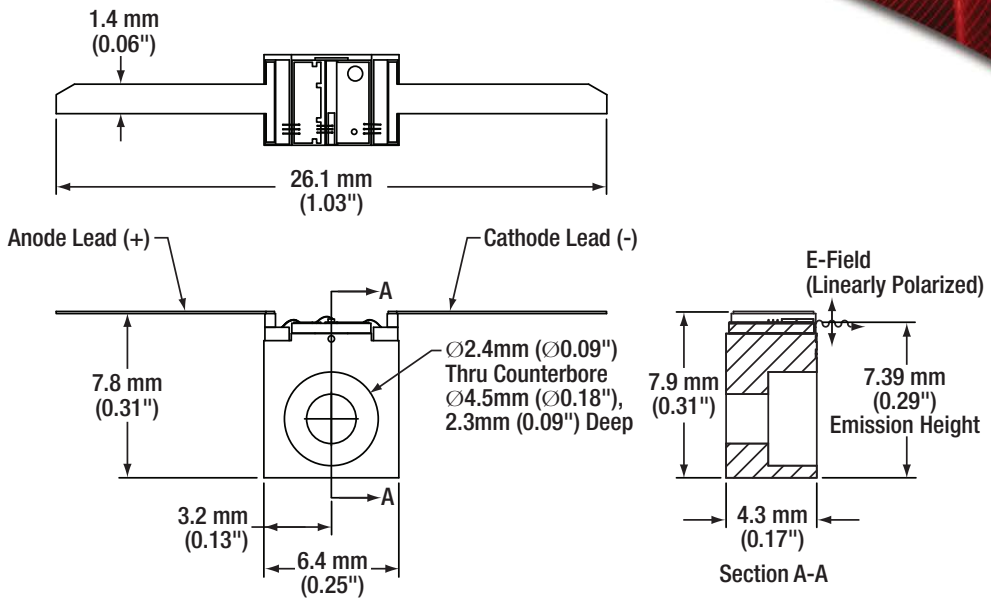






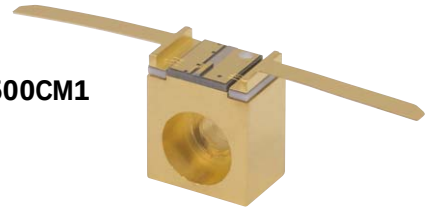
Far field divergence values are measured at 25 °C and at a distance of 89.4 mm from the laser. The detector's aperture is Ø10 mm, and the sampling step size is 3°. The angle subtended by the detector is 6.4°.

Drawings for QD9500CM1



Quantum Cascade Laser, 40 mW, CWL between 10 and 11 µm

QD10500CM1



Description

The QD10500CM1 is a single spatial mode, single longitudinal mode, Distributed Feedback Quantum Cascade Laser designed and manufactured by Thorlabs. This laser operates in Continuous Wave (CW) mode at room temperature. The QD10500CM1 is mounted on an open heatsink C-mount package with both the cathode and the anode isolated from the heatsink base. This discrete semiconductor laser is a compact light source suited to many applications. There is no monitor photodiode.

Specifications

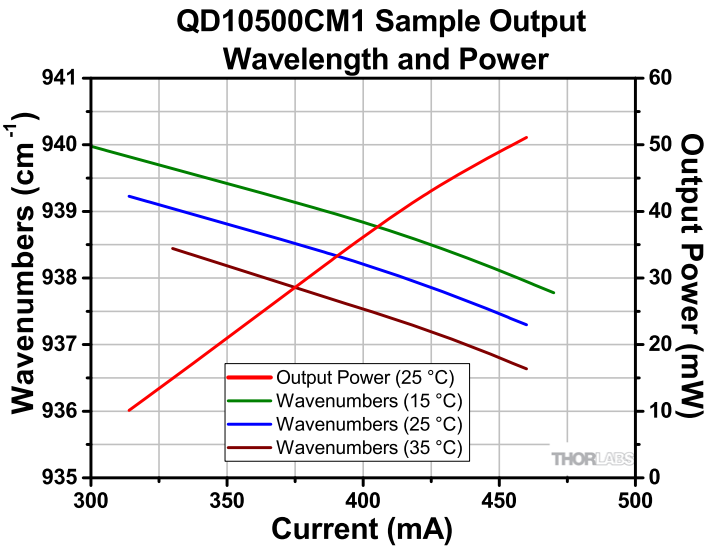
QD10500CM1	
LD Reverse Voltage (Max)	1 V
PD Reverse Voltage (Max)	N/A
Absolute Max Current	Varies Between Devices[a]
Absolute Max Power	200 mW
Operating Temperature[b]	15 to 50 °C
Storage Temperature[b]	-40 to 85 °C

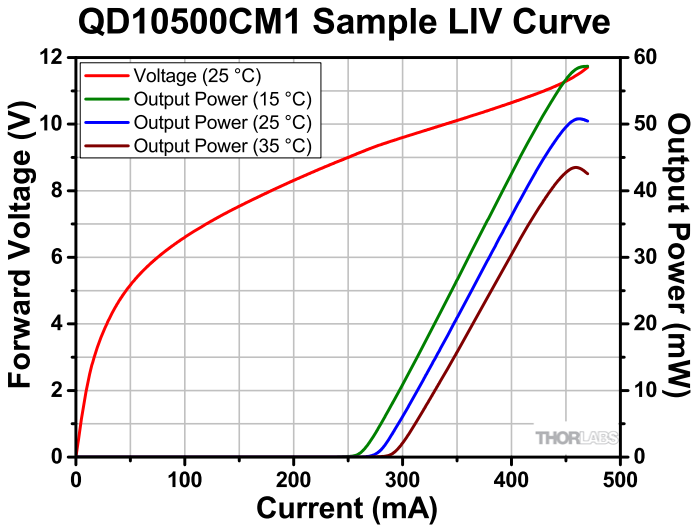
[a]The absolute maximum current is determined on a device-by-device basis and is listed on the device's data sheet.
[b]Non-Condensing Environment

T_{Case} = 25 °C, CW Current Operation

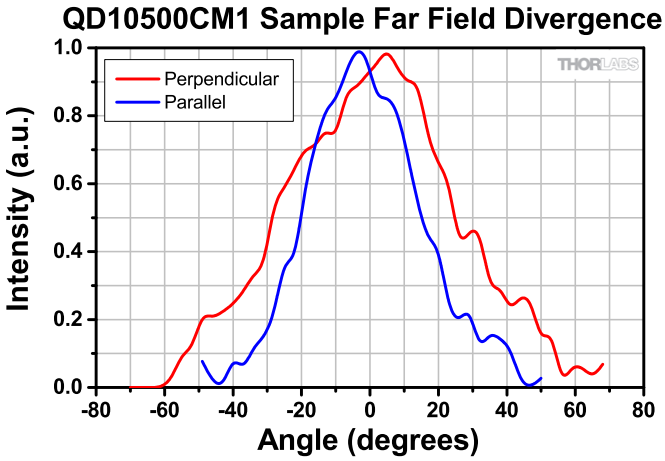
QD10500CM1				
	Symbol	**Min**	**Typical**	**Max**
Center Wavelength	λ_c	10.00 µm	-	11.00 µm
Tuning Range	TR	1 cm^{-1}	2 cm^{-1}	-
Temperature Tuning	$\Delta\bar{\nu}/\Delta T$	-	-0.07 cm^{-1}/°C	-
Side Mode Suppression	SMSR	20 dB	-	-
Output Power	P_{out}	10 mW	40 mW	-
Operating Current	I_{pp}	-	-	600 mA
Threshold Current	I_{TH}	-	300 mA	-
Forward Voltage	V_F	-	10.0 V	14.0 V
Slope Efficiency	$\Delta P/\Delta I$	-	0.3 W/A	-
Perpendicular Beam Divergence Angle (FWHM)	$\theta_\perp$	-	55°	-
Parallel Beam Divergence Angle (FWHM)	$\theta_\parallel$	-	40°	-

Sample Performance Plots





Sample Performance Plots (Cont.)



Far field divergence values are measured at 25 °C and at a distance of 89.4 mm from the laser. The detector's aperture is Ø10 mm, and the sampling step size is 3°. The angle subtended by the detector is 6.4°.

Drawing

